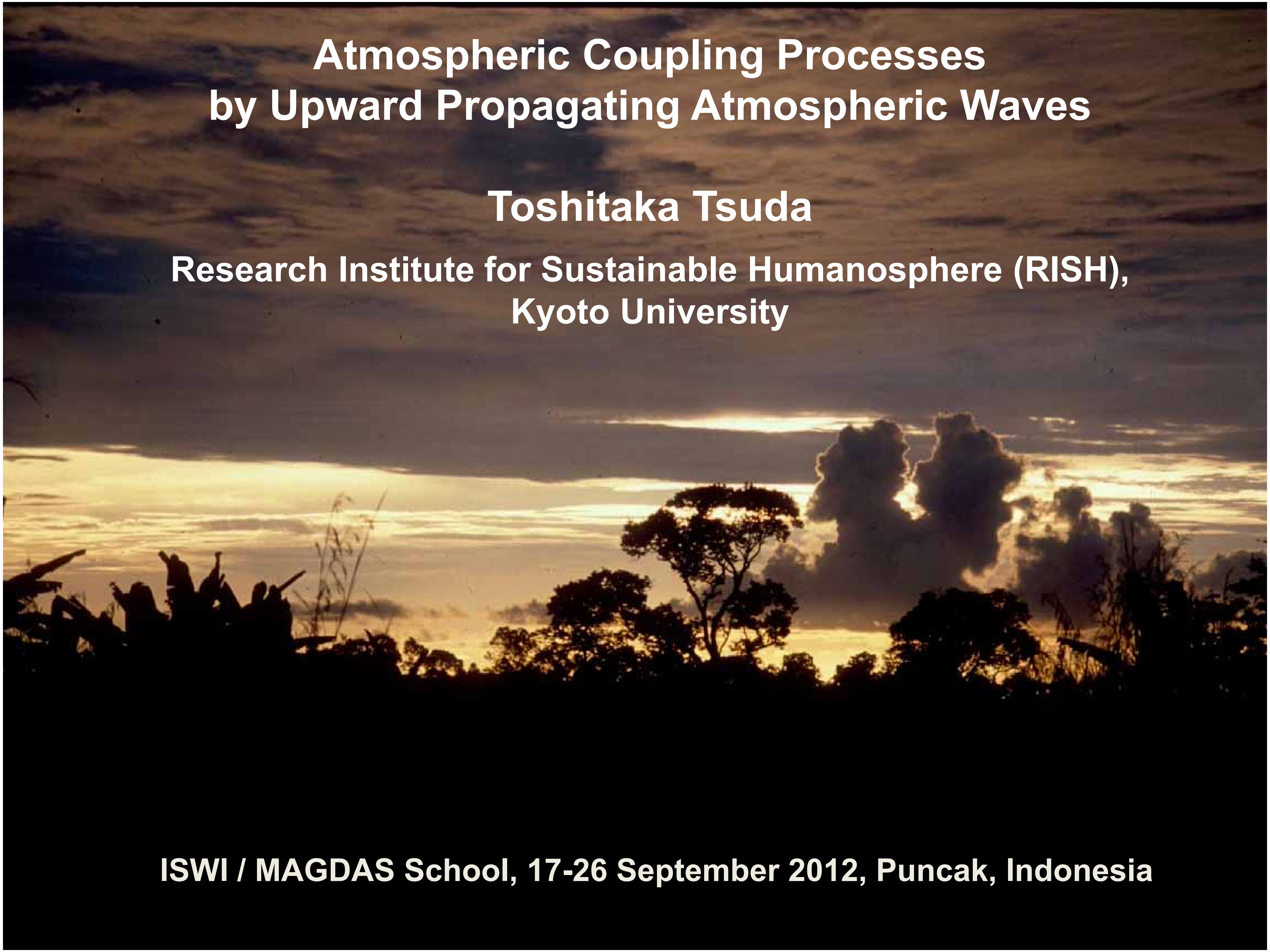

Atmospheric Coupling Processes by Upward Propagating Atmospheric Waves

Toshitaka Tsuda

Research Institute for Sustainable Humanosphere (RISH), Kyoto University

ISWI / MAGDAS School, 17-26 September 2012, Puncak, Indonesia

Outline of this lecture: Atmospheric Coupling Processes

- ✓ **A linear theory of atmospheric gravity wave**
  - Dispersion relation of atmospheric gravity waves
  - Convective instability and wave breaking/saturation
  - Critical level interaction between a gravity wave and wind shear
  - Importance of wave drag force (wave breaking) to maintain the general circulation of the middle atmosphere
- ✓ **Radar observations of wave breaking process**:
  - gravity wave saturation and turbulence generation (the MU radar).
- ✓ **Global distribution of gravity wave activity with GPS radio occultation (RO) measurements**:
  - Generation mechanisms; tropical convection, topography (mountain waves), Jet stream & polar night-jet, etc.
- ✓ **Correlation between sporadic E and stratospheric gravity waves**
  - Generation of orographic waves over Andes and Antarctica
  - A global distribution of sporadic E revealed with GPS-RO
- ✓ **Coupling between the lower atmosphere and the MLT (mesosphere lower thermosphere) winds in the tropics**
  - Tropical convection and gravity waves in the stratosphere
  - Correlation between short-period GW and Mesospheric SAO
  - Relation between S-QBO and M-QBO (M-QB Enhancement)

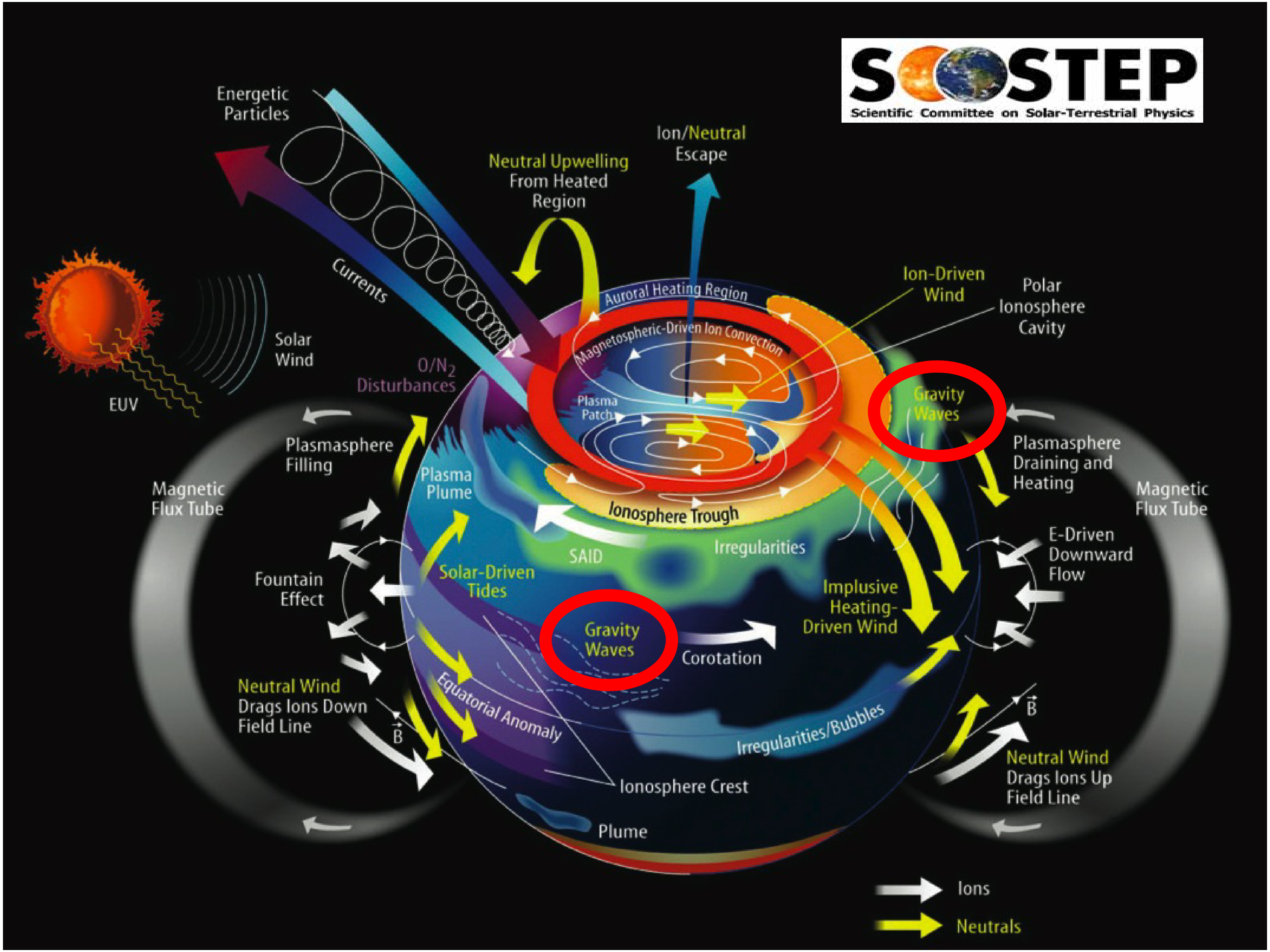
SCOSTEP
Scientific Committee on Solar-Terrestrial Physics
Energetic Particles
Ion/Neutral Escape
Neutral Upwelling From Heated Region
Currents
Solar Wind
EUV
O/N_2 Disturbances
Auroral Heating Region
Magnetospheric-Driven Ion Convection
Ion-Driven Wind
Polar Ionosphere Cavity
Plasma Patch
Gravity Waves
Plasmasphere Filling
Plasmasphere Draining and Heating
Magnetic Flux Tube
Plasma Plume
Ionosphere Trough
Magnetic Flux Tube
E-Driven Downward Flow
SAID
Irregularities
Fountain Effect
Solar-Driven Tides
Implusive Heating-Driven Wind
Gravity Waves
Corotation
Neutral Wind Drags Ions Down Field Line
Equatorial Anomaly
Irregularities/Bubbles
B
Neutral Wind Drags Ions Up Field Line
Ionosphere Crest
Plume
Ions
Neutrals

Classification of atmospheric waves

(Middle atmosphere dynamics by D.G. Andrews, J.R. Holton and C.B. Leovy)

(1) Restoring mechanism

Planetary (Rossby) waves: Coriolis Effects (meridional potential vorticity gradient)

Gravity (buoyancy) waves: Gravity (stratification) (*)

(Inertio-gravity waves; combination of stratification and Coriolis effects)

(2) Forced waves

Forced waves are continually maintained by an excitation mechanism of given phase speed and wave number.

Thermal tides excited by diurnal solar heating

Free waves: gravity waves, normal modes

(3) Propagation

Some waves can propagate in all directions.

Horizontally propagating planetary waves can be trapped in the vertical under some circumstances.

Equatorial waves can propagate vertically and zonally, but are trapped around the equator. Kelvin wave, mixed-Rossby-grabity (MRG) wave

(*) Typical scales of gravity waves

Wave periods: buoyancy (5-10 min.) to inertial (12hrs - several days) periods

Vertical wave length: shorter than 3-5 km

Horizontal scale: a few tens to thousands km

Generation Mechanisms of Atmospheric Gravity Waves

- **Atmospheric gravity waves are an oscillation characterized by a restoring force by buoyancy, and they are generated by**
  - **meteorological disturbances, like typhoon, cyclone, fronts, etc.**
  - **cloud convection in the tropics**
  - **unstable behavior of jet stream, like wind shear, geostrophic adjustment, etc**
  - **interaction of surface winds and topography (orographic waves)**

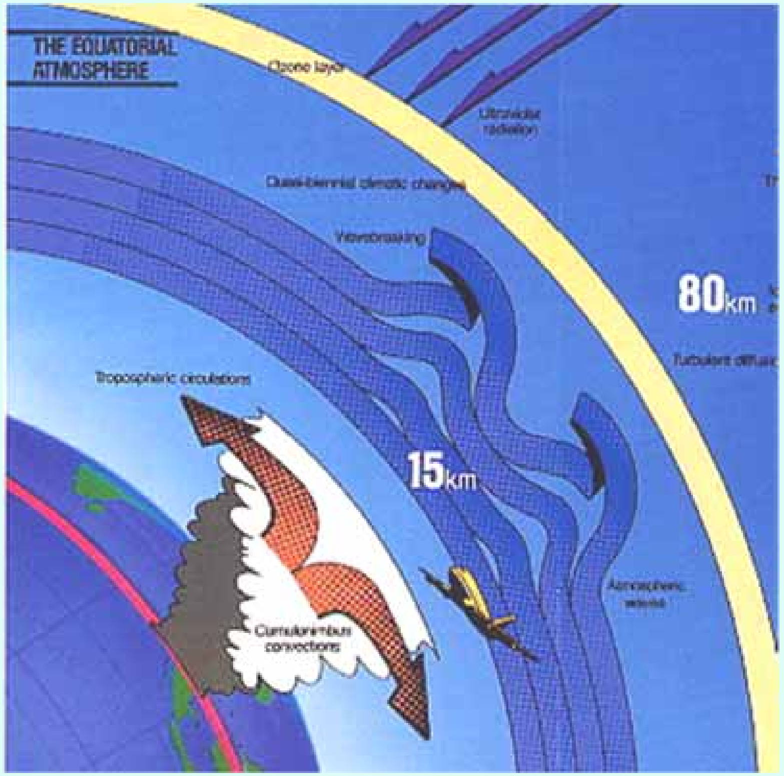

Gravity wave generation by cloud convection in the tropics

Numerical model of gravity wave generation by tropical convection
T. Lane and M. Reeder (2001)

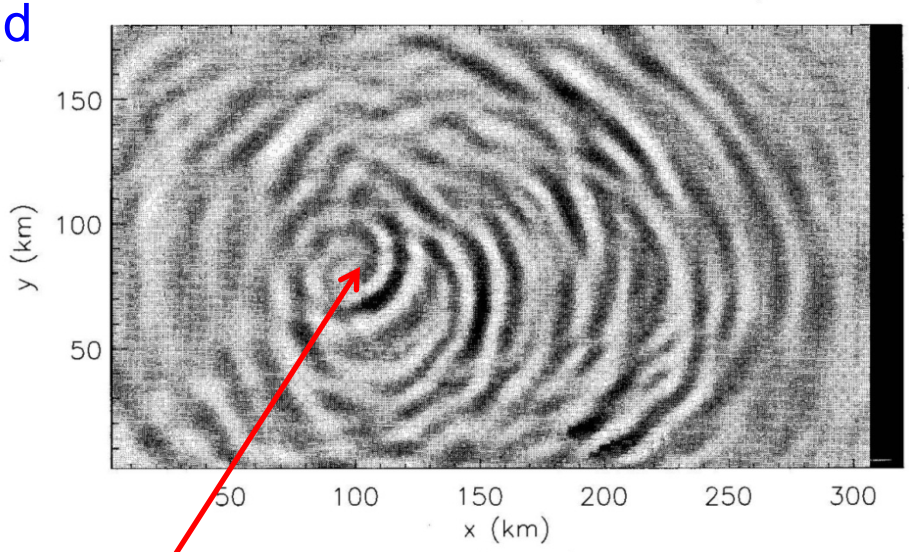

Figure 5. Horizontal cross-section of vertical velocity at $z = 40$ km in Domain 1 at 1330 LST.

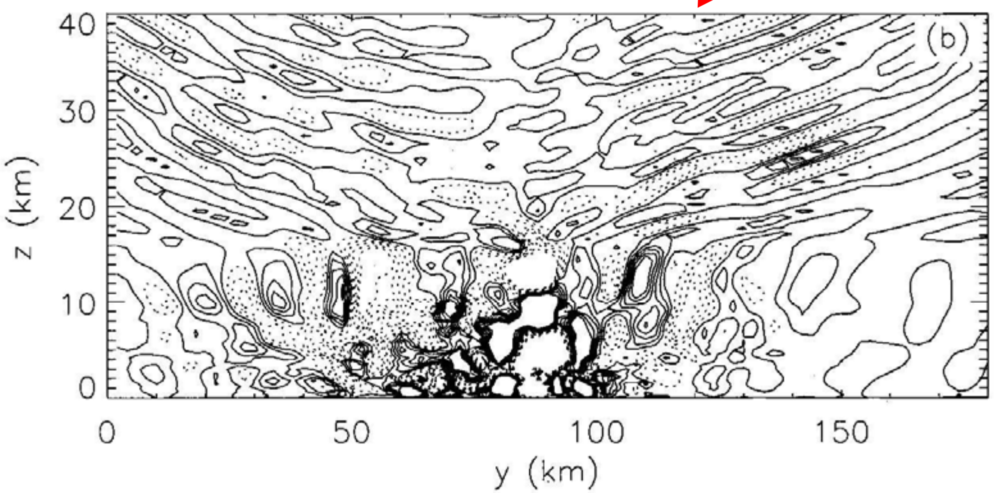

Figure 4. (a) Zonal cross-section of vertical velocity through $y = 100$ km for Domain 1. (b) Meridional cross-section of vertical velocity through $x = 100$ km for Domain 1. Vertical velocity is contoured at 0.1 m s^{-1} intervals, with the negative values dashed. Both plots are valid at 1300 LST. Note that (b) has a different horizontal scale from (a).

- ✓Horizontal (top) and Height-meridional (left) cross section of vertical velocity
- ✓Typical wave parameters
  - λx ~ 15-20 km
  - λz ~ 4-6 km
- ✓ No preferential direction for horizontal propagation

Generation and propagation characteristics of atmospheric gravity waves

Any vertical displacement in a stratified layer due to gravity produces an oscillation, which can propagate upward/downward from the position of generation .

Vertical group velocity of atmospheric gravity waves (downward in the figure below) is opposite direction to the wave phase velocity (upward).

This animation is copied from Prof. Satoshi Sakai's HP
http://dennou-k.gaia.h.kyoto-u.ac.jp/library/gfd_exp/exp_e/index.htm

Atmospheric gravity waves are generated due to interaction of surface winds with topography (mountains): mountain waves or orographic waves

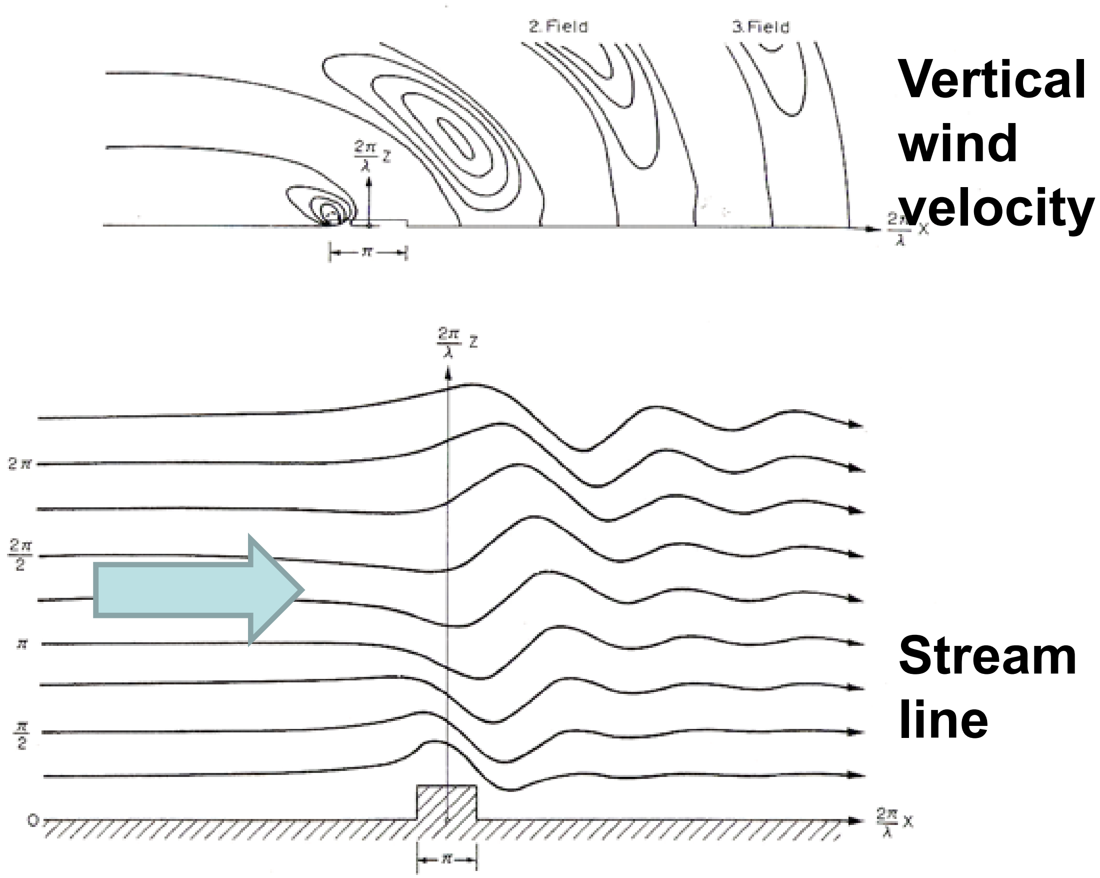

(e.g., Gossard and Hooke, 1975)

Experiment on generation of mountain (orographic) waves

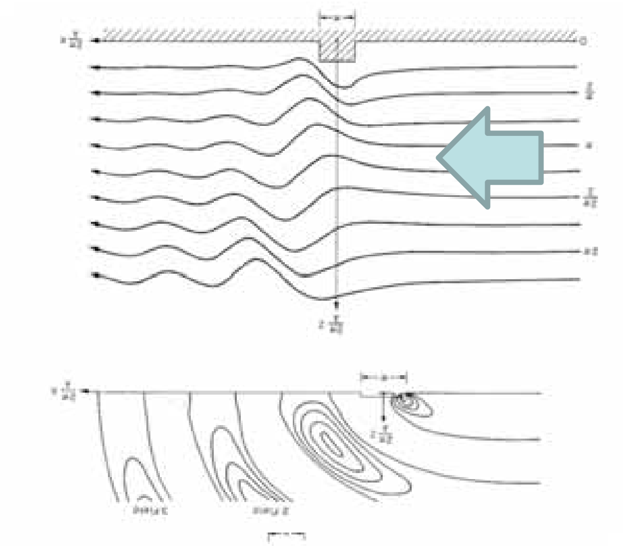

This animation is copied from Prof. Satoshi Sakai’s HP
http://dennou-k.gaia.h.kyoto-u.ac.jp/library/gfd_exp/exp_e/index.htm

Outline of this lecture: Atmospheric Coupling Processes

- ✓ A linear theory of atmospheric gravity wave
  - Dispersion relation of atmospheric gravity waves
  - Convective instability and wave breaking/saturation
  - Critical level interaction between a gravity wave and wind shear
  - Importance of wave drag force (wave breaking) to maintain the general circulation of the middle atmosphere
- ✓ Radar observations of wave breaking process:
  - gravity wave saturation and turbulence generation (the MU radar).
- ✓ Global distribution of gravity wave activity with GPS radio occultation (RO) measurements:
  - Generation mechanisms; tropical convection, topography (mountain waves), Jet stream & polar night-jet, etc.
- ✓ Correlation between sporadic E and stratospheric gravity waves
  - Generation of orographic waves over Andes and Antarctica
  - A global distribution of sporadic E revealed with GPS-RO
- ✓ Coupling between the lower atmosphere and the MLT (mesosphere lower thermosphere) winds in the tropics
  - Tropical convection and gravity waves in the stratosphere
  - Correlation between short-period GW and Mesospheric SAO
  - Relation between S-QBO and M-QBO (M-QB Enhancement)

Fundamental equations of an atmospheric gravity wave (GW)

The backgroud atmosphere is assumed to be motionless, and density stratified due to gravity.

$$\overline{\vec{v}} = 0 \quad (1)$$

Hydrostatic equation

$$\frac{\partial \overline{p}(z)}{\partial z} = -\overline{\rho}(z) g \quad (2)$$

When the atmosphere is isothermal, pressure and air density can be expressed as follows by using scale height $H = RT_0/g$.

$$\overline{p}(z) = p_0 e^{-z/H} \quad (3)$$

$$\overline{\rho}(z) = \rho_0 e^{-z/H} \quad (4)$$

Atmospheric density decreases exponentially along height

We can derive perturbed equations of motion, mass conservation low, and thermodymanics as:

Equation of Motion

$$\overline{\rho}\left(\frac{\partial \vec{v}}{\partial t} + f\vec{e}_z \times \vec{v}\right) = -\nabla p - \rho g \vec{e}_z \quad (5)$$

Mass conservation

$$\frac{\partial \rho}{\partial t} + w\frac{\partial \overline{\rho}}{\partial z} + \overline{\rho}\nabla\vec{v} = 0 \quad (6)$$

Thermodynamics

$$\frac{\partial p}{\partial t} + w\frac{\partial \overline{p}}{\partial z} = \gamma R T_0\left(\frac{\partial \rho}{\partial t} + w\frac{\partial \overline{\rho}}{\partial z}\right) \quad (7)$$

where $\gamma = C_p/C_v$ is specific heat ratio.

z: height
t: time
v: velocity
p: pressure
ρ: density
T: temperature
g: gravity acceleration
f: Coriolis frequency
γ: specific heat ratio
R: gas constant

In order to normalize exponential growth of variables, we apply following transformations.

$$\tilde{v} = \vec{v}e^{-z/2H} \tag{8}$$

When wave energy ρv^2 is conserved, the amplitude of wind velocity perturbations increase exponentially along height in response to the density decrease.

$$(\tilde{p}, \tilde{\rho}) = (p, \rho)e^{z/2H} \tag{9}$$

Furthermore, all of variables are expanded into harminic functions.

$$\tilde{a}(x, y, z, t) = A\exp(ikx + imz - i\omega t) \tag{10}$$

$\partial/\partial x = ik$、$\partial/\partial z = im$、$\partial/\partial t = -i\omega$

where k and m are horizontal and vertical wavenumber, and ω is wave frequency. Dispersion relation can be derived as

$$\boxed{m^2 = \frac{k^2(N^2 - \omega^2)}{\omega^2 - f^2} + \frac{\omega^2 - \omega_a^2}{c_s^2}} \tag{11}$$

$c_s = \sqrt{\gamma RT_0}$, N and $f = 2\Omega\sin(latitude)$ are speed of sound, Brunt-Väisälä and inertial frequencies.

Since m^2 must be positive for vertically propagating wave, two solutions can be obtained.

(1) Acoustic wave: $\omega > \omega_a = \sqrt{c_s^2/4H^2}$

(2) Gravity wave: $N > \omega > f$

C. O. Hine, 1974
Upper atmosphere in motion,
AGU monograph

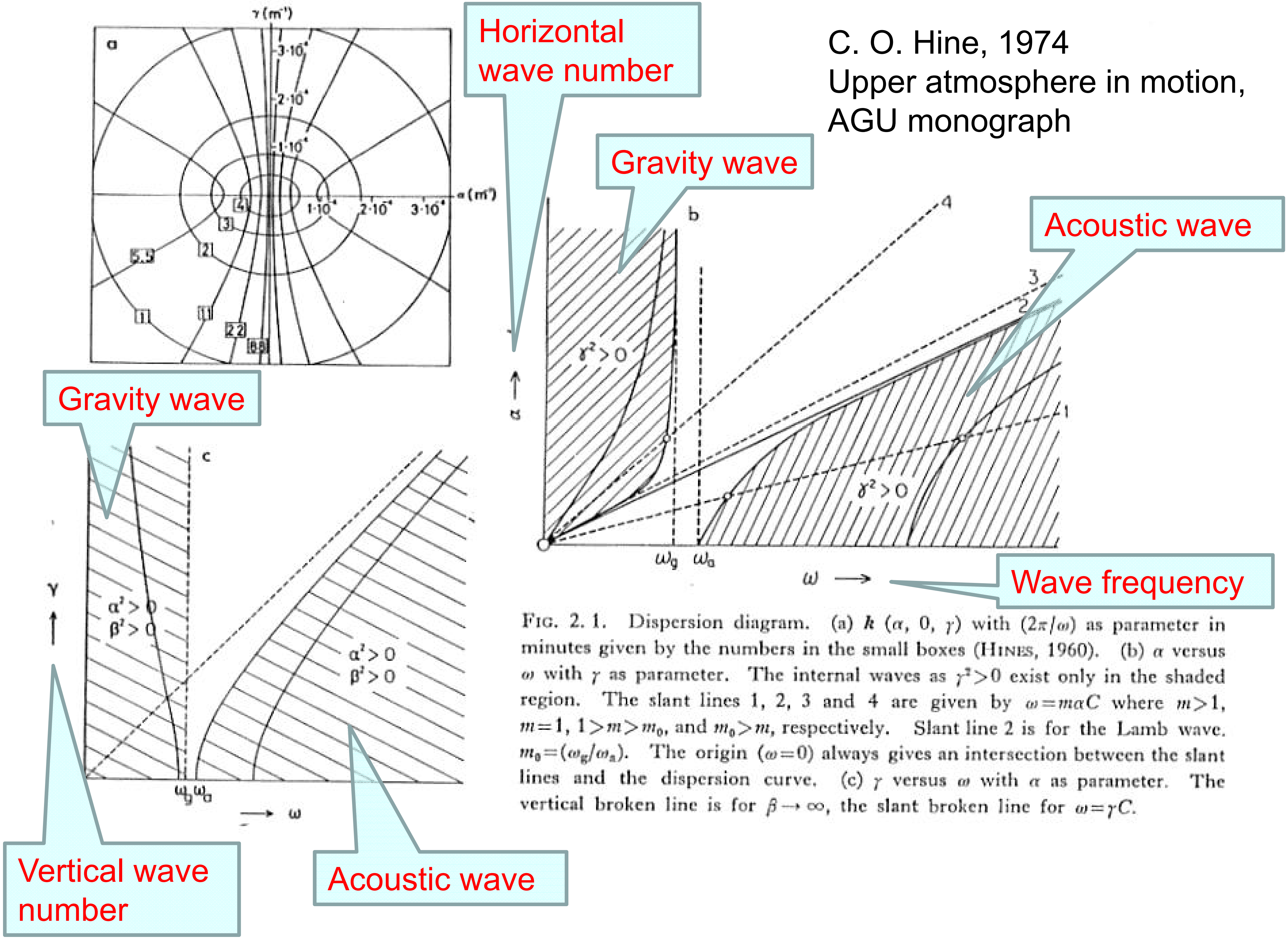

FIG. 2. 1. Dispersion diagram. (a) $\boldsymbol{k}$ (α, 0, γ) with ($2\pi/\omega$) as parameter in minutes given by the numbers in the small boxes (HINES, 1960). (b) α versus ω with γ as parameter. The internal waves as $\gamma^2>0$ exist only in the shaded region. The slant lines 1, 2, 3 and 4 are given by $\omega=m\alpha C$ where $m>1$, $m=1$, $1>m>m_0$, and $m_0>m$, respectively. Slant line 2 is for the Lamb wave. $m_0=(\omega_g/\omega_a)$. The origin ($\omega=0$) always gives an intersection between the slant lines and the dispersion curve. (c) γ versus ω with α as parameter. The vertical broken line is for $\beta\to\infty$, the slant broken line for $\omega=\gamma C$.

Dispersion relations of atmospheric gravity wave

$$m^2 = \frac{k^2(N^2-\omega^2)}{\omega^2 - f^2} \quad \text{where} \quad \omega = k(c-\overline{u})$$ Eq. (12)

$$\boxed{\begin{aligned} v' &= -\left(\frac{if}{\omega}\right)u' \\ w' &= -\left(\frac{k}{m}\right)u' \end{aligned}}$$ Eq. (13)

$$\theta' = -\frac{i d\overline{\theta}/dz}{m(\overline{u}-c)}u'$$

Perturbation components due to gravity wave.

u' : horizontal wind in the direction of wave propagation

v' : orthogonal wind component

w' : vertical wind velocity

θ' : potential temperature

Radiosonde (balloon) observation of wind velocity (solid: Eastward, dashed: Northward) and temperature (dot-dash) profiles at Watukosek, Indonesia on March 8, 1990.

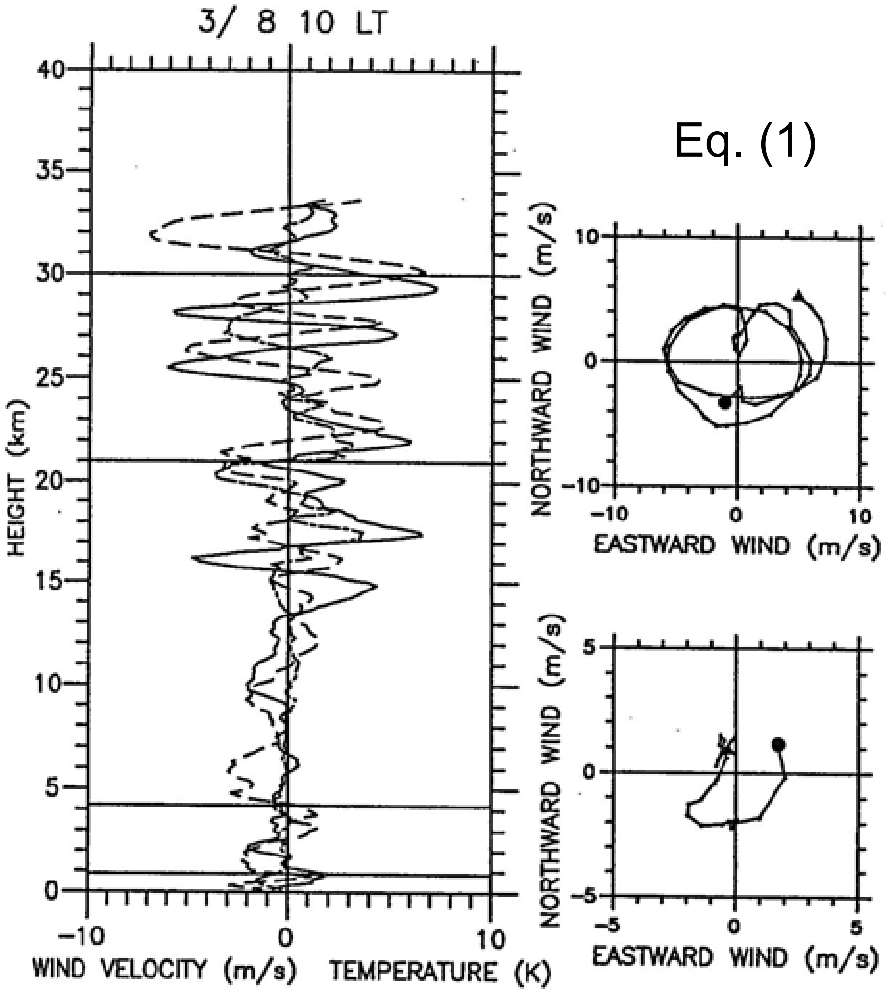

Outline of this lecture: Atmospheric Coupling Processes

- ✓ A linear theory of atmospheric gravity wave
  - Dispersion relation of atmospheric gravity waves
  - Convective instability and wave breaking/saturation
  - Critical level interaction between a gravity wave and wind shear
  - Importance of wave drag force (wave breaking) to maintain the general circulation of the middle atmosphere
- ✓ Radar observations of wave breaking process:
  - gravity wave saturation and turbulence generation (the MU radar).
- ✓ Global distribution of gravity wave activity with GPS radio occultation (RO) measurements:
  - Generation mechanisms; tropical convection, topography (mountain waves), Jet stream & polar night-jet, etc.
- ✓ Correlation between sporadic E and stratospheric gravity waves
  - Generation of orographic waves over Andes and Antarctica
  - A global distribution of sporadic E revealed with GPS-RO
- ✓ Coupling between the lower atmosphere and the MLT (mesosphere lower thermosphere) winds in the tropics
  - Tropical convection and gravity waves in the stratosphere
  - Correlation between short-period GW and Mesospheric SAO
  - Relation between S-QBO and M-QBO (M-QB Enhancement)

Taylor-Goldstein equation of a gravity wave

Liner gravity wave theory including the effects of background mean winds. (e.g., E.E. Gossard and W.H. Hooke, Waves in the atmospherie, Chapter 3, Elsevier, 1975)

$$\frac{\partial^2 W}{\partial z^2} + [\frac{N^2}{(u_0 - C)^2} - k^2 - \frac{\partial^2 u_0 / \partial z^2}{(u_0 - C)} - \frac{2\Gamma \partial u_0 / \partial z}{u_0 - C} - \Gamma^2] W = 0 \qquad \text{Eq. (14)}$$

W: vertical wind velocity perturbation due to a gravity wave
z: height, N: Brunt-Vaisala frequency, u_0: background mean winds
Γ=1/2H (H; scale height)
C: horizontal phase velocity of GW, k; horizontal wave number

$$m^2 = k^2 (\frac{N^2}{\omega^2} - 1) - \Gamma^2 - \frac{2\Gamma}{u_0 - C}\frac{\partial u_0}{\partial z} - \frac{1}{u_0 - C}\frac{\partial^2 u_0}{\partial z^2} \qquad \text{Eq. (15)}$$

When m^2 is negative, wave dissipation occurs along height, while a positive m^2, the gravity wave can propagate upward/downward.

Reference
Wave equation: $d^2f/dt^2 = c^2\, d^2f/dx^2$
Simple harmonic oscillation: $d^2A/dx^2 + Bx = 0$

Wave breaking due to convective instability

By assuming N^2 is constant, and du^2/dz^2, 1/2H and k^2 are negligible, Eq (14) becom

$$\frac{\partial^2 W}{\partial z^2} + [\frac{N^2}{(u_0 - C)^2}]W = 0$$

Eq. (16)

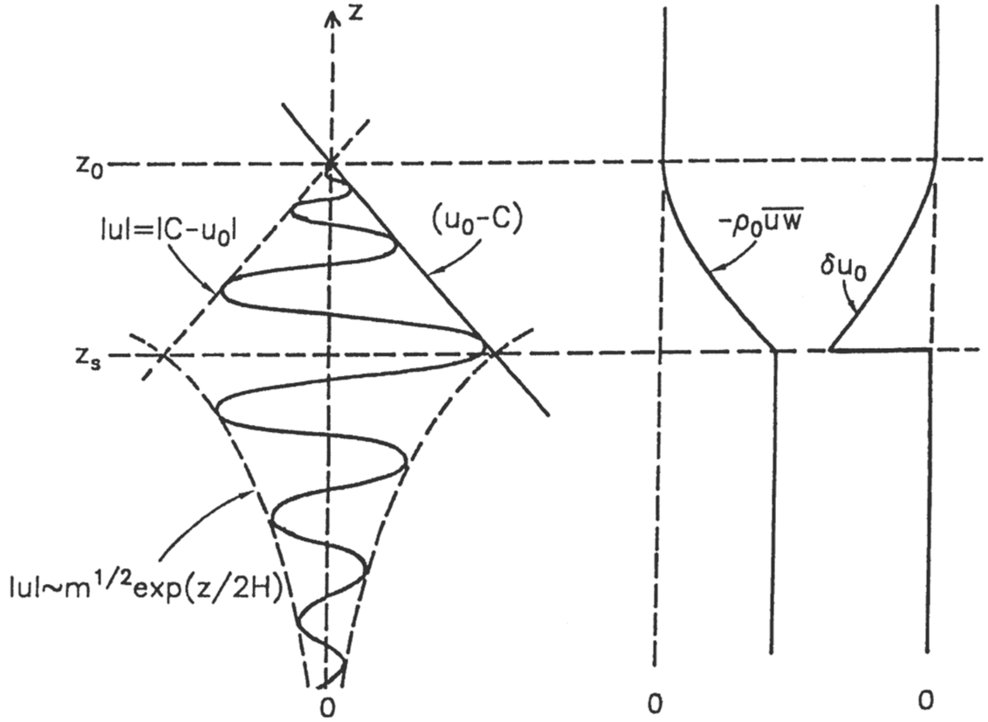

A gravity wave becomes unstable when the total horizontal wind velocity by adding the mean wind and the wave perturbation component exceeds the wave phase velocity, i.e., $u_o+u'>C$.

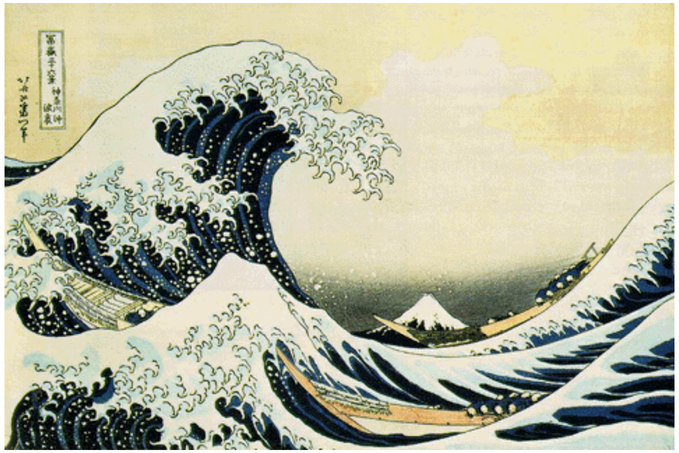

Schematic of the growth with height and saturation of a gravity wave due to convective instability. Wave dumping produces both a divergence of the vertical flux of horizontal momentum an acceleration of the mean flow toward the phase speed of wave. Deceleration and diffusion cease above the critical level ($z=z_0$) in the liner theory. [Fritts, 1984]

Kelvin-Helmholtz Instability (KHI)

When a large velocity difference (wind shear) exists across an interface between two layers, dynamical instability is induced, which is called KHI.

This animation is copied from Prof. Satoshi Sakai's HP
http://dennou-k.gaia.h.kyoto-u.ac.jp/library/gfd_exp/exp_e/index.htm

Critical level interaction between a gravity wave and wind shear

By neglecting both du^2/dz^2 and 1/2H, Eq (15) becomes

$$m^2 = \frac{N^2}{(u_0 - c)^2} - k^2 = k^2\left(\frac{N^2}{\omega^2} - 1\right) \qquad \text{Eq. (17)}$$

The vertical group velocity of a wave becomes very small as the wave approaches to the height of C=u_0, which is called the critical level. Then, the wave cannot propagate upward acrossing this level.

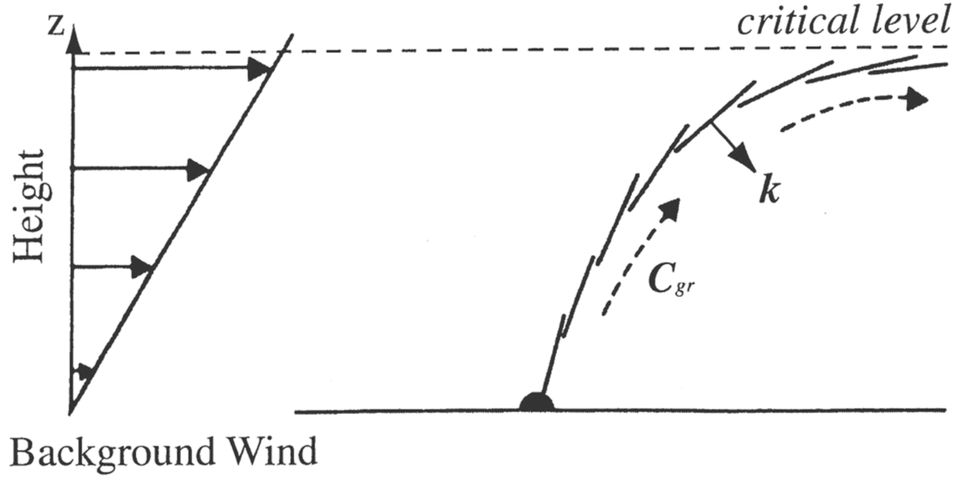

Schematic diagram of vertical propagation of a gravity wave in the vertical wind shear. Short solid lines show phase surface of the gravity wave [adapted from Matsuno and Shimazaki, 1981].
C_{gr} is the phase velocity of the wave. k is the vector perpendicular to the wave propagating direction.

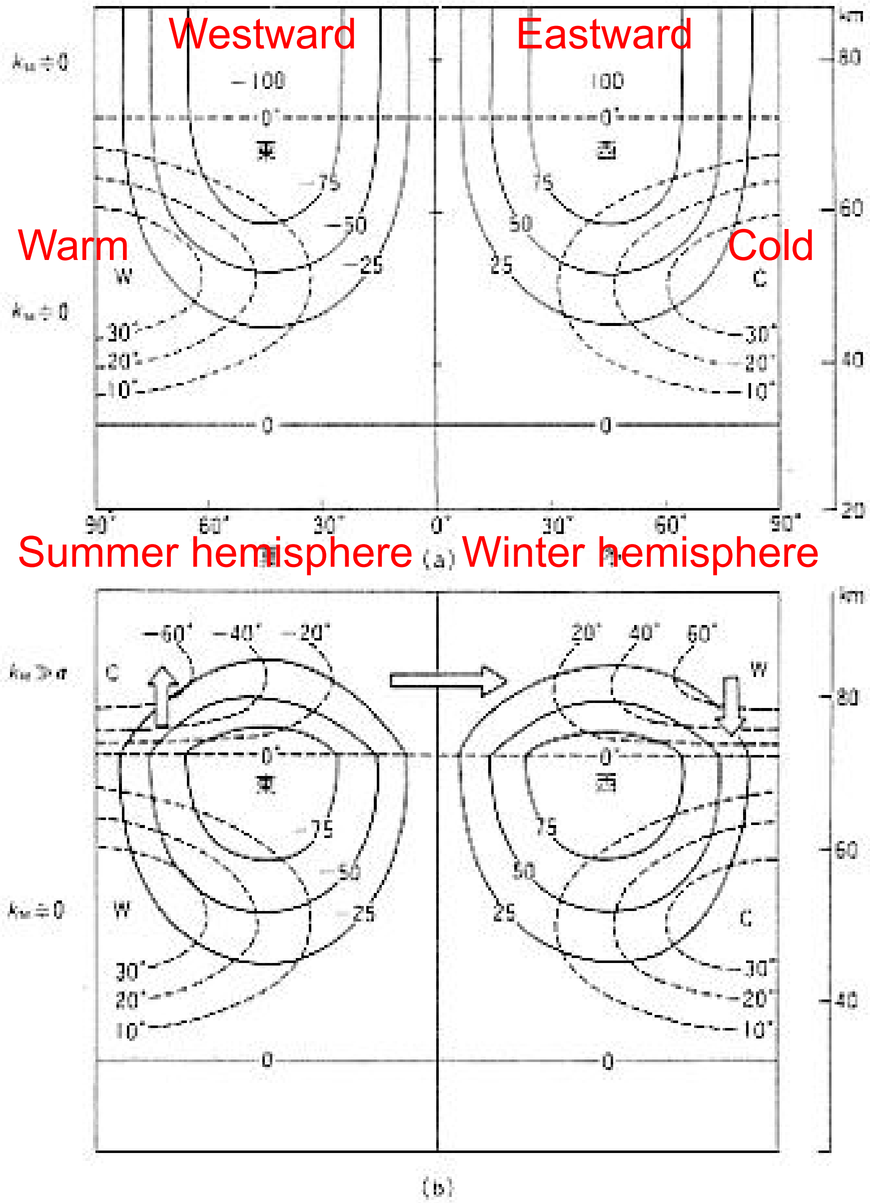

図 4.10　中層大循環の機構を説明するための模式図．実線は東西風速，破線は気温の偏差（同一高度内での）の等値線を示す．(a)は上部に摩擦層がない場合，(b)は摩擦層がある場合を示す．(b)では矢印で示すような子午面流・上下流がつくられ，逆センスの温度分布が生まれる((a)は Lindzen, 1968)．

(TOP)
Predicted structure of the middle atmosphere in 1970's by assuming only radiation balance due to photo-chemical processes.

Solid line: zonal winds (eastward positive)

Dashed line: temperature

(BOTTOM)
Observed structure of the middle atmosphere in 1980's.
Zonal winds become weak at around 80 km altitude (mesopause), closing the jet stream of the middle atmosphere.
Temperature gradient along latitude is reversed, producing a colder mesopause in summer.
A cross equator flow from summer to winter hemisphere occurs.

Mean zonal (eastward positive) wind velocity at mid-latitudes in the northern hemisphere
Summer (assuming radiative equilibrium only)

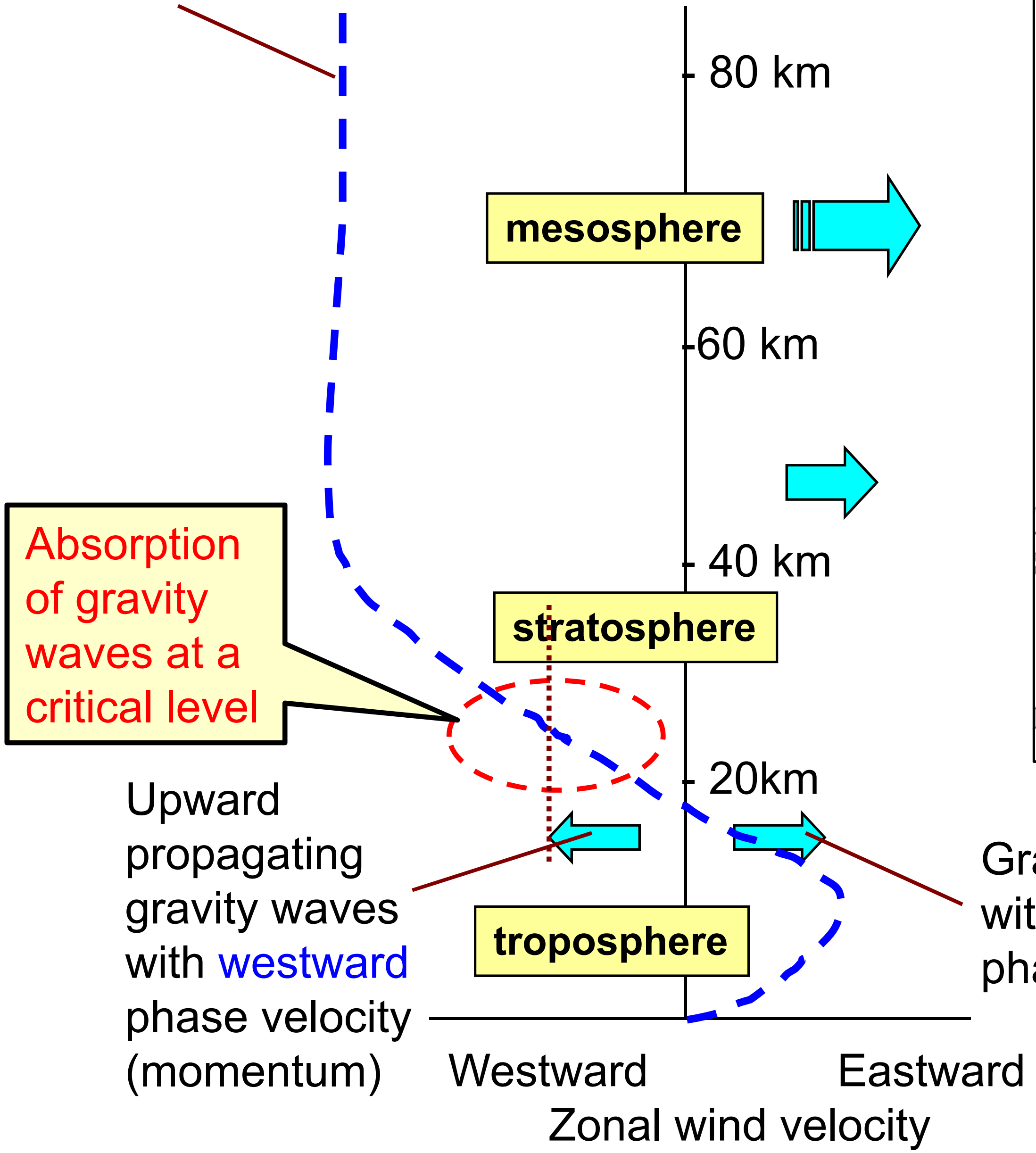

CRITICAL LEVEL

Vertical propagation of a gravity wave in the vertical wind shear (LEFT). Short solid lines (RIGHT) show phase surface of the gravity wave [adapted from Matsuno and Shimazaki, 1981].

C_{gr} is the phase velocity of the wave.

$\boldsymbol{k}$ is the vector perpendicular to the wave propagating direction.

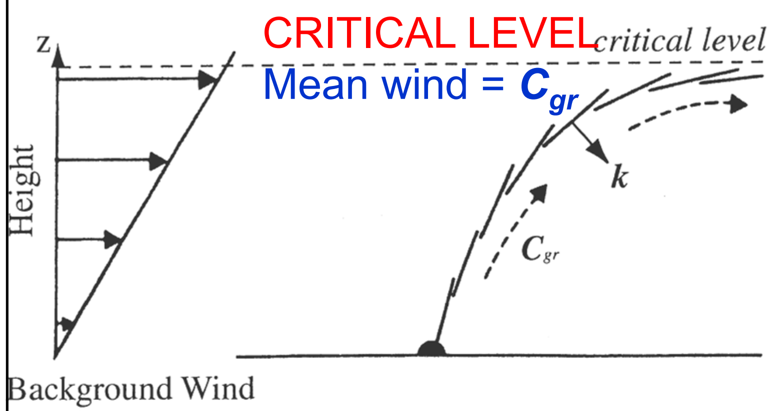

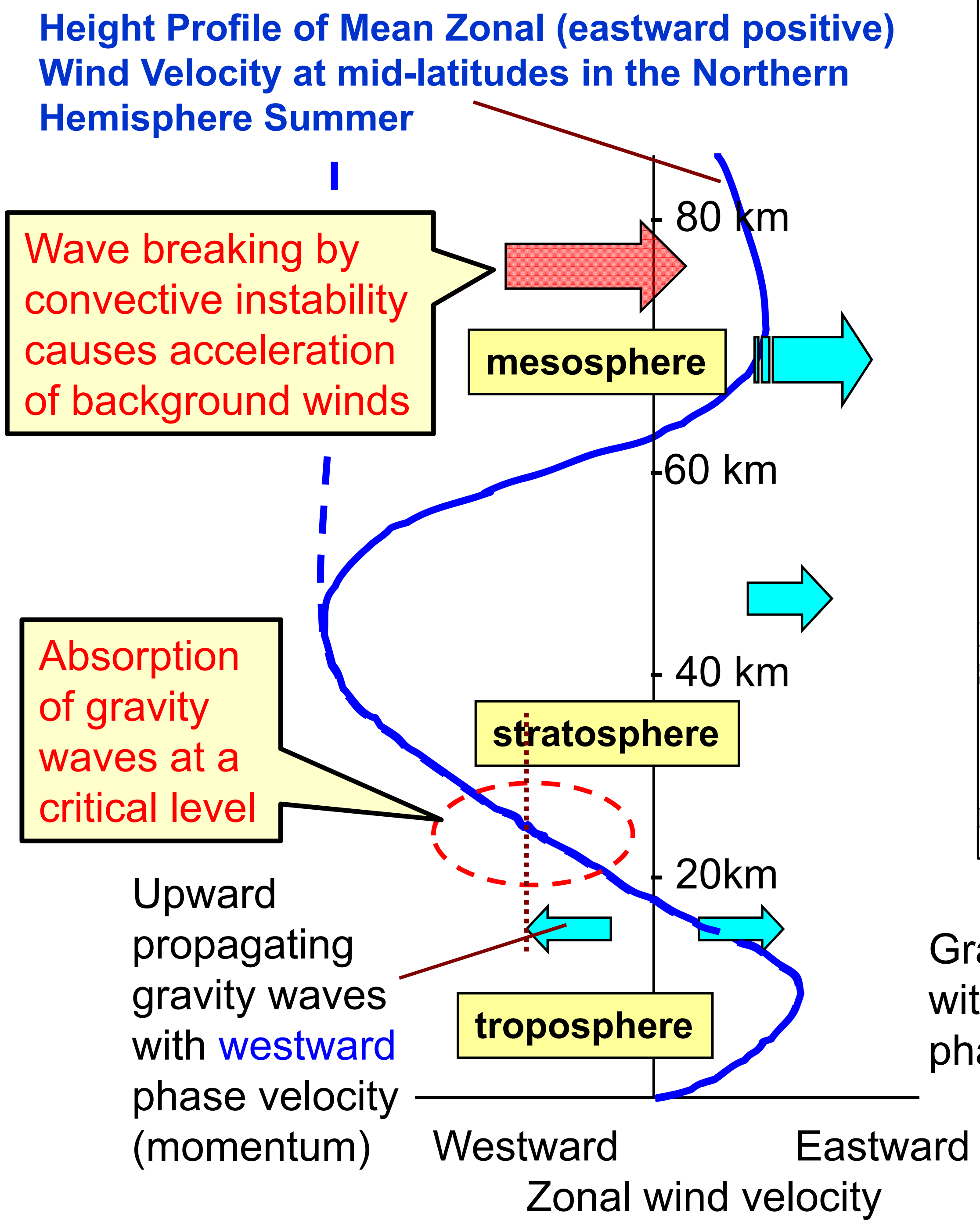

CRITICAL LEVEL

Vertical propagation of a gravity wave in the vertical wind shear (LEFT). Short solid lines (RIGHT) show phase surface of the gravity wave [adapted from Matsuno and Shimazaki, 1981].

C_{gr} is the phase velocity of the wave.

k is the vector perpendicular to the wave propagating direction.

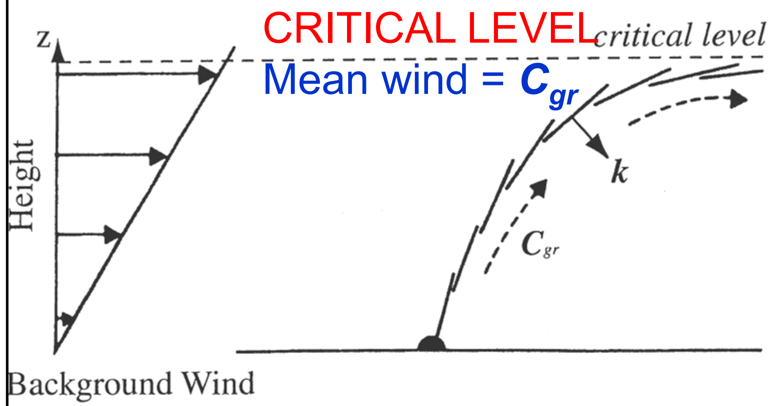

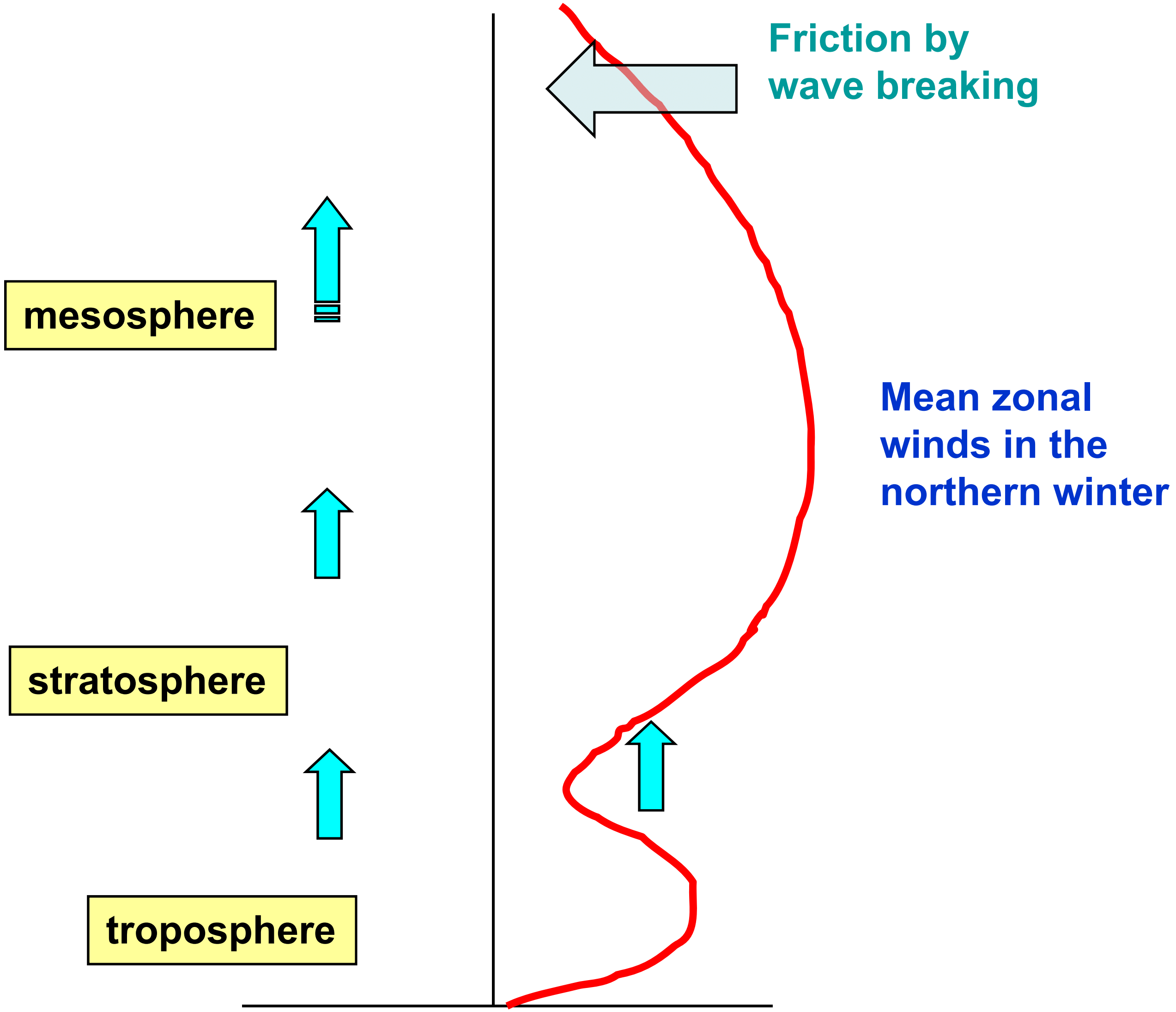
Friction by
wave breaking
mesosphere
Mean zonal
winds in the
northern winter
stratosphere
troposphere

Characteristics of Atmospheric Gravity Waves

- Gravity waves are generated by a variety of processes including the interaction of surface winds with topography, meteorological disturbances, deep convective storms, unbalanced flow in the jet stream, and so on.
- Circulation changes associated with gravity wave dissipation are now known to have wide-ranging effects on numerical weather prediction models, climate change response patterns, forecasts of stratospheric ozone recovery, and space weather.
- The global scale of these issues requires global knowledge of gravity wave properties despite the fact that the scales of the waves themselves are too small to be fully simulated in a global model.
- The problem of gravity waves and their effects on the general circulation thus requires a broad range of studies, those using local high-resolution observations, global observational data sets such as those acquired from satellite as well as wave-resolving numerical models.
- Ground-based atmospheric radars, such as MST, MF meteor radars, can observe the detailed time-height behavior of gravity waves.
- Recent satellite missions, like GPS radio occultation, have a very good height resolution, which provide a unique opportunity to study a global morphology of gravity waves.

Outline of this lecture: Atmospheric Coupling Processes

- ✓ A linear theory of atmospheric gravity wave
  - Dispersion relation of atmospheric gravity waves
  - Convective instability and wave breaking/saturation
  - Critical level interaction between a gravity wave and wind shear
  - Importance of wave drag force (wave breaking) to maintain the general circulation of the middle atmosphere
- ✓ Radar observations of wave breaking process:
  - gravity wave saturation and turbulence generation (the MU radar).
- ✓ Global distribution of gravity wave activity with GPS radio occultation (RO) measurements:
  - Generation mechanisms; tropical convection, topography (mountain waves), Jet stream & polar night-jet, etc.
- ✓ Correlation between sporadic E and stratospheric gravity waves
  - Generation of orographic waves over Andes and Antarctica
  - A global distribution of sporadic E revealed with GPS-RO
- ✓ Coupling between the lower atmosphere and the MLT (mesosphere lower thermosphere) winds in the tropics
  - Tropical convection and gravity waves in the stratosphere
  - Correlation between short-period GW and Mesospheric SAO
  - Relation between S-QBO and M-QBO (M-QB Enhancement)

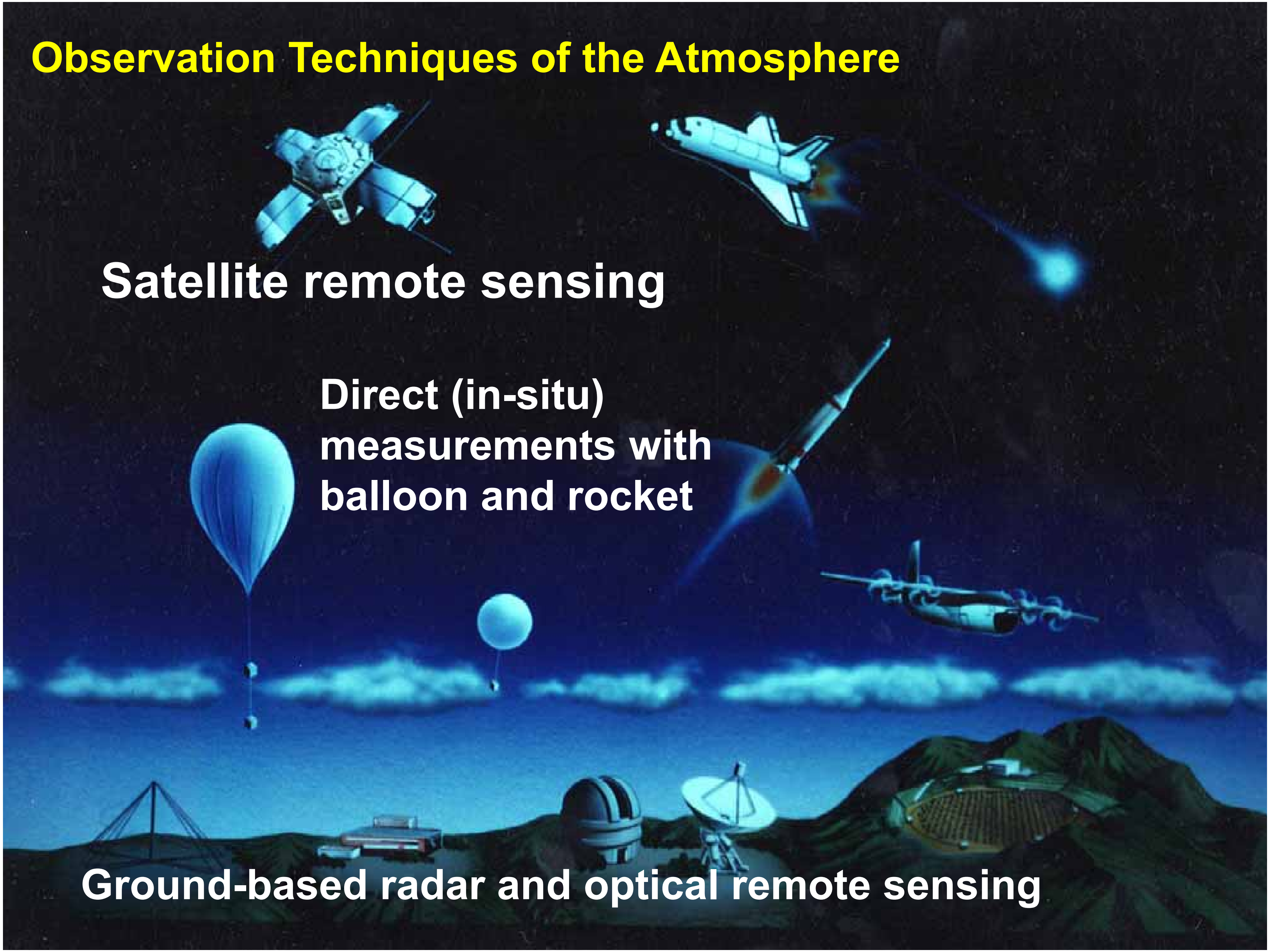
Observation Techniques of the Atmosphere
Satellite remote sensing
Direct (in-situ) measurements with balloon and rocket
Ground-based radar and optical remote sensing

Shigaraki MU Observatory
The MU (middle and upper atmosphere) Radar

Boundary Layer Radar with RASS (radio acoustic sounding system)
Frequency: 1.375 GHz
Antenna: 10mx10m, coaxial-colinear array
Acoustic horn x4

Radar system	monostatic pulse radar; active phased array system
Operation frequency	46.5MHz
Antenna	475 crossed yagis
Aperture	8,330 m^2 (103 m in diameter)
Transmitter	475 solid state amplifiers
Peak power	1 MW
Average power	50 kW
Polarization	linear and circular

Refractive Index (N) and Atmospheric Parameters

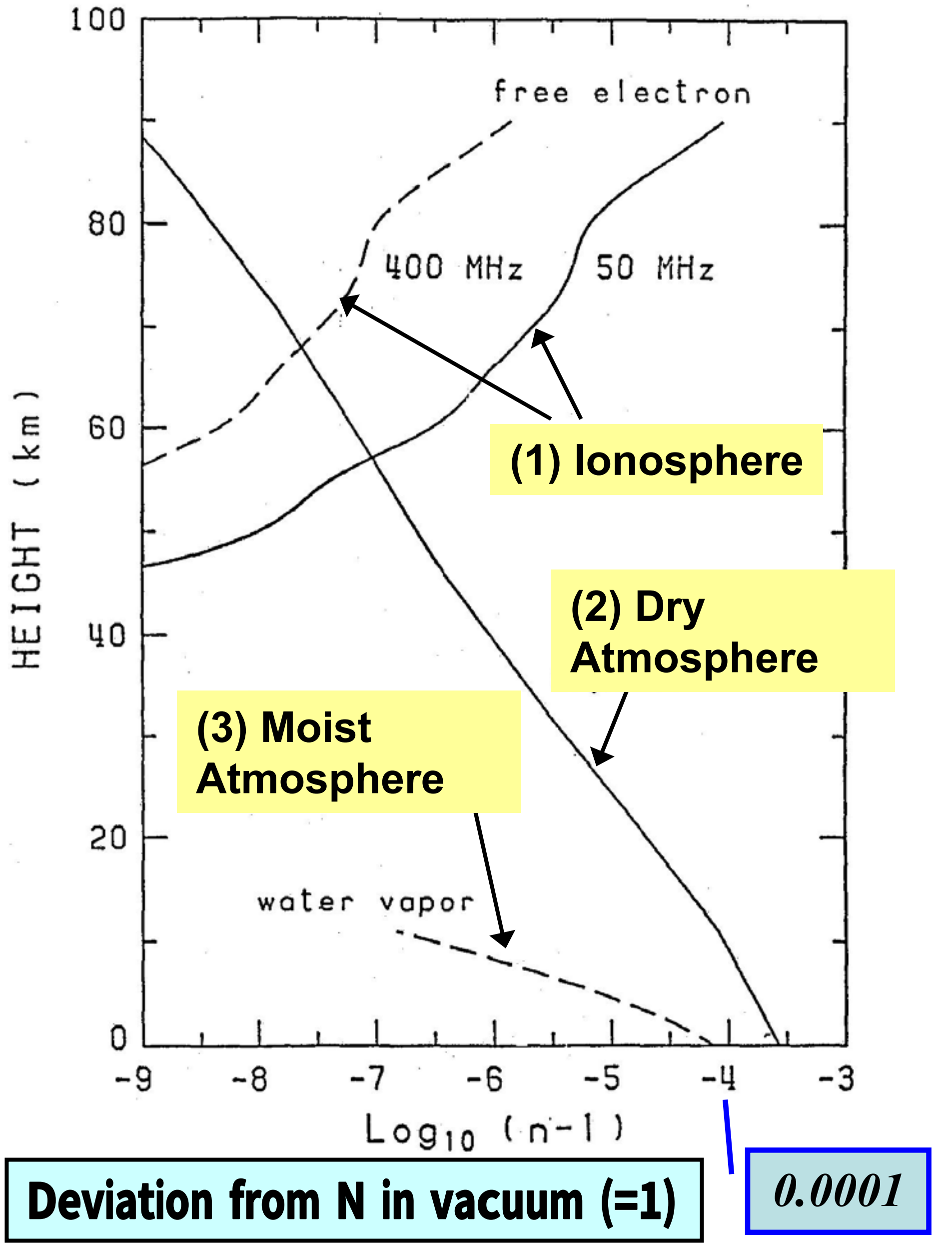

$$
\begin{aligned}
N = 1 &+ C_1 \times Ne / f^2 \quad \text{(1) Ionosphere} \\
&+ C_2 \times p / T \quad \text{(2) Dry atmosphere} \\
&+ C_3 \times e / T^2 \quad \text{(3) Moist Atmosphere}
\end{aligned}
$$

$C_{1,2,3}$: Constants

p: Pressure T: Temperature

e: Partial pressure of water vapor

f: Radio frequency,

Ne: Electron density

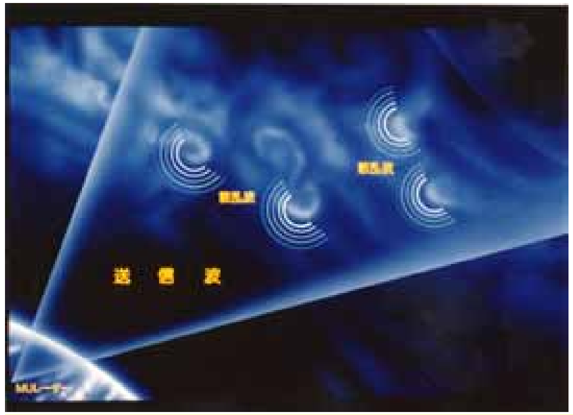

We can detect radio wave scattering from refractive index caused by atmospheric turbulence.

Measurement of 3D wind velocity

By steering the radar antenna beam into (at least) 3 independent directions, we can decompose 2 horizontal and vertical wind velocity components.

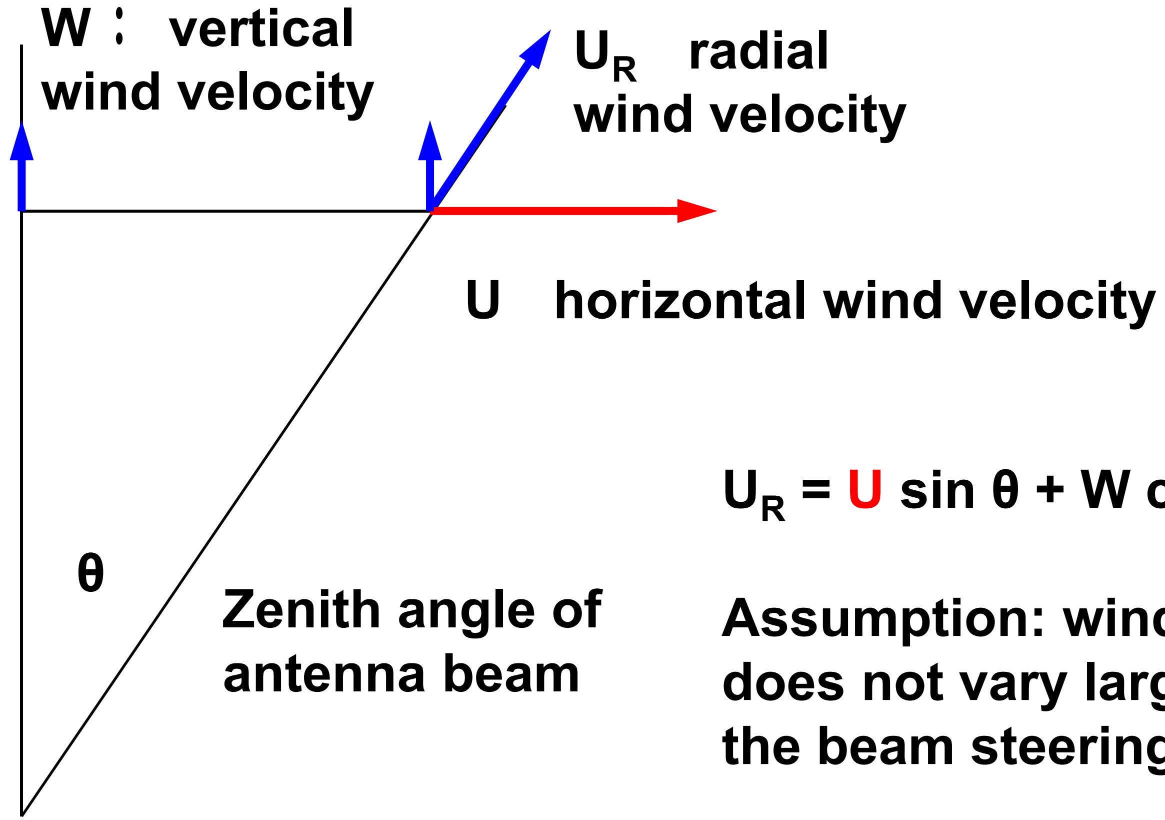

$$U_R = U \sin\theta + W \cos\theta$$

Assumption: wind velocity does not vary largely within the beam steering volume.

Horizontal Wind Velocity

Radiosonde

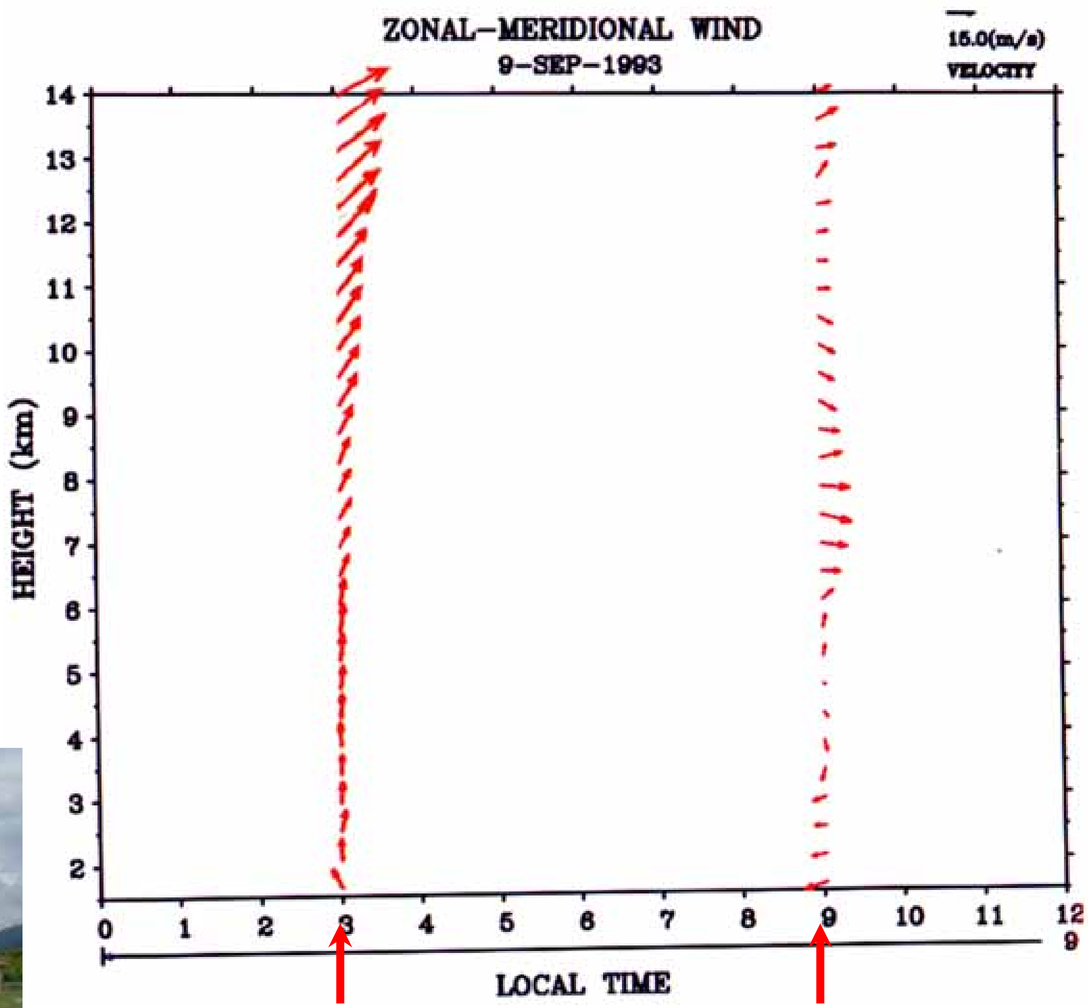

6 hr interval

Continuous Monitoring of Horizontal Wind Velocity Fluctuations with the MU Radar

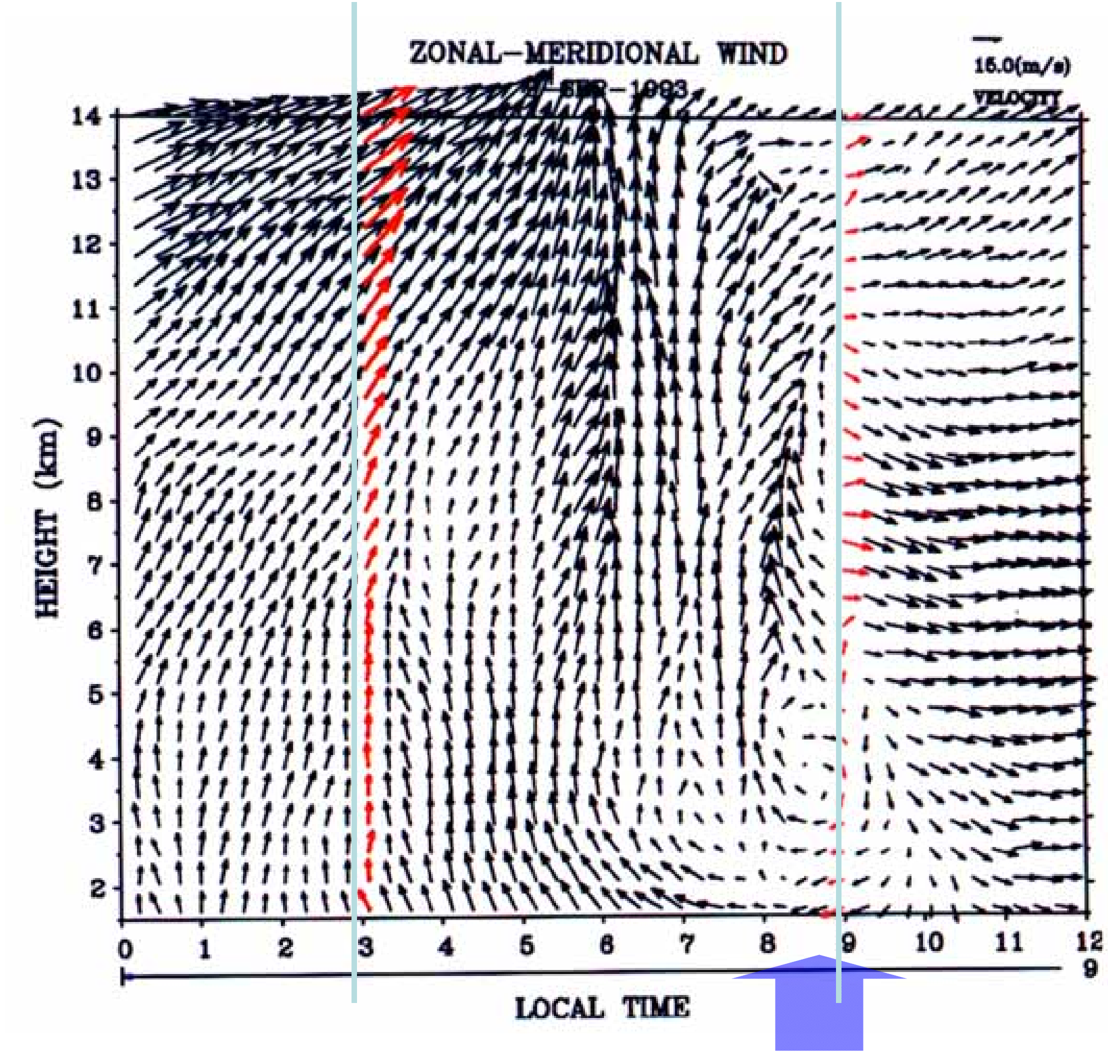

Passage of
a typhoon

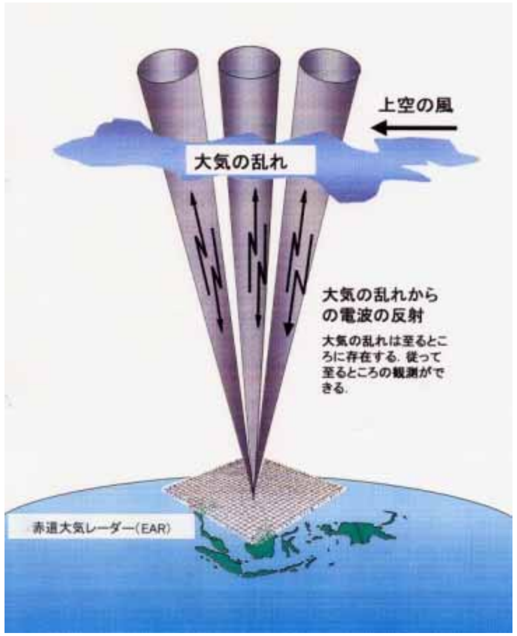

EAR site is now a comprehensive equatorial atmosphere observatory

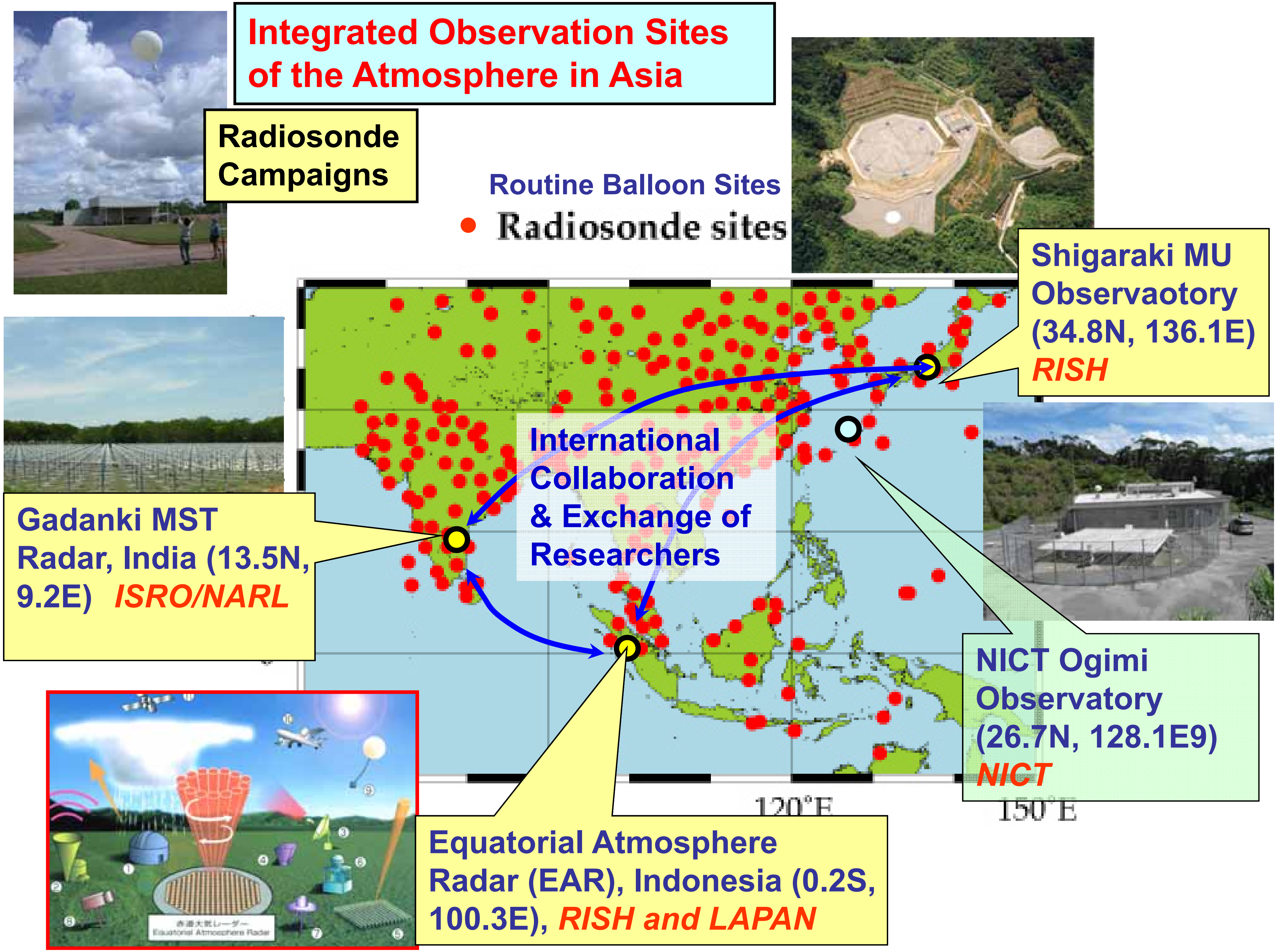
Integrated Observation Sites of the Atmosphere in Asia
Radiosonde Campaigns
Routine Balloon Sites
Radiosonde sites
Shigaraki MU Observaotory (34.8N, 136.1E) RISH
International Collaboration & Exchange of Researchers
Gadanki MST Radar, India (13.5N, 9.2E) ISRO/NARL
NICT Ogimi Observatory (26.7N, 128.1E9) NICT
120°E
150°E
Equatorial Atmosphere Radar (EAR), Indonesia (0.2S, 100.3E), RISH and LAPAN

Wind velocity profiles observed with the MU radar, radiosondes and rocketsondes

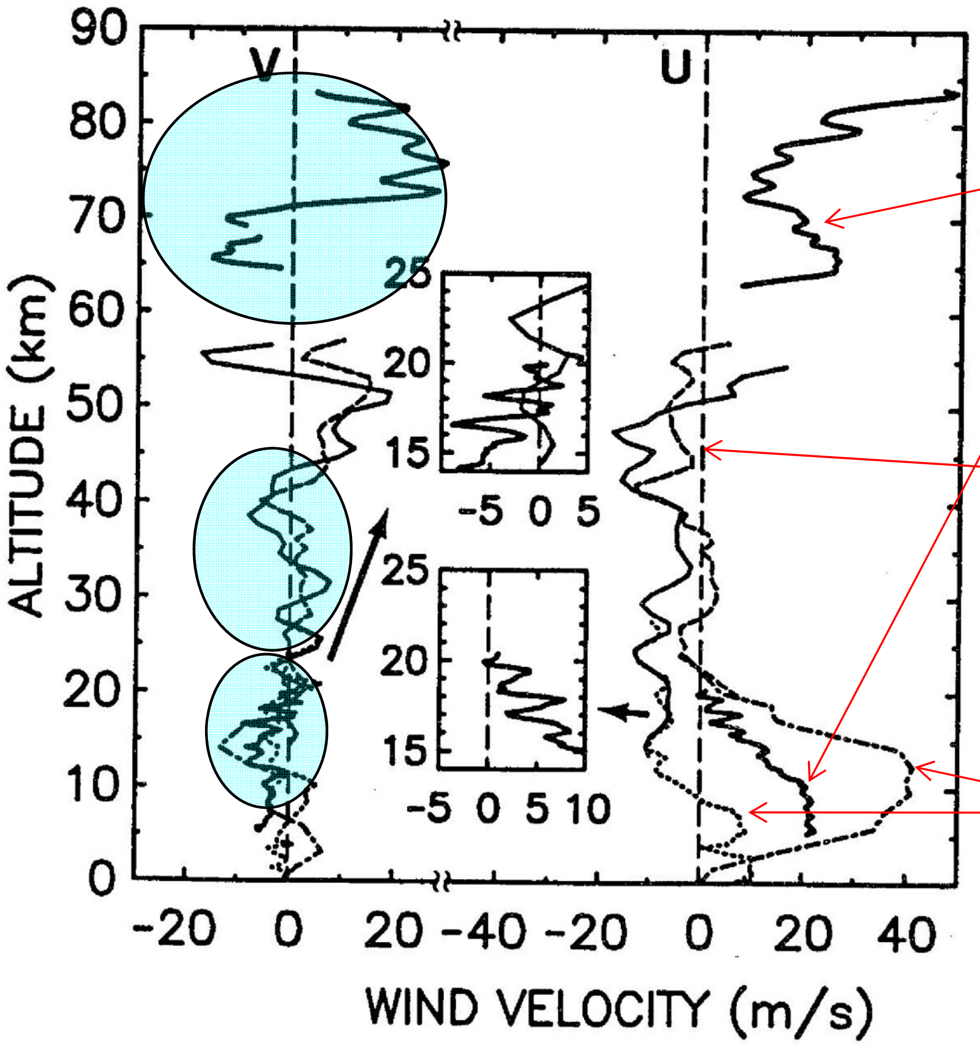

Both wave amplitudes and wave lengths (λ_z) increase along height.
λ_z =2 – 3 km in the lower stratosphere; λ_z =5km in the middle stratosphere;
λ_z =10km in the mesosphere

Hourly northward wind velocity (solid line) and turbulence layer observed with the MU radar during 8-16 LT on 18 October 1986

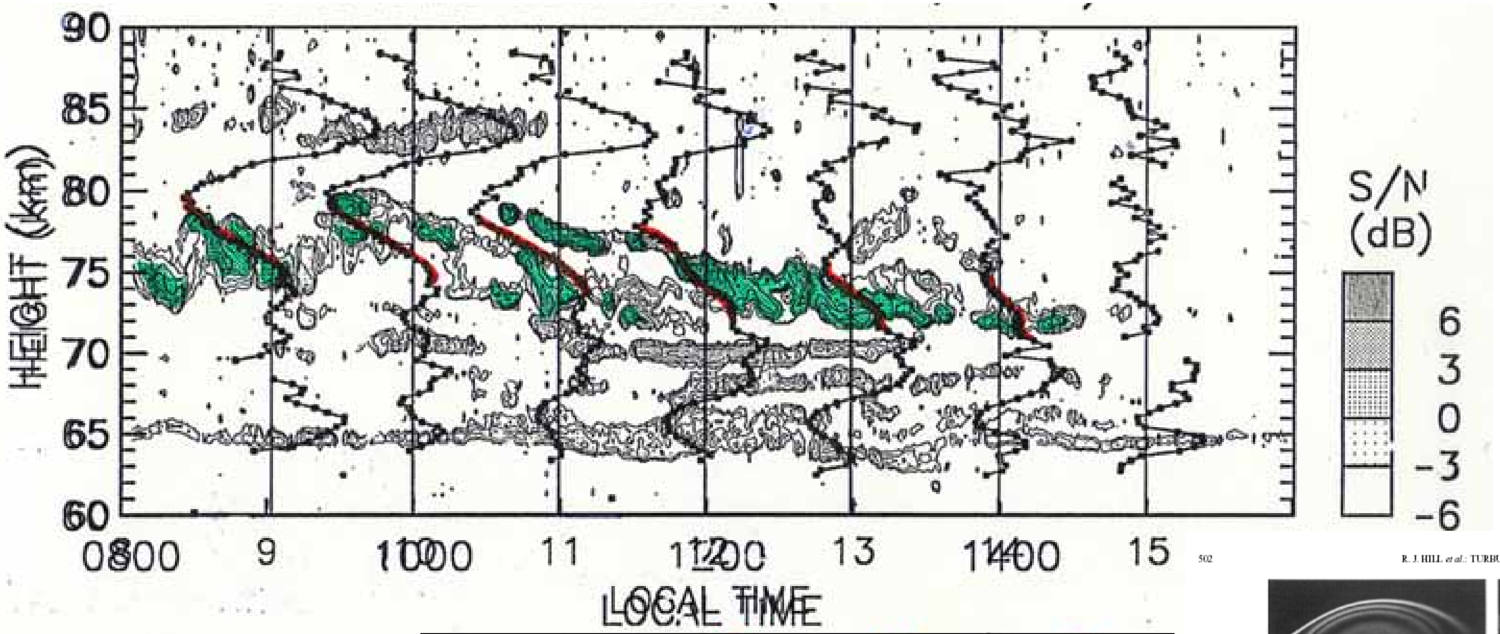

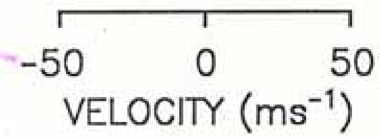

Generation of turbulence due to convective instability of gravity waves (breaking)

356 David C. Fritts PAGEOPH,

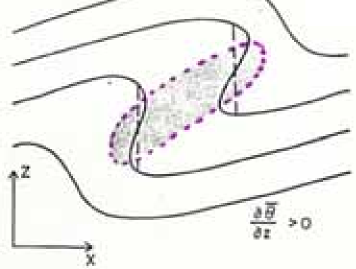

Figure 7
Schematic of the occurrence of turbulence due to an unstable gravity wave. The shaded region is convectively unstable and is a region in which strong turbulence will cause only a small diffusion.

502 R. J. HILL *et al.*: TURBULENCE AND PMSE

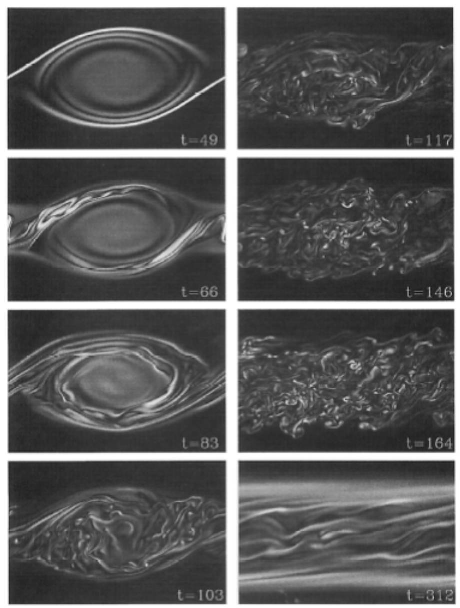

Fig. 1. Cross sections in a streamwise vertical plane displaying the 3D evolution of vorticity magnitude. The 8 nondimensional times span the dynamical evolution, including early quasi-2D billow roll-up ($t = 49$), transition to 3D structure consisting of streamwise-aligned convective rolls ($t = 66$ and 83), creation of a turbulent layer ($t \sim 83$ to 164), and eventual restratification and stabilization of the flow ($t > 200$).

Time-height variations of turbulence echo layers in the mesosphere

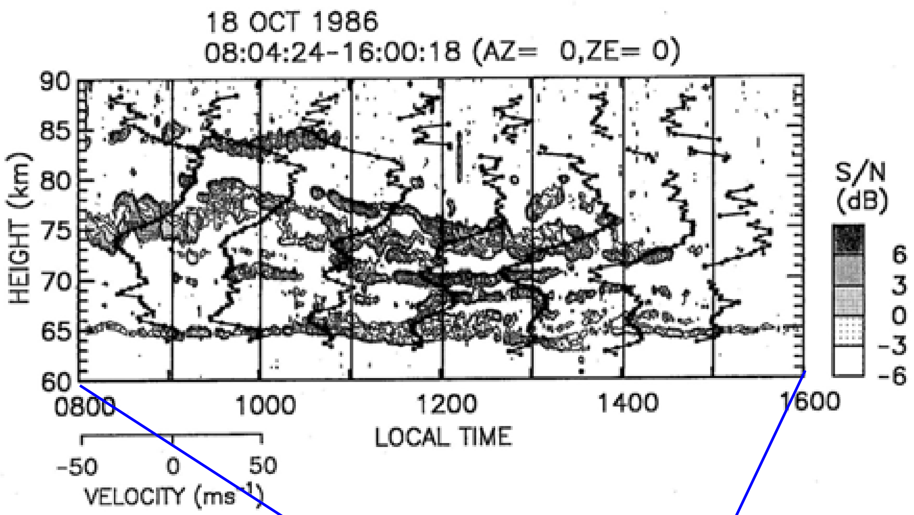

Turbulence layer in PBL (top) and mesopsphere (bottom)

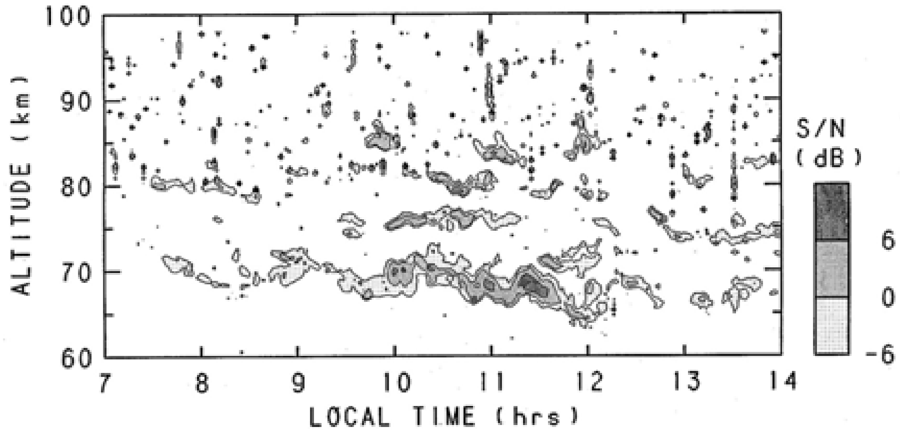

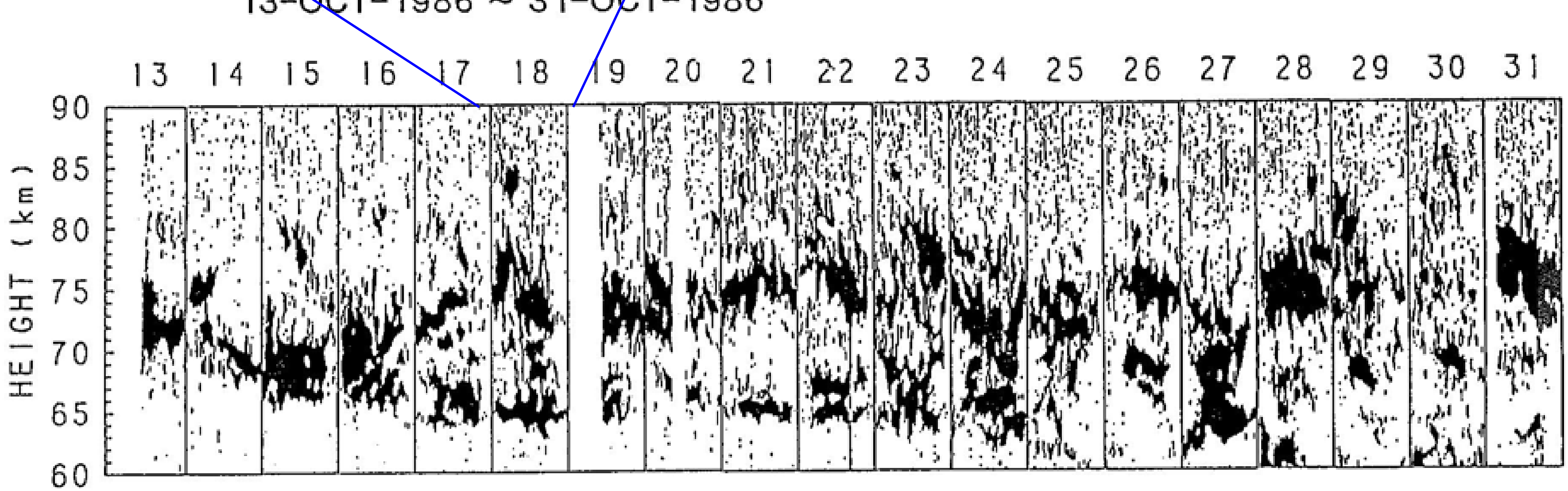

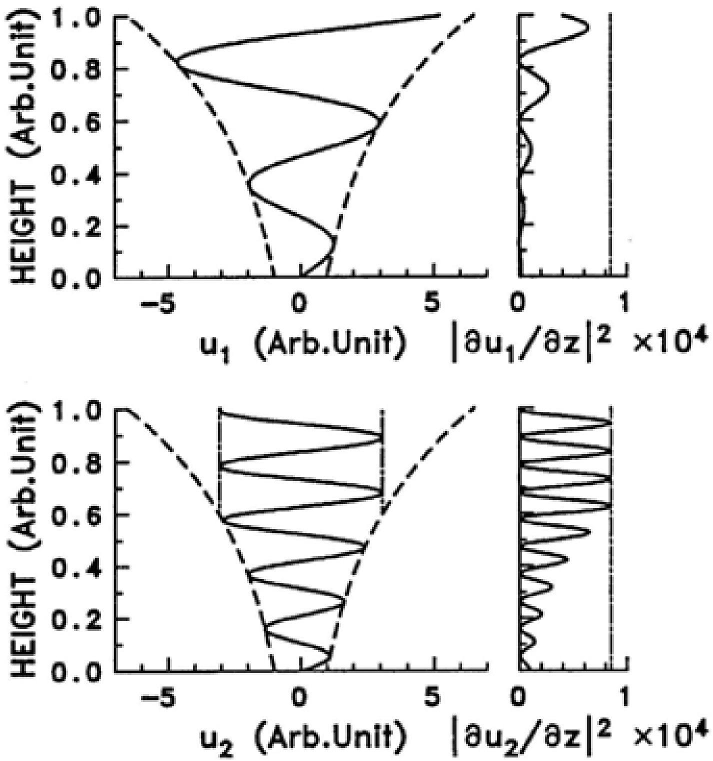

Atmospheric gravity waves grow amplitudes of temperature (T) and wind velocity (U) perturbations as they propagate upward. A wave with a short vertical wave length reaches unstable condition at lower altitude, because the vertical shear of T and U shear rapidly becomes larger.

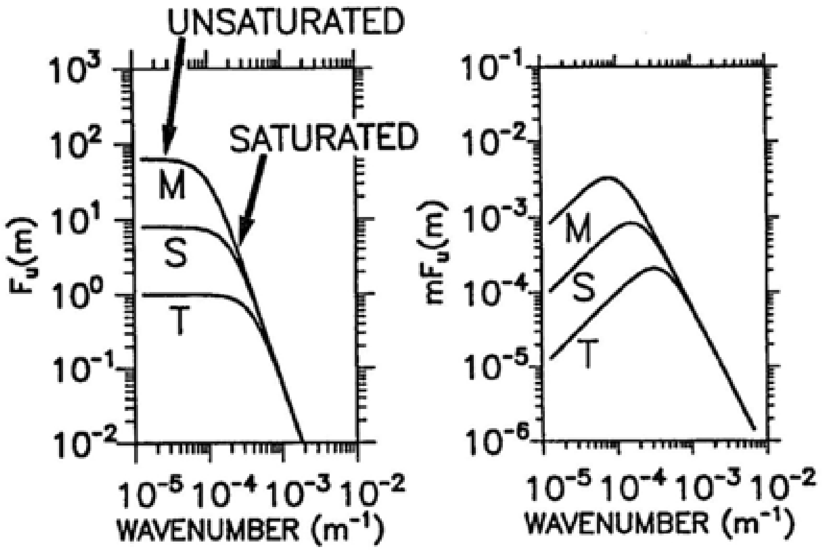

Considering a convectively unstable condition of gravity waves and their dispersion relations, a vertical wave number spectrum (m) of T and U becomes saturated at large m, being proportional to m^{-3}. At small m, the spectral density increases along altitude.

Momentum flux measurements with a beam pair method

Radial wind velocity is measured with a pair of antenna at the same zenith angle

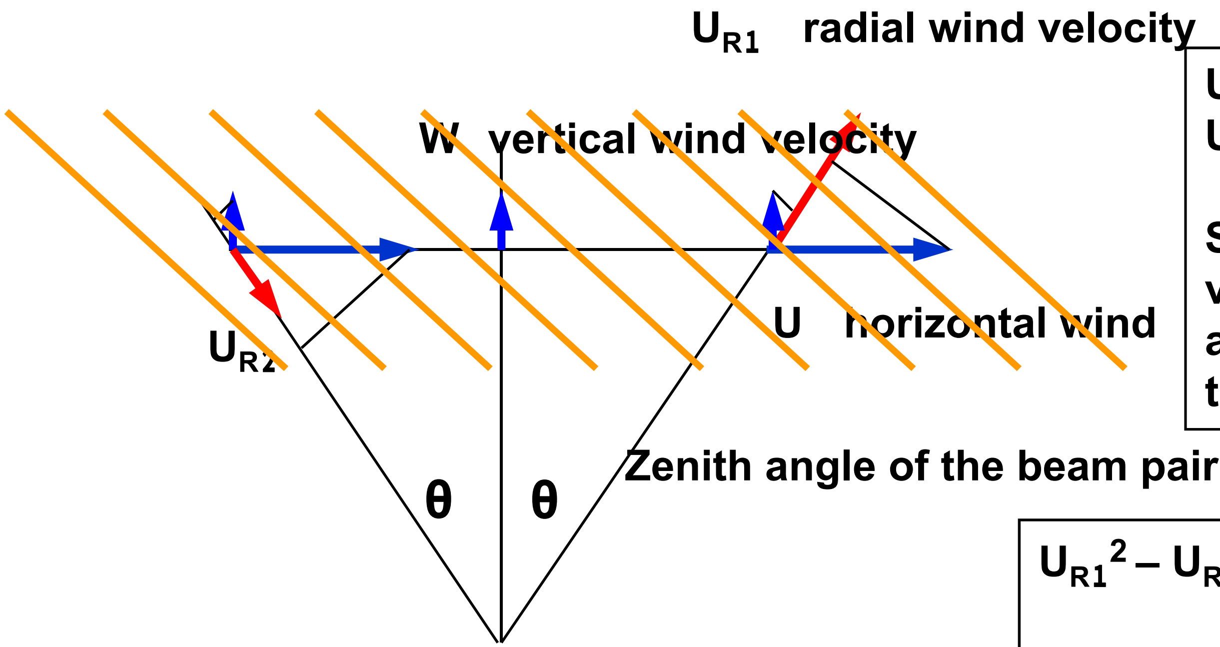

$U_{R1} = U \sin\theta + W \cos\theta$
$U_{R2} = - U \sin\theta + W \cos\theta$

Statistical behavior of the wind velocity fluctuations is assumed to be the same within the beam steering region.

$U_{R1}^2 - U_{R2}^2 = 4\,UW \sin\theta \cos\theta$

By subtracting the two radial wind velocity variance, we can calculate momentum flux (U'W').
By multiplying air density, and take a height derivative, acceleration (friction) can be estimated.

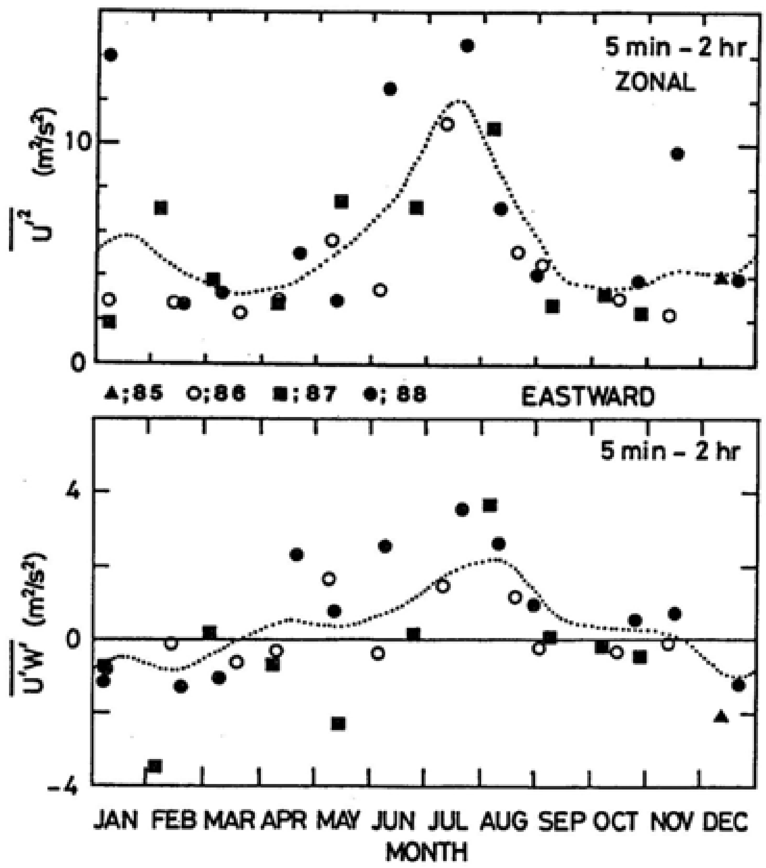

図 6-6. 1985–88 年の MU レーダー定常観測から求めた、周期 5 分から 2 時間の東西視線風速変動についての分散値 (上) と、東向きの単位体積あたりの運動量フラックス (下)。

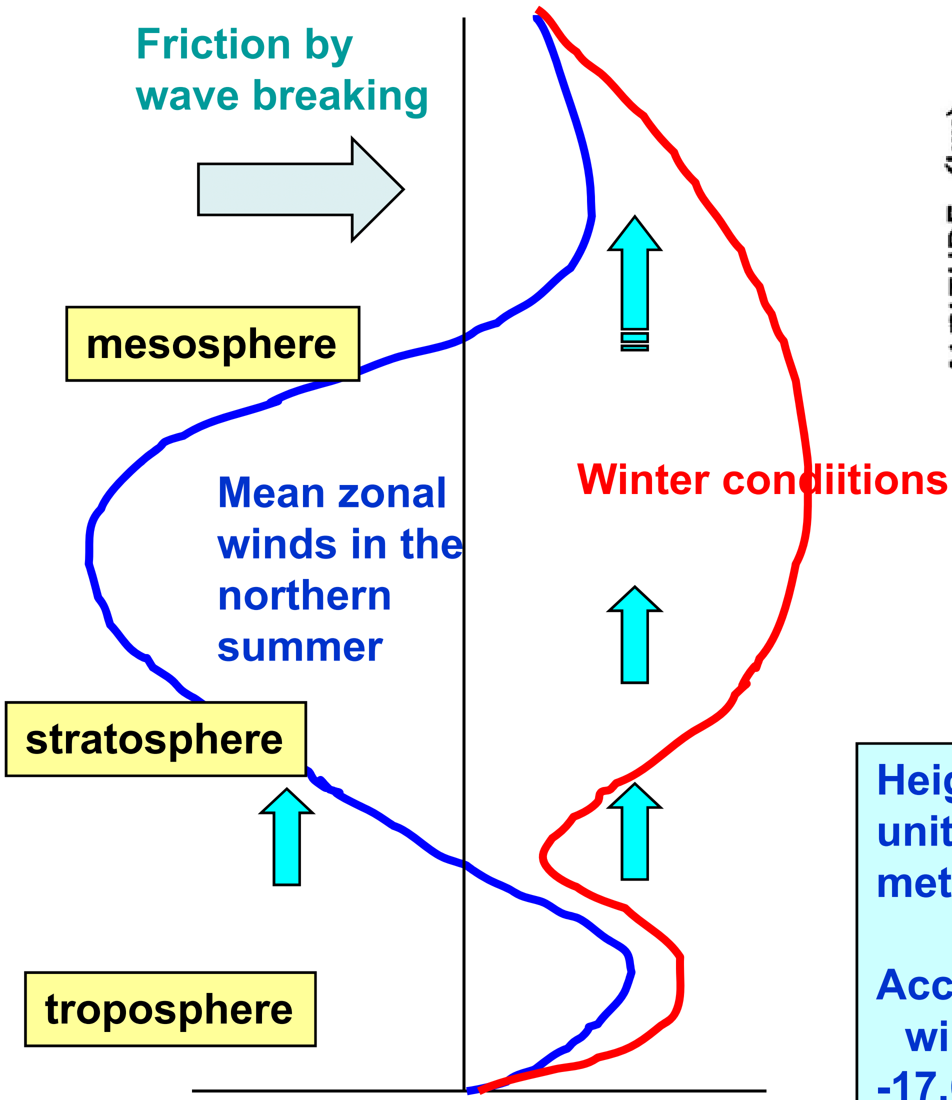

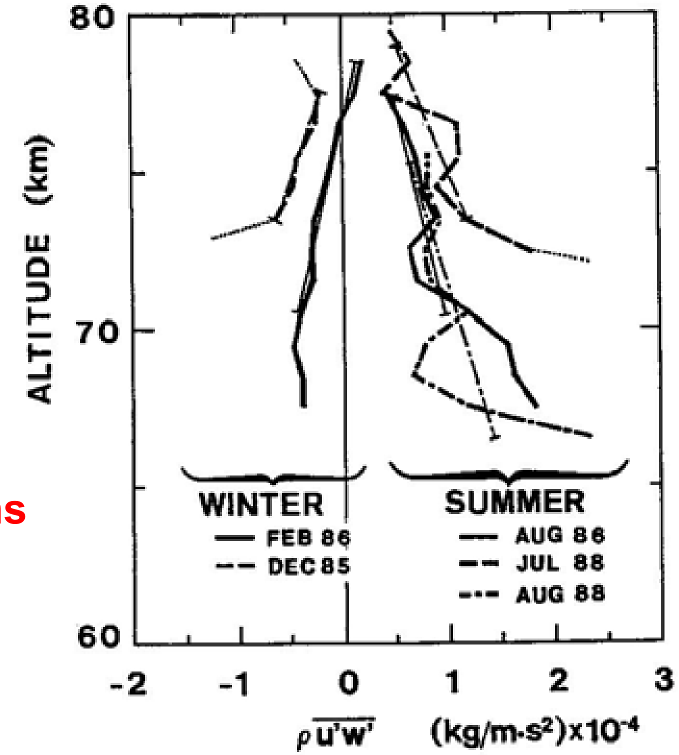

Height variation of momentum flux (per unit mass) observed by the beam pair method with the MU radar.

Acceleration: $-1/\rho \; d(\rho u'w')/dz$

winter	summer
-17.6 m/s/day	7.2 m/s/day
-11.0 m/s/day	12.8 m/s/day
	9.4 m/s/day

Model prediction

-13 m/s/day 26 m/s/day

Outline of this lecture: Atmospheric Coupling Processes

- ✓ A linear theory of atmospheric gravity wave
  - Dispersion relation of atmospheric gravity waves
  - Convective instability and wave breaking/saturation
  - Critical level interaction between a gravity wave and wind shear
  - Importance of wave drag force (wave breaking) to maintain the general circulation of the middle atmosphere
- ✓ Radar observations of wave breaking process:
  - gravity wave saturation and turbulence generation (the MU radar).
- ✓ Global distribution of gravity wave activity with GPS radio occultation (RO) measurements:
  - Generation mechanisms; tropical convection, topography (mountain waves), Jet stream & polar night-jet, etc.
- ✓ Correlation between sporadic E and stratospheric gravity waves
  - Generation of orographic waves over Andes and Antarctica
  - A global distribution of sporadic E revealed with GPS-RO
- ✓ Coupling between the lower atmosphere and the MLT (mesosphere lower thermosphere) winds in the tropics
  - Tropical convection and gravity waves in the stratosphere
  - Correlation between short-period GW and Mesospheric SAO
  - Relation between S-QBO and M-QBO (M-QB Enhancement)

GPS: precise satellite positioning

*** Accuracy of GPS**

code: a few m

carrier phase: 1 mm

⇒ prediction of volcano eruption and/or earthquake

Ultimate accuracy of GPS is determined by the propagation delay and bending in the atmosphere.

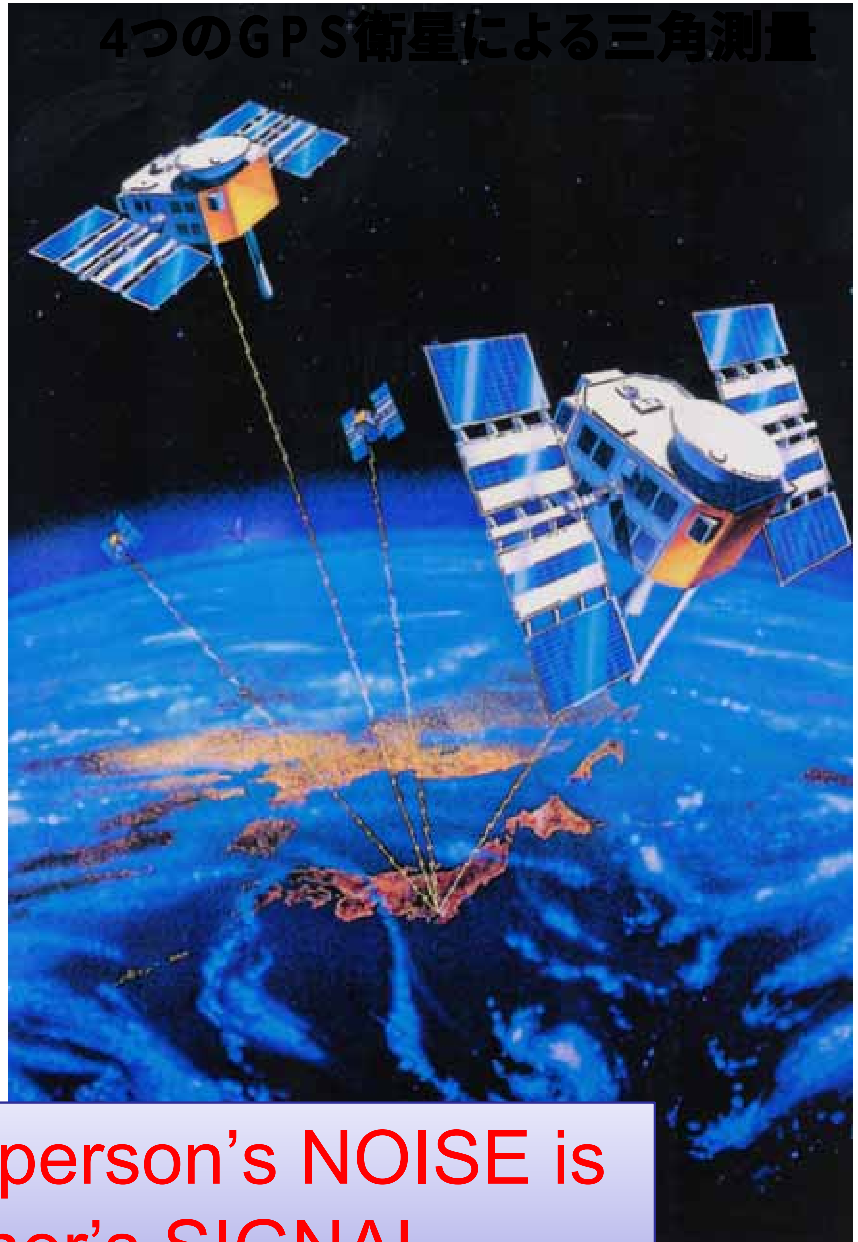

These noise/error (delay and bending) are, however, useful to measure water vapor content, temperature and electron density perturbations. (GPS Meteorology)

One person’s NOISE is another’s SIGNAL

Occultation (solar eclipse, lunar eclipse)

Radio occultation technique

Exploration of planetary atmosphere and ionosphere by analyzing radio signals emitted from an interplanetary spacecraft.

- Mariner IV: Mars, 1965
- Mariner V: Venus, 1967
- Voyager: Saturn, Jupiter

Application of the radio occultation to the Earth's atmosphere was studied in 1980's in US and Russia. It was realized by the GPS/MET project in 1995-7 by using a stable GPS radio signal and accurate orbital elements of a satellite (position: 10cm, speed: 0.1mm/s)

Radio and optical ray path bends at an interface of two layers with different refractive index values.

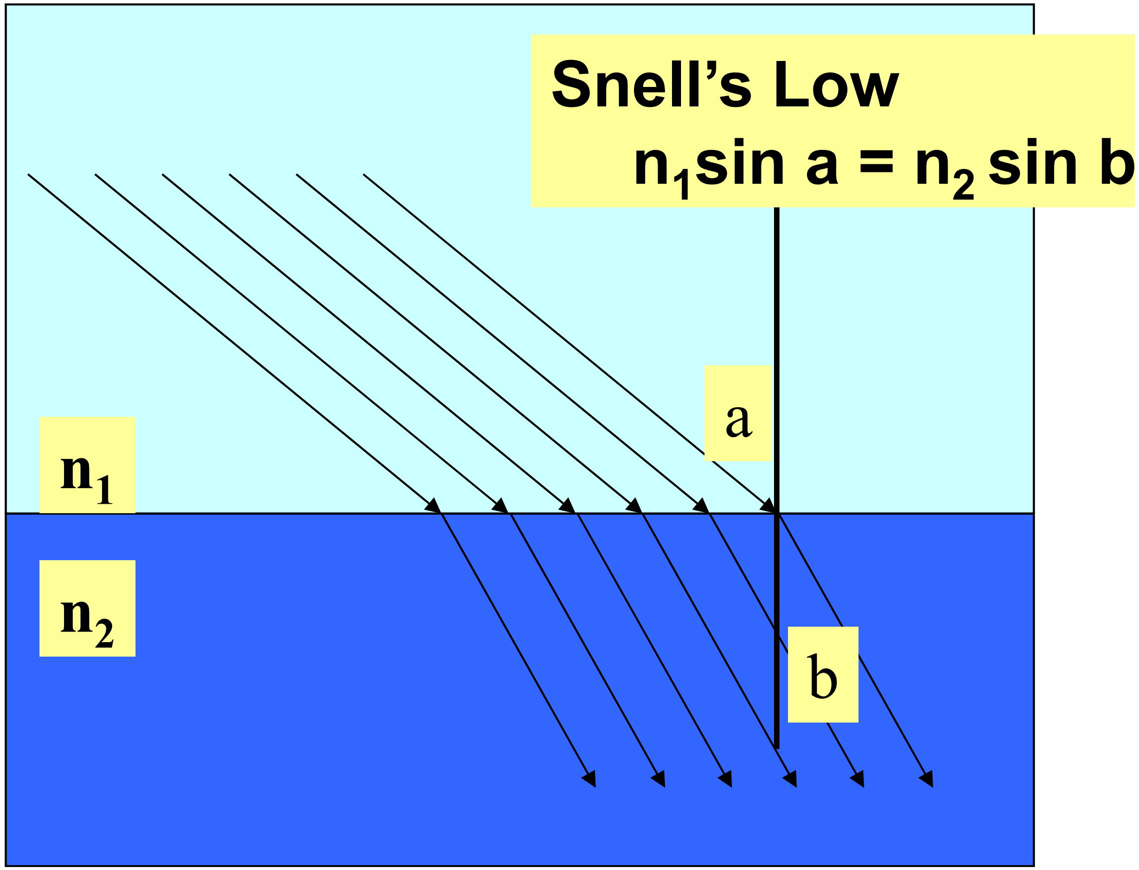

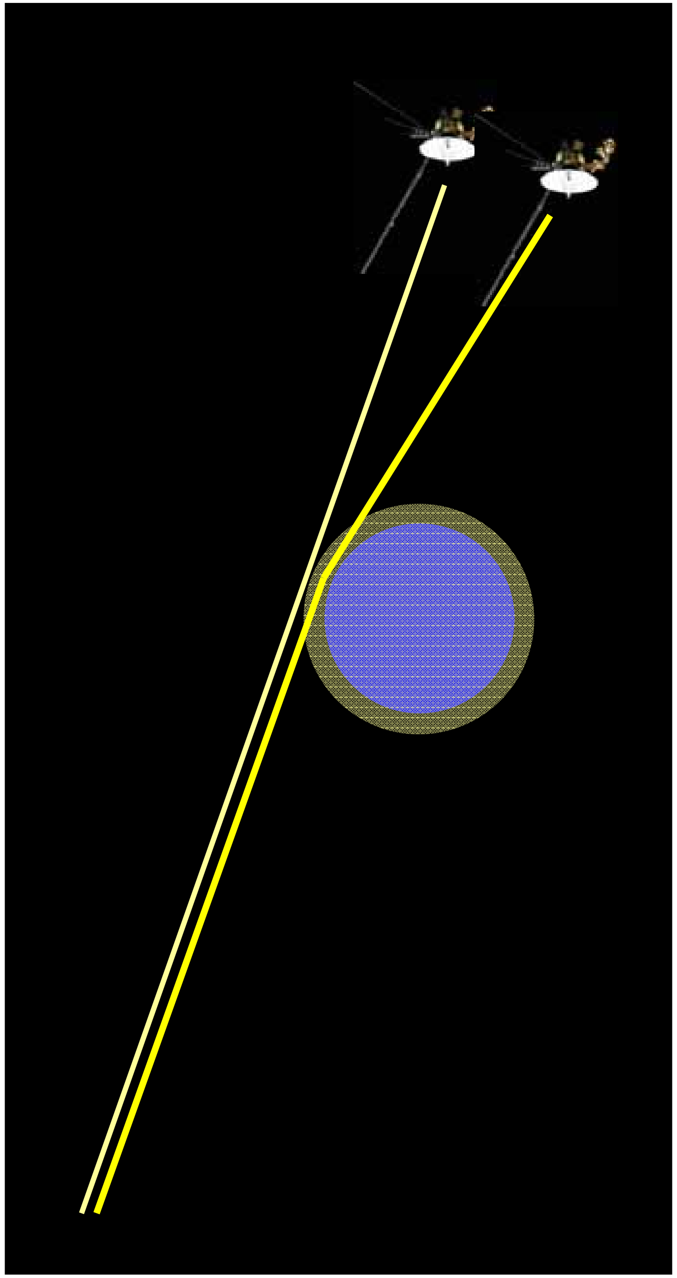

Refractive Index (N) and Atmospheric Parameters

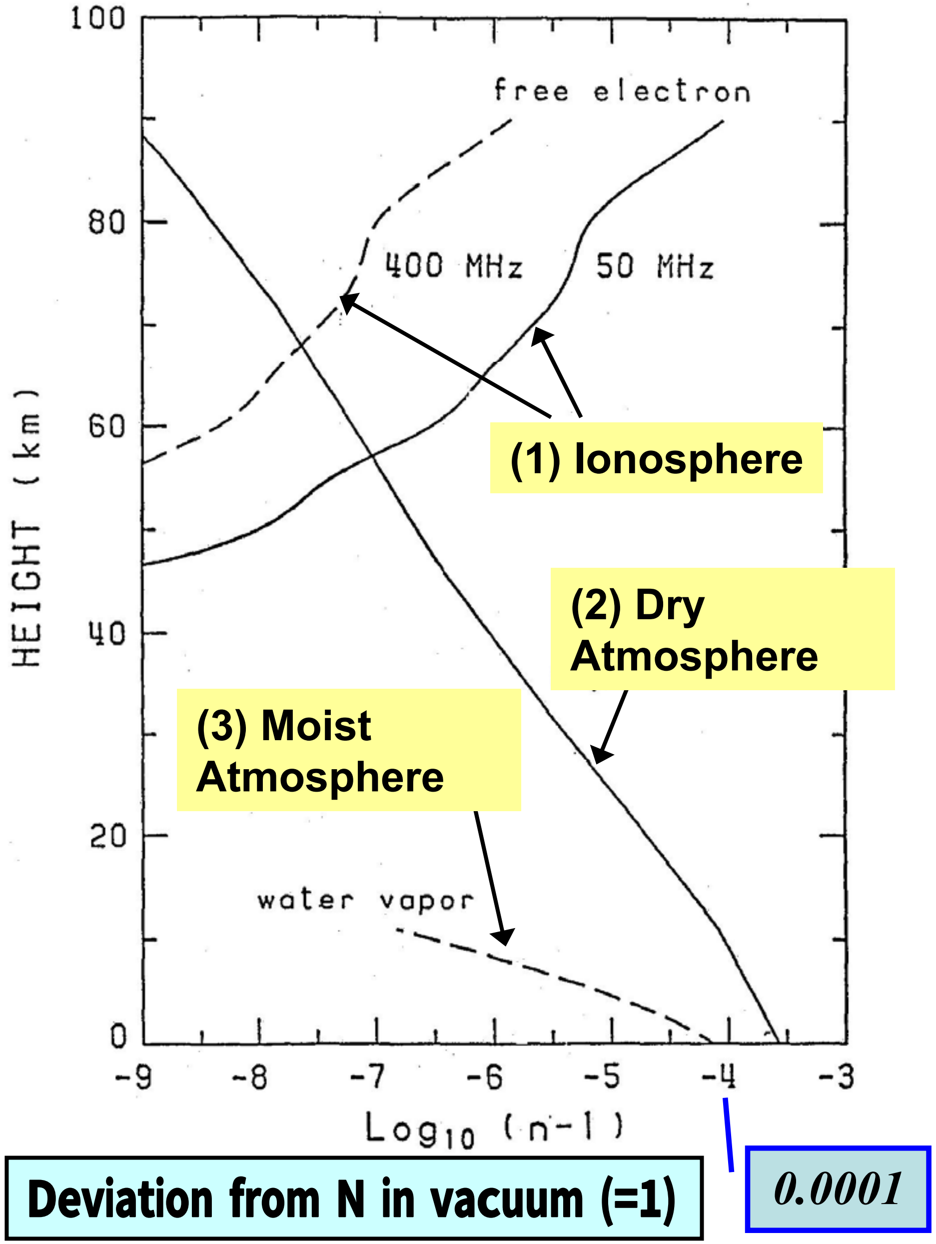

$N = 1 + C_1 \times Ne / f^2$ (1) Ionosphere

$+ C_2 \times p / T$ (2) Dry atmosphere

$+ C_3 \times e / T^2$ (3) Moist Atmosphere

$C_{1,2,3}$: Constants

p: Pressure T: Temperature

e: Partial pressure of water vapor

f: Radio frequency,

Ne: Electron density

Fermat ｓ’s theorem: For propagation of light, the path length becomes minimum.

Ray Tracing: When a plane wave propagates in inhomogeneous medium at the velocity **v**, propagation direction (normal to the plane wave) changes in an infinitesimal time ⊿ t by $\Delta\alpha = -\partial v / \partial l \Delta t$ (derivative is taken parallel to the wave front.)

Considering group velocity $v=c/n$ (c: speed of light), **v** varies depending on the gradient of *n*, along the wave front.

$$\Delta\alpha = c/n^2 (\partial n/\partial l)\Delta t$$

Using a small distance along the propagation path

$\Delta s = v\Delta t$, $\Delta\alpha = 1/n (\partial n/\partial l)\Delta s$

Using a unit vector in the propagation direction **T**

$$d\alpha = 1/n (T \times \nabla n)\, ds$$

The resulting bending angle can be obtained by the following integration.

$$\alpha = \int 1/n (T \times \nabla n) ds$$

When **n** is discontinuous, we apply Snell’s law.

Using a unit vector **N** normal to the discontinuity, **n(TxN)** must be continuous across the boundary.

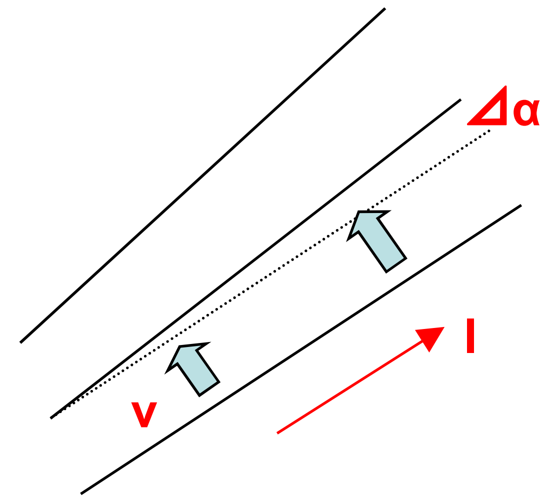

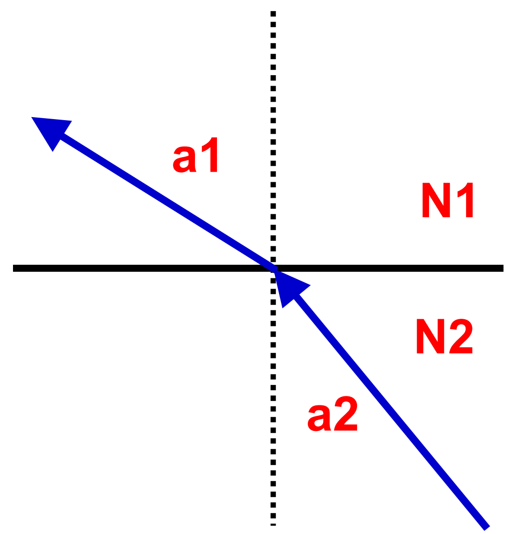

N1 sin a1 = N2 sin a2

GPS Radio Occultation

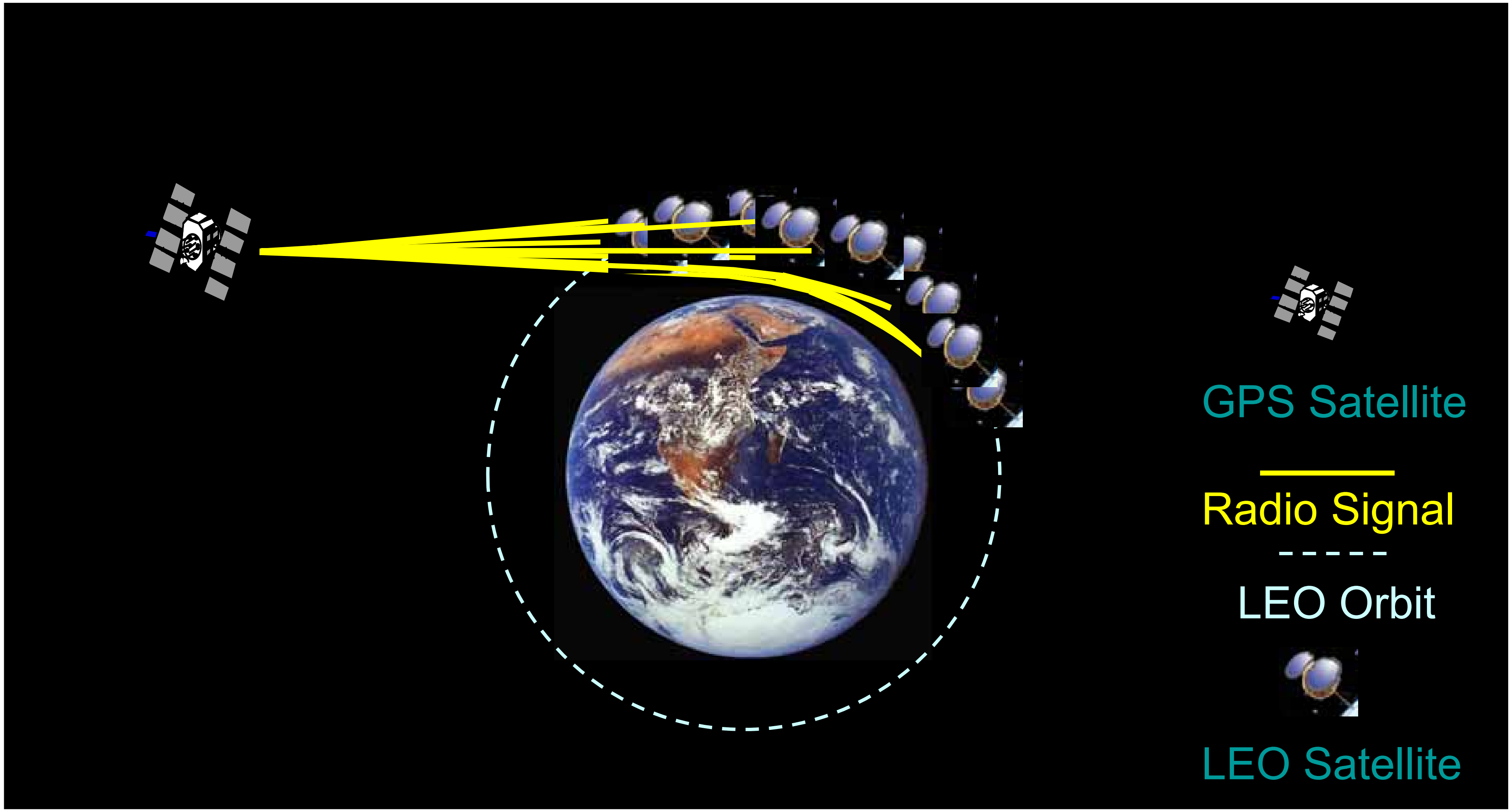

Courtesy by NSPO, Taiwan

Geometry of GPS Occultation Measurement

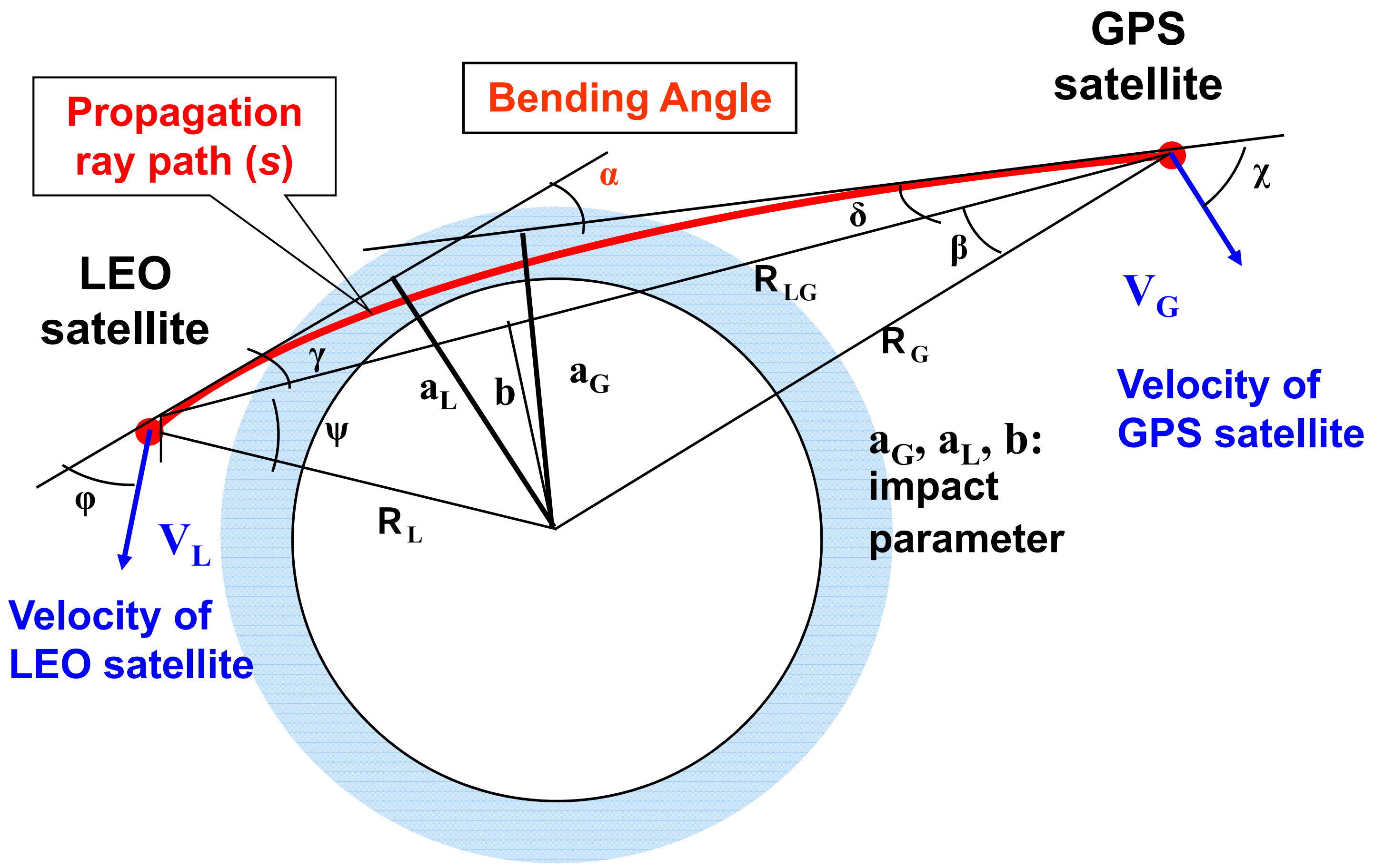

Melbourne, W. G., E. S. Davis, C. B. Duncan, G. A. Haji, K. R. Hardy, E. R. Kursinski, T. K. Meehan, L. E. Young, and T. P. Yunck, April 1994, "The application of spaceborne GPS to atmospheric limb sounding and global change monitoring", JPL Publ., 94-18, NASA.

Propagation delay of GPS waves with the tangent height at 35 km: 1m

Bending angle of GPS ray path (α) = 4×10^{-6} deg (4 ppm)

Difference in the relative satellite velocity ($V_1 - V_2$) = 0.4 mm/s

Requirement for satellite POD (position and velocity) = 10 cm, 0.1 mm/s

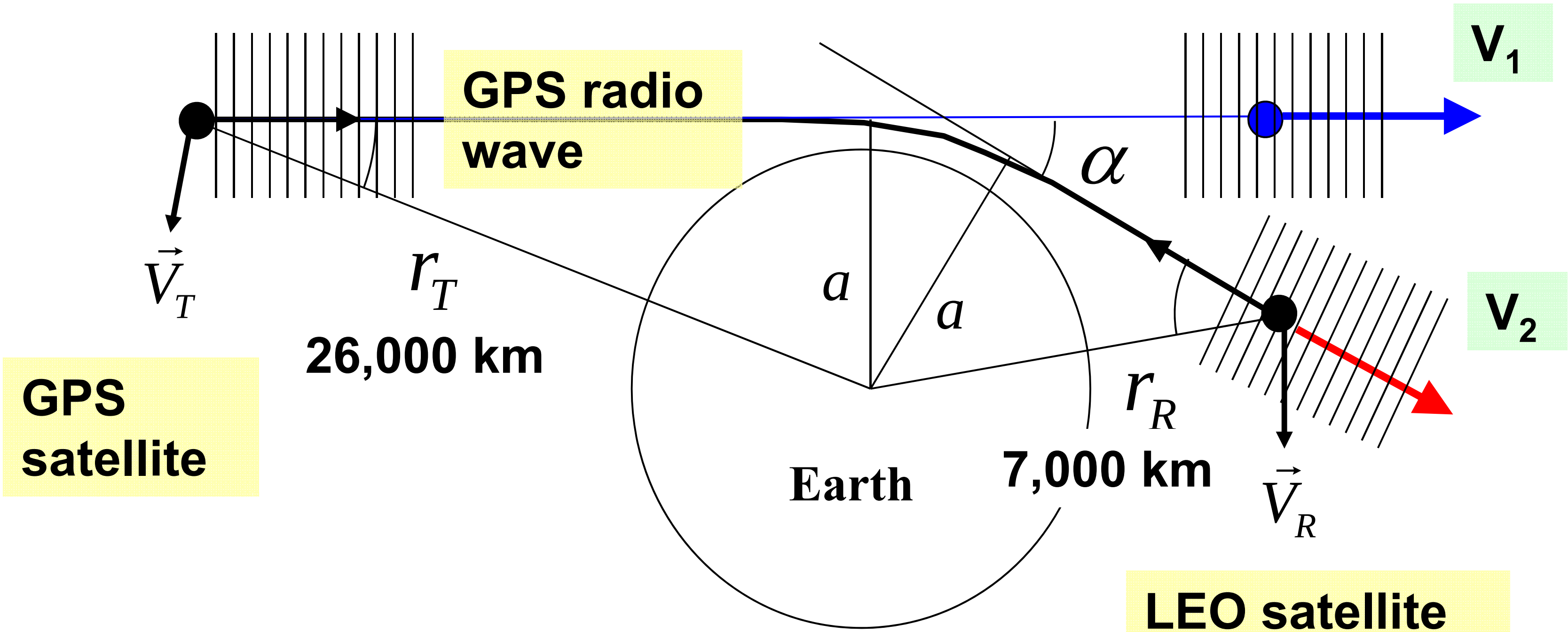

LEO satellite with a GPS receiver

Note: Delay becomes about 1 km near the surface; α=5/1000 deg

Basic Concept of GPS Occultation Measurement

GPS Signals received on a low earth orbiting (LEO) satellite are used for an active limb sounding of the atmosphere and ionosphere.

During a rising or setting of a GPS satellite (occultation), the radio rays between the GPS and LEO satellites successively scan the atmosphere (and the ionosphere) from the receiver height down to the surface. A refractive index profile can be retrieved from the time variations of the ray bending angles.

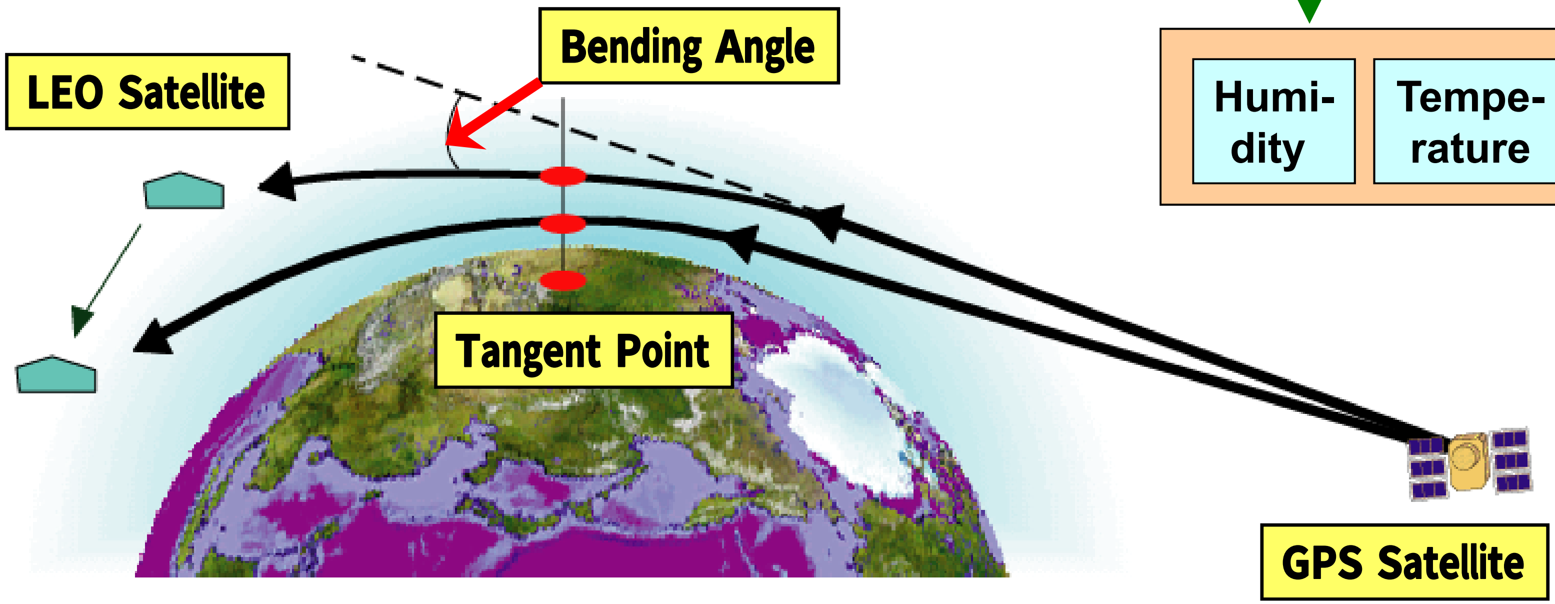

Propagation Delay of GPS Signals

Determination of LEO Orbit

↓

Bending of Radio Ray Path

↓

Refractive Index Profile near the Tangent Point

↓

Humi-dity	Tempe-rature	Electron Density

Comparison of temperature profiles between the two COSMIC GPS RO results (#49 and #50) and radiosonde at Kuching, Malaysia.
Profiles are shifted by 5K each.

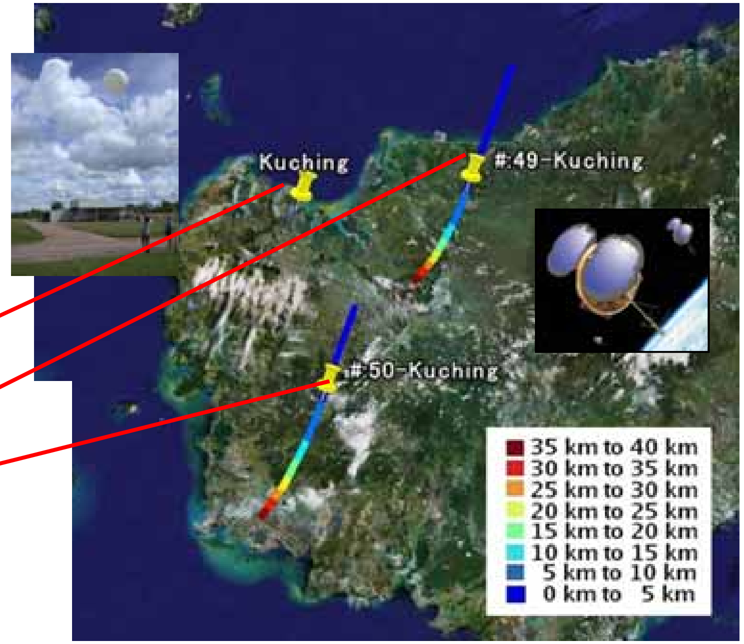

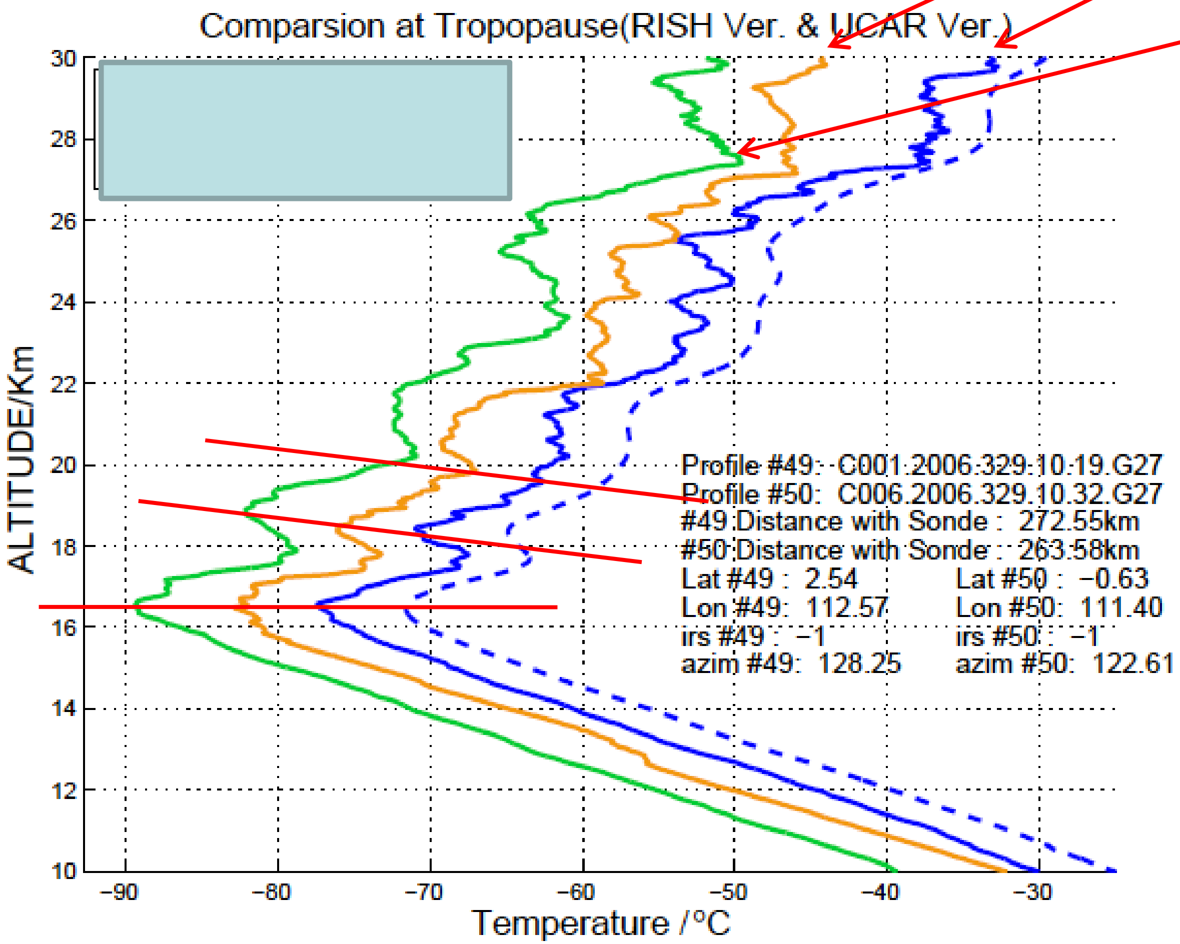

Temperature profiles with GPS RO have a height resolution comparable to a radiosonde.

- detailed structure of the tropopause
- perturbations due to atmospheric waves

Tropical convection and gravity waves in the stratosphere

Generation, Propagation and Dissipation of Atmospheric Waves in the Equatorial Region

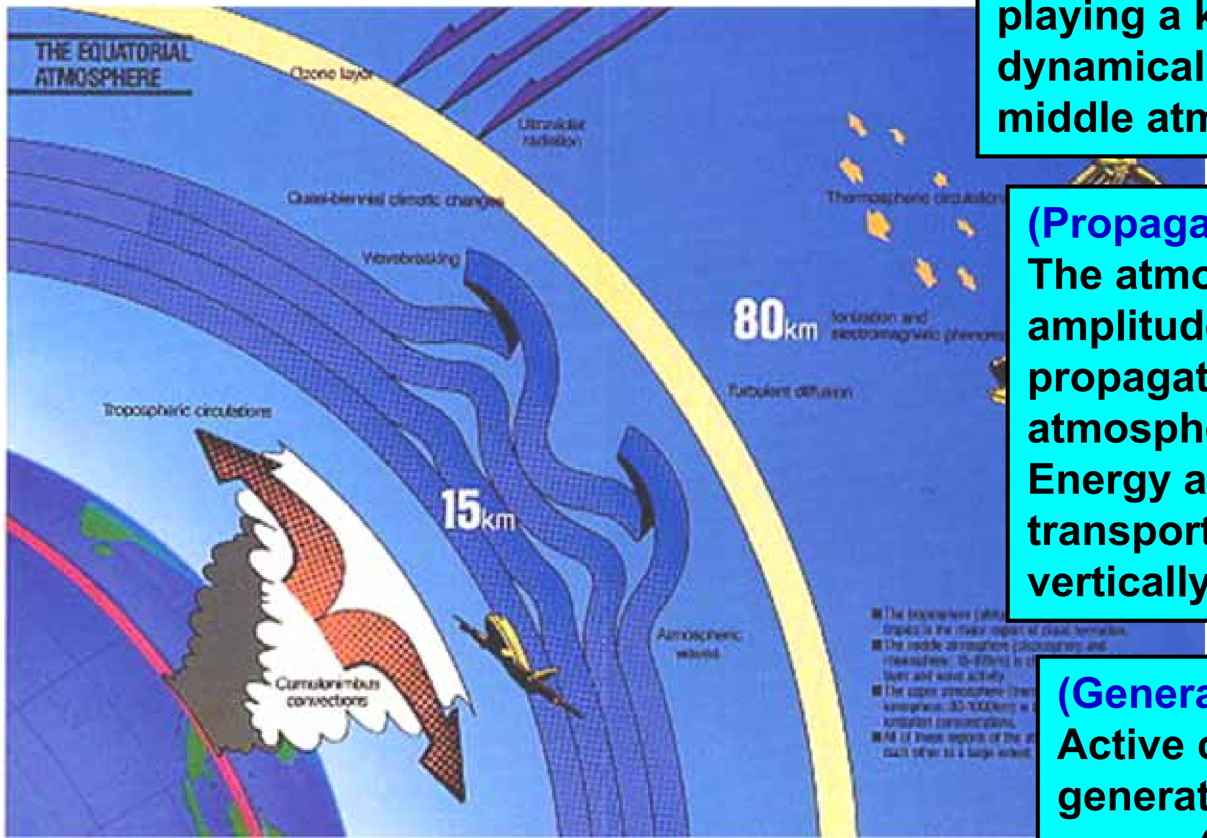

(Dissipation)
The waves dissipate through various instability processes, and deposit the momentum to the background winds, playing a key role to maintain the dynamical structure of the equatorial middle atmosphere.

(Propagation)
The atmospheric waves grow the amplitudes during upward propagation in the middle atmosphere (15-100 km).
Energy and momentum are transported both horizontally and vertically by these waves.

(Generation)
Active convection in the tropics generates various atmospheric waves (equatorial Kelvin wave, atmospheric tide, gravity waves, etc).

Correlation between Gravity Wave Energy (PE) and Tropical Clouds

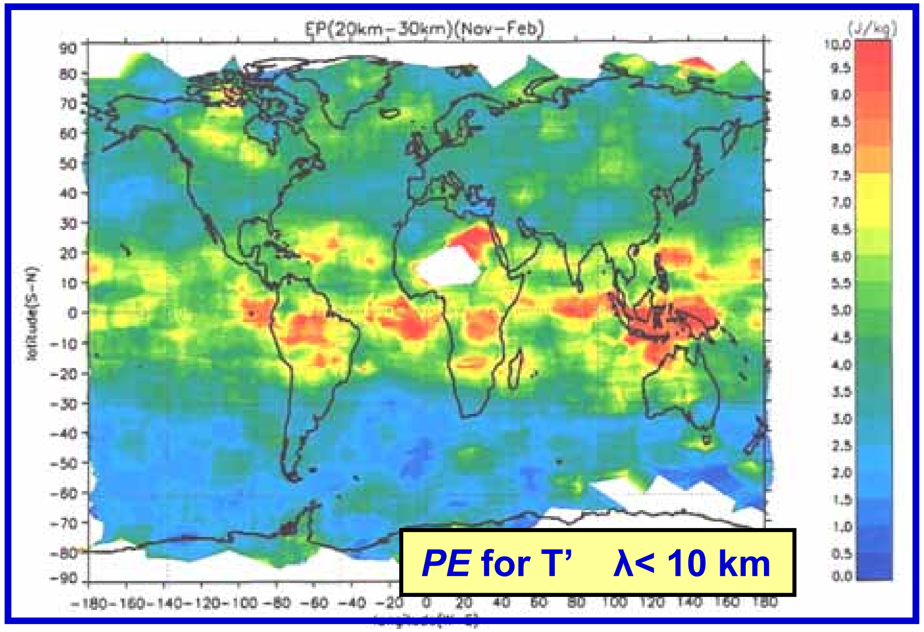

(Left) Latitude-longitude distribution of the wave potential energy $PE=1/2(g/N)^2(T'/T)^2$ at 20-30 km in Nov-Feb from GPS/MET in 1995-1997

(Bottom) Black body temperature (OLR) in Feb, 1997

Large PE values are detected at low latitudes (25°N - 25°S), and they are particularly enhanced over the regions of active convection , i.e, Indonesia to Indian ocean, Africa and South America.

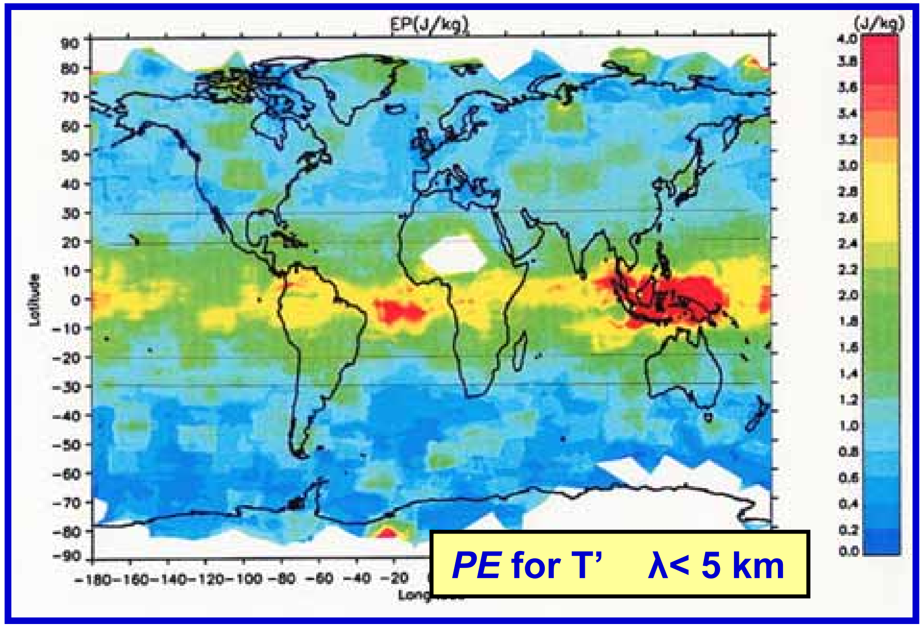

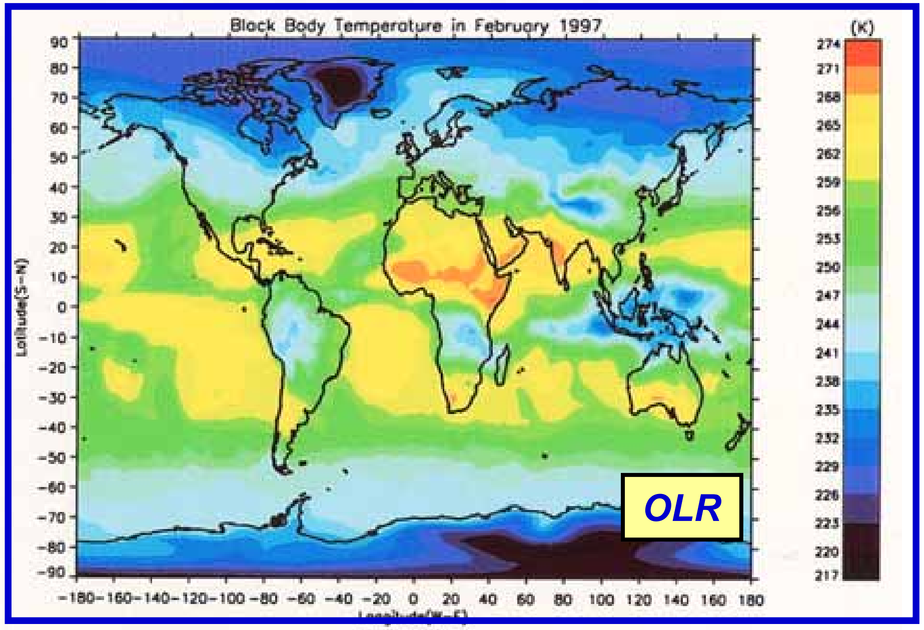

Dec 2003 / Jan-Feb 2004

Cloud top height /OLR(K)

Atmospheric wave energy Ep (J/kg) at 19-26 km

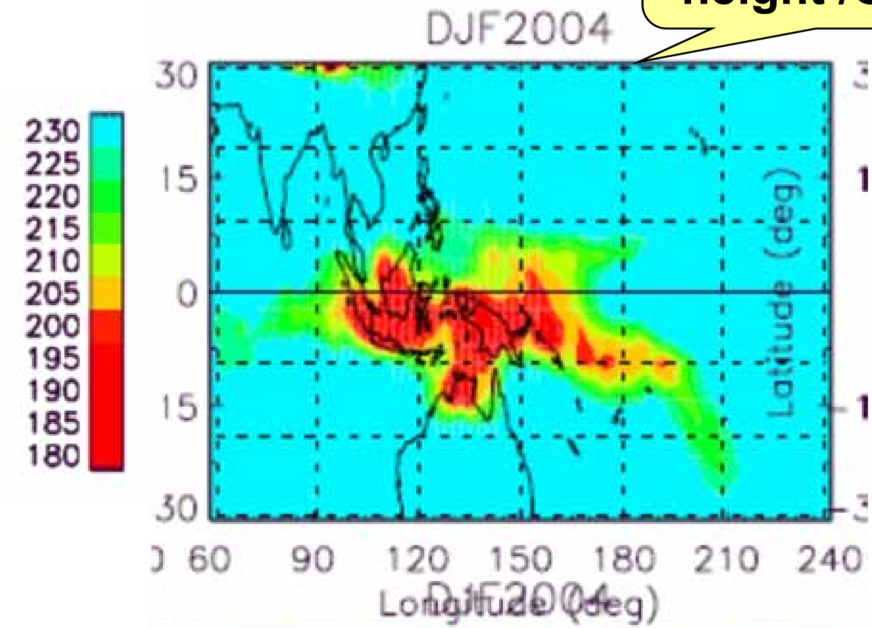

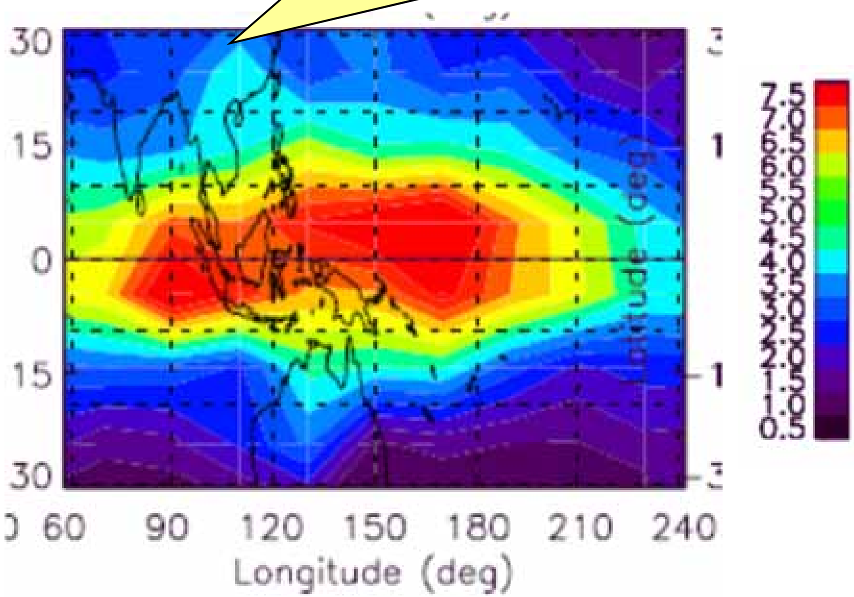

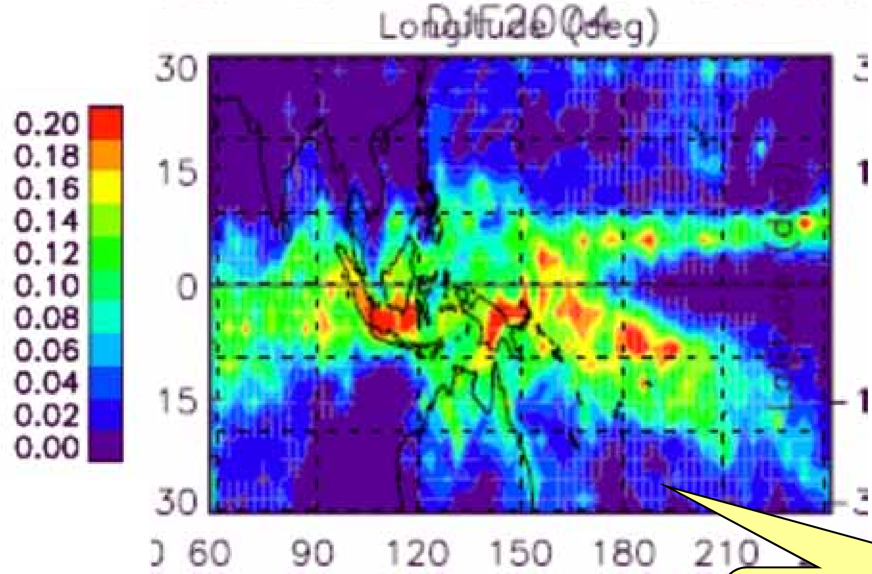

Convective rain rate (mm) / TRMM-PR

In the northern winter months (Dec/Jan/Feb), intense cloud convections are located over Indonesia and western Pacific, which actively generates atmospheric gravity waves as well as Kelvin wave-like disturbances in the equatorial region.

CHAMP

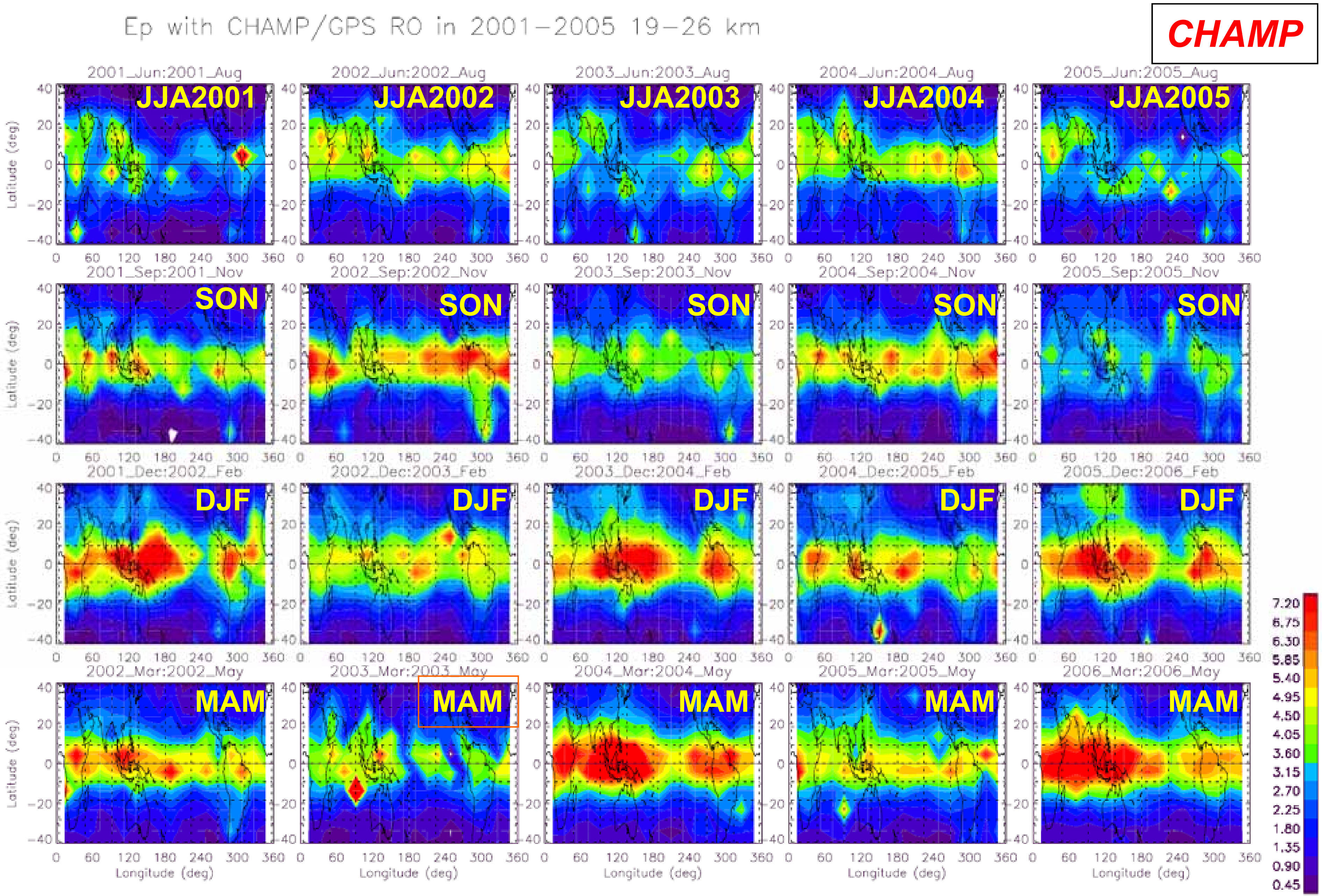

Ep with CHAMP/GPS RO in 2001–2005 19–26 km
CHAMP
2001_Jun:2001_Aug
JJA2001
2002_Jun:2002_Aug
JJA2002
2003_Jun:2003_Aug
JJA2003
2004_Jun:2004_Aug
JJA2004
2005_Jun:2005_Aug
JJA2005
2001_Sep:2001_Nov
SON
2002_Sep:2002_Nov
SON
2003_Sep:2003_Nov
SON
2004_Sep:2004_Nov
SON
2005_Sep:2005_Nov
SON
2001_Dec:2002_Feb
DJF
2002_Dec:2003_Feb
DJF
2003_Dec:2004_Feb
DJF
2004_Dec:2005_Feb
DJF
2005_Dec:2006_Feb
DJF
2002_Mar:2002_May
MAM
2003_Mar:2003_May
MAM
2004_Mar:2004_May
MAM
2005_Mar:2005_May
MAM
2006_Mar:2006_May
MAM
Latitude (deg)
Longitude (deg)
7.20
6.75
6.30
5.85
5.40
4.95
4.50
4.05
3.60
3.15
2.70
2.25
1.80
1.35
0.90
0.45

Season-height section of zonal mean PE at 25.S-2.5N from Sep 2006 to Apr 2008

COSMIC

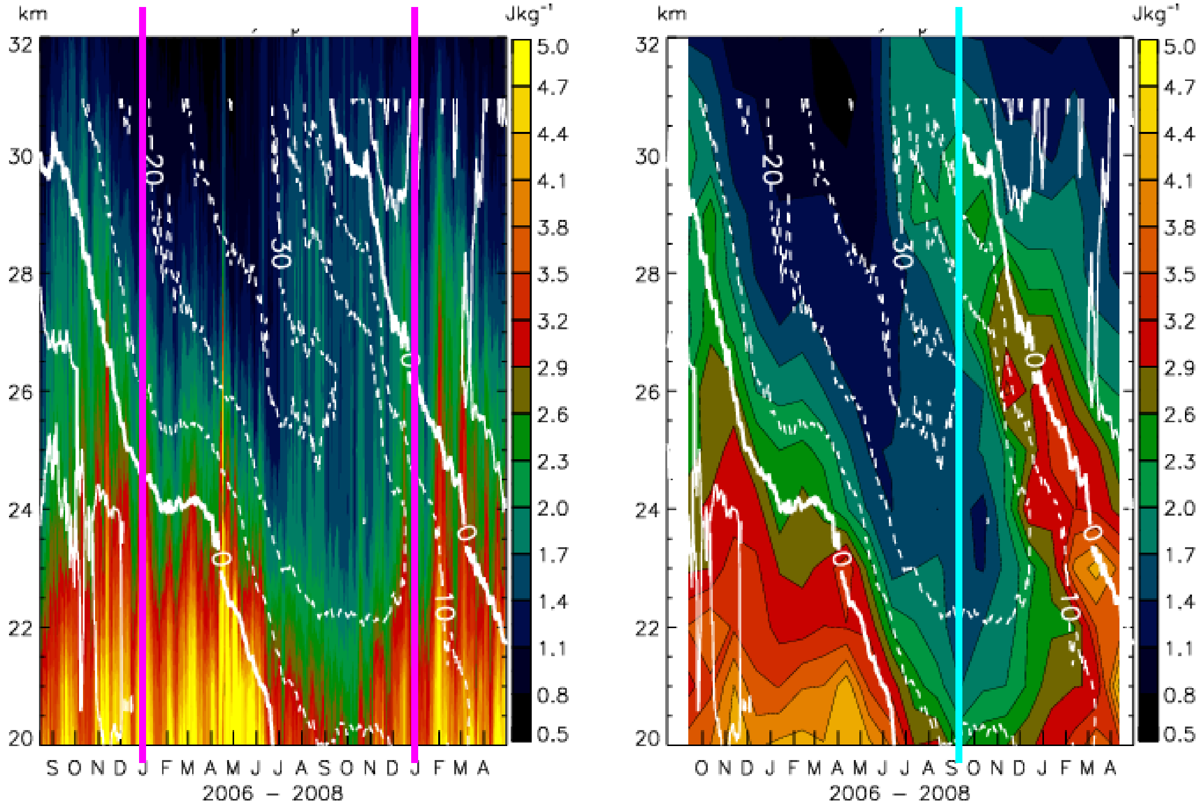

- QBO westward shear initially, then eastward shear after mid-2007.
- QBO removes gravity waves, especially close to the 0 m/s phase line.

LEFT:

- **Grid size: 20°x5°x7 days,**
- **7km high-passed perturbations from individual profiles, and get PE by integrating vertically over 7km, stepping up by 1km and forward by 1 day.**
- **Mainly meso-scale GWs with minor MRGW and higher speed KW contributions.**

RIGHT

- **Grid size: 20°x5°x one month**
- **Height independent (1km) data by assuming that all wave phases are represented at that particular height**
- **Slower speed KWs but still mainly consists of GWs**

White contours: NCEP zonal mean zonal wind, units m/s, east/westward; solid dashed

Year-to-year variations of wave energy (Ep), OLR and convective rain rate in Dec/Jan/Feb in 2001-2005

CHAMP

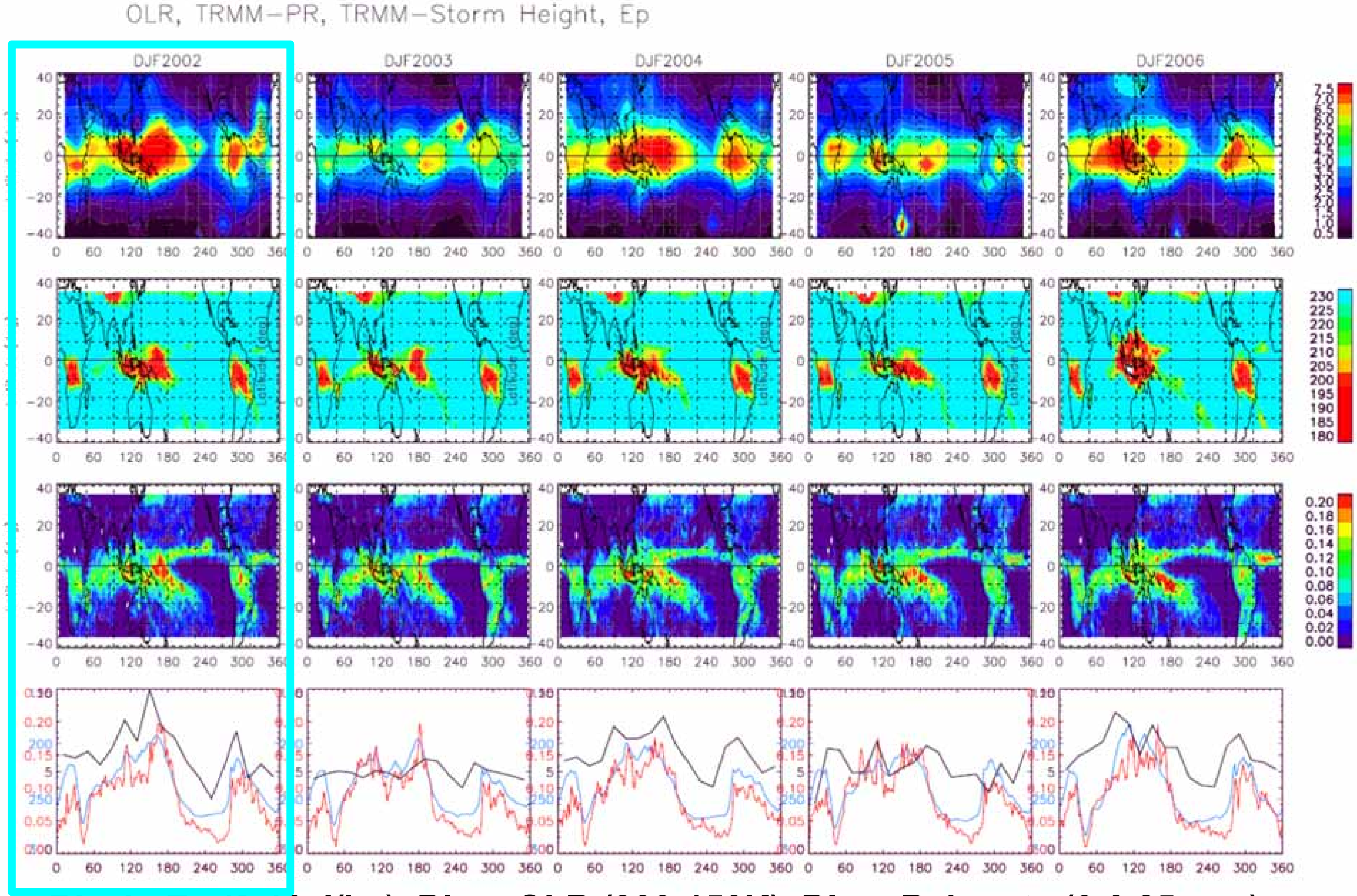

Black: Ep (0-10 J/kg), Blue: OLR (300-150K), Blue: Rain rate (0-0.25 mm)

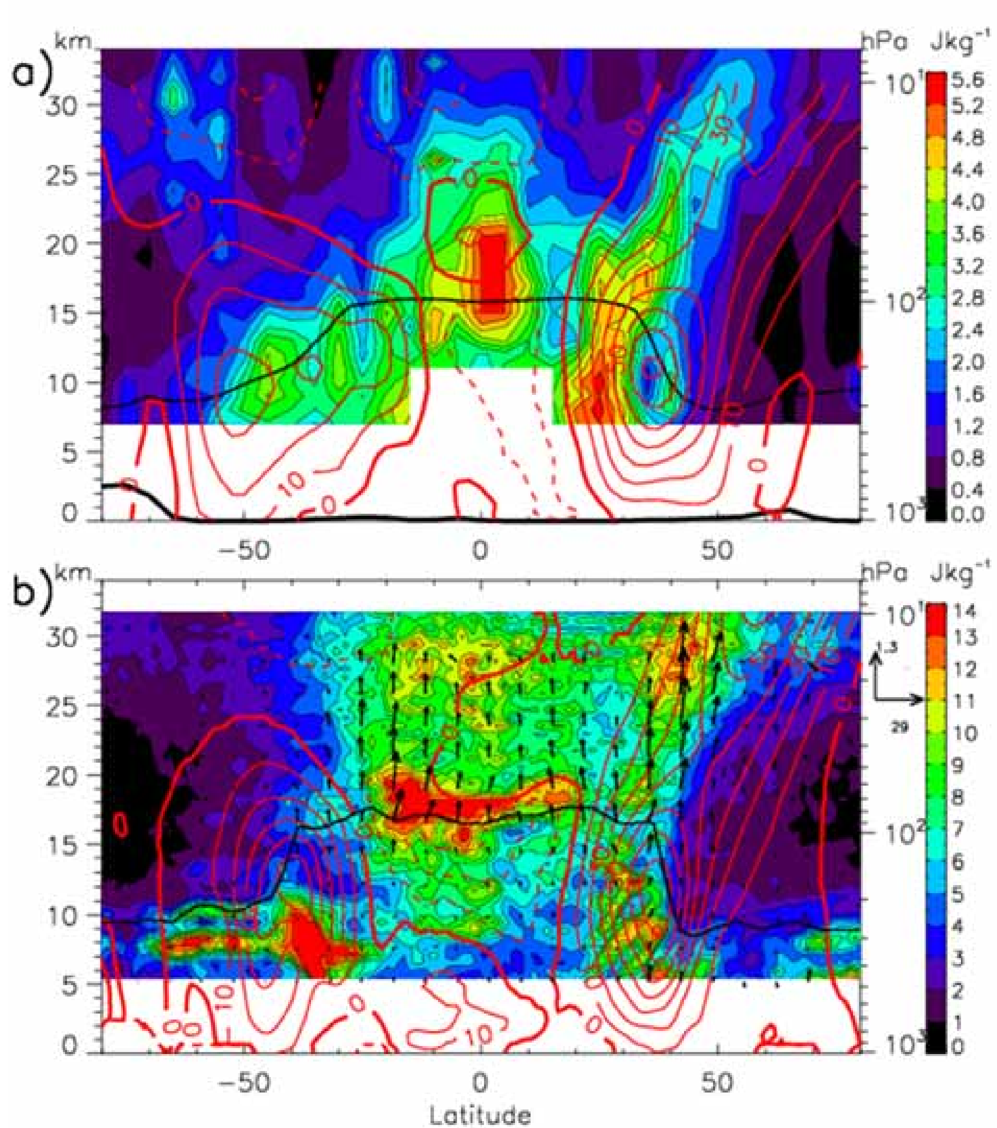

Latitude-height section of gravity wave energy (PE)

COSMIC

COSMIC PE at 140E during 12 – 18 Dec 2006

- Strong winter time sub-tropical jet
- Large PE from mid-troposphere up to polar night jet

AGCM PE 140E, 1 – 7 Jan (similar wind conditions to COSMIC)

- PE from waves with periods 6hr – 1 month, λ_z < 7km, 380 < λ_x < 40,000km
- Note different colour scale
- Vectors show meridional and vertical energy fluxes due to λ_z < 7km

- The polar night jet itself generates gravity waves which propagate upward and downward, as evident in (b) by the downward flux vectors on the polar side of the jet above 20 hPa.
- Another consistency between the COSMIC and AGCM data is relatively low values of UTLS potential energy at 20N, which is a region that also corresponds to weaker energy flux.

COSMIC

Latitude-height section of PE at 140E (130-150E) during 12-18 Dec 2006 from COSMIC GPS RO temperature data

Red: NCEP 7-day averaged u, with solid eastward and dashed westward

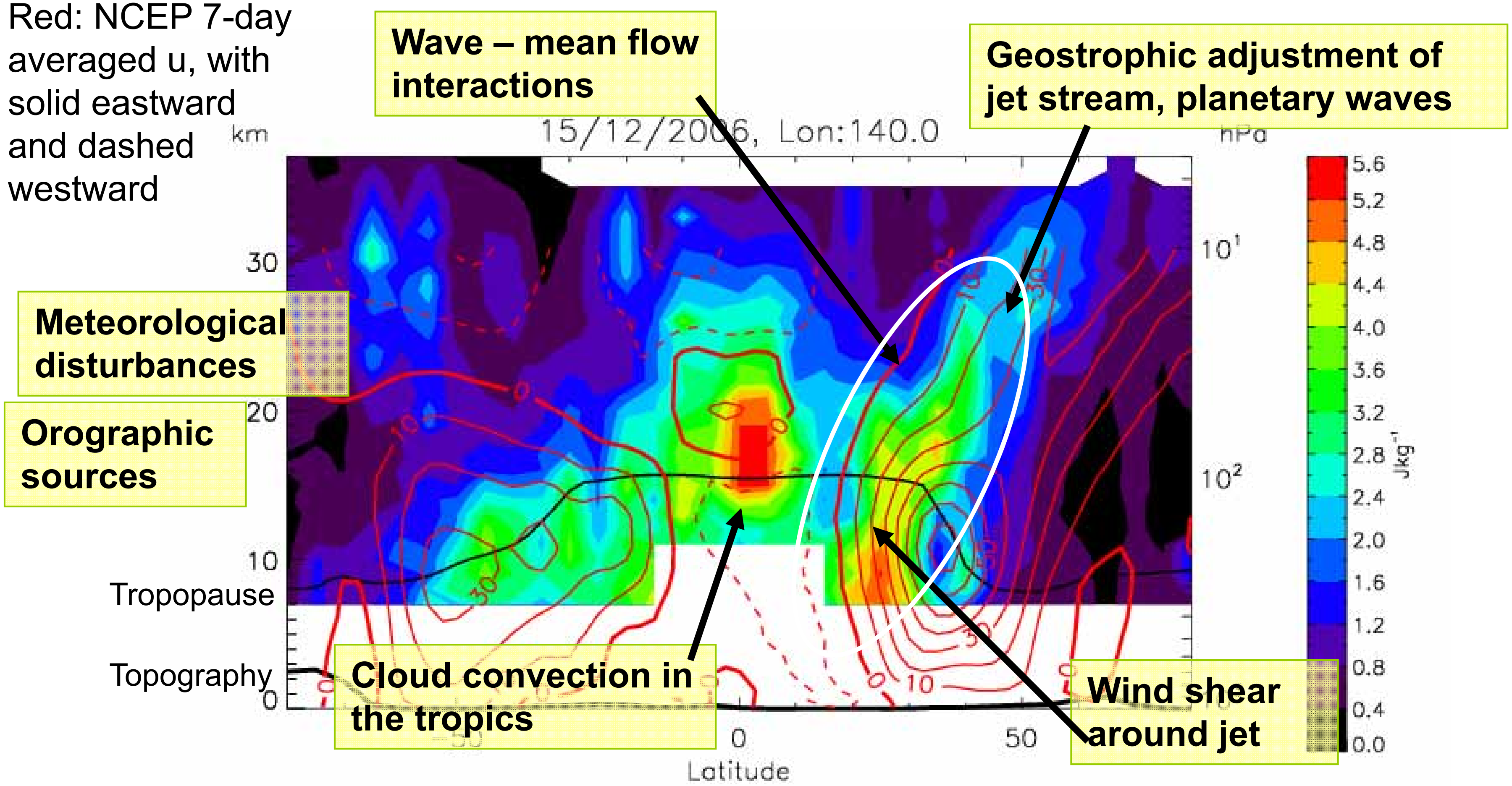

COSMIC

Gravity wave potential energy (PE) at 17–23 km altitude in winter 2006/07 (Dec-Feb) by using the COSMIC GPS RO temperature data.

Red contour: the winter mean NCEP u at 500–100 hPa in units of ms^{-1}.
Black contour: winter mean GPCP precipitation in mm day^{-1}

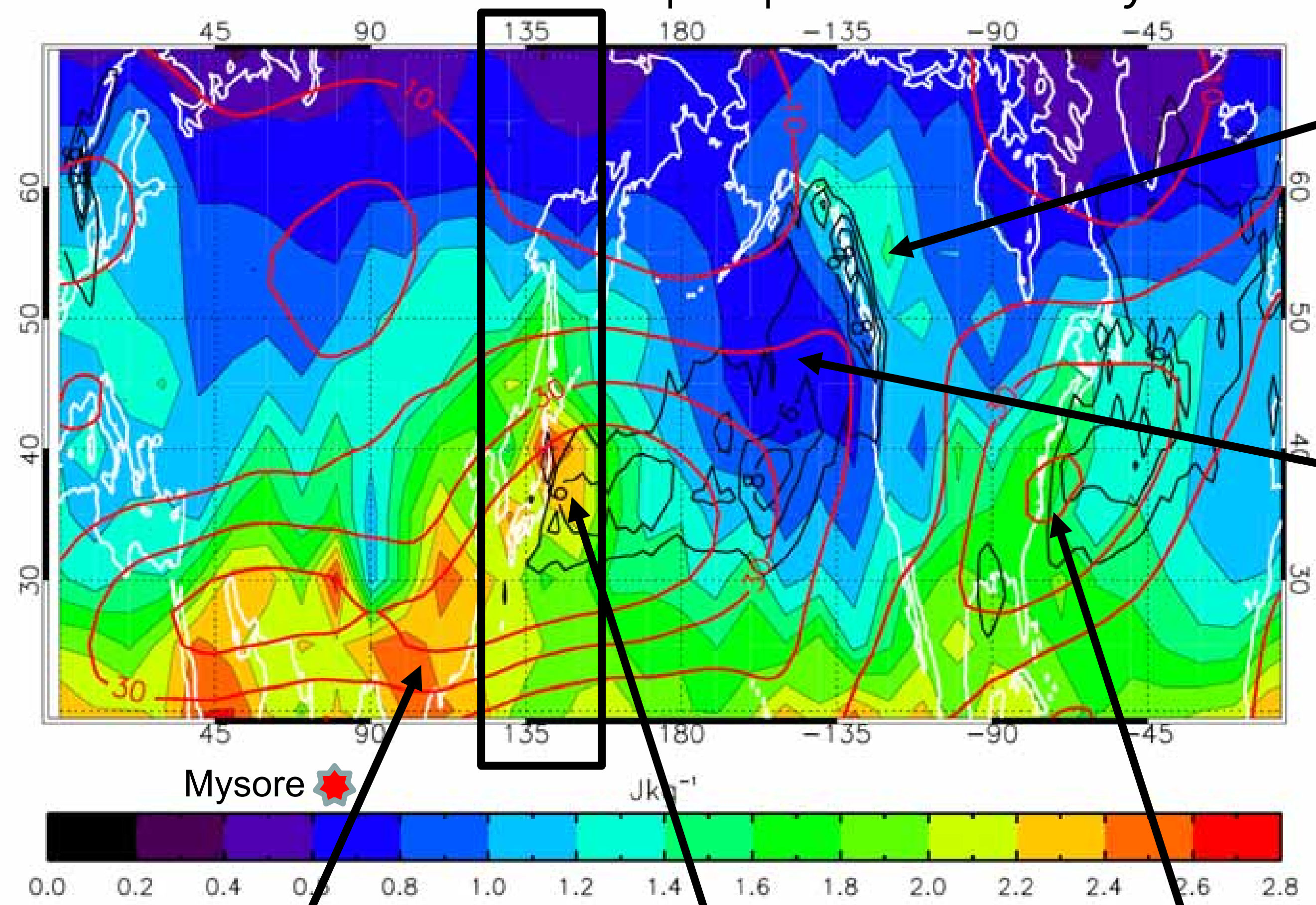

Large PE over Canadian Rockies due to orographic effects

PE is low over Pacific despite large oceanic precipitation

Himalayas & Tibet have large PE – some orographic effects but also jet stream

Japan – separate large PE: strong jet & orography

Large Eastern USA PE associated with strong winter jet

Gravity waves over Arctic and Antarctic regions

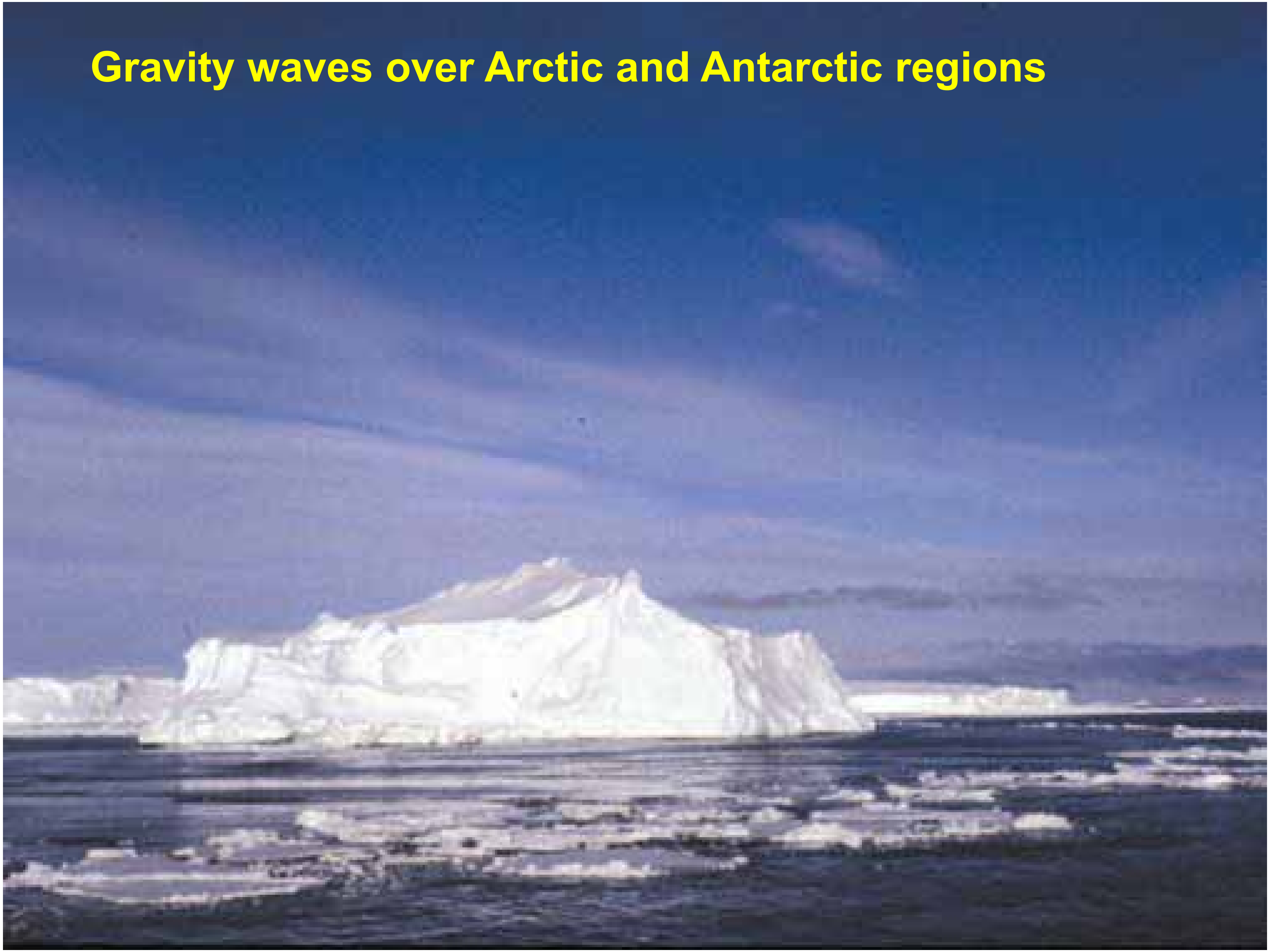

Generation Sources of Gravity Waves

COSMIC

A height-latitude section of the wave potential energy (Ep) (T' with vertical wave lengths < 7 km) from the COSMIC GPS RO data in 7 days centered on December 29, 2006 at the longitude of 140°E (130°-150°E).
Zonal winds from NCEP and topography (elevation) at 140°E are also plotted in red and black curves, respectively.

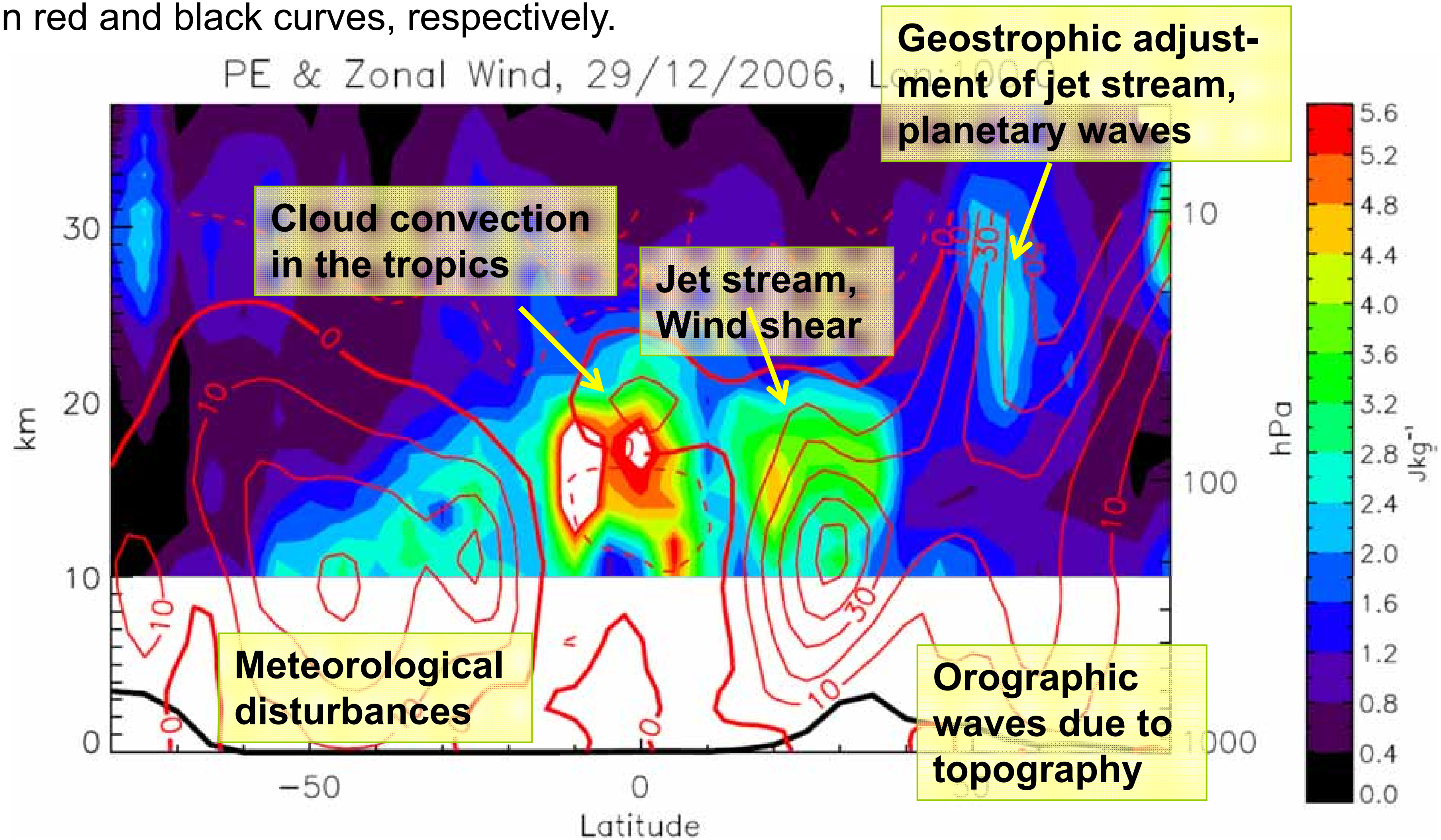

COSMIC

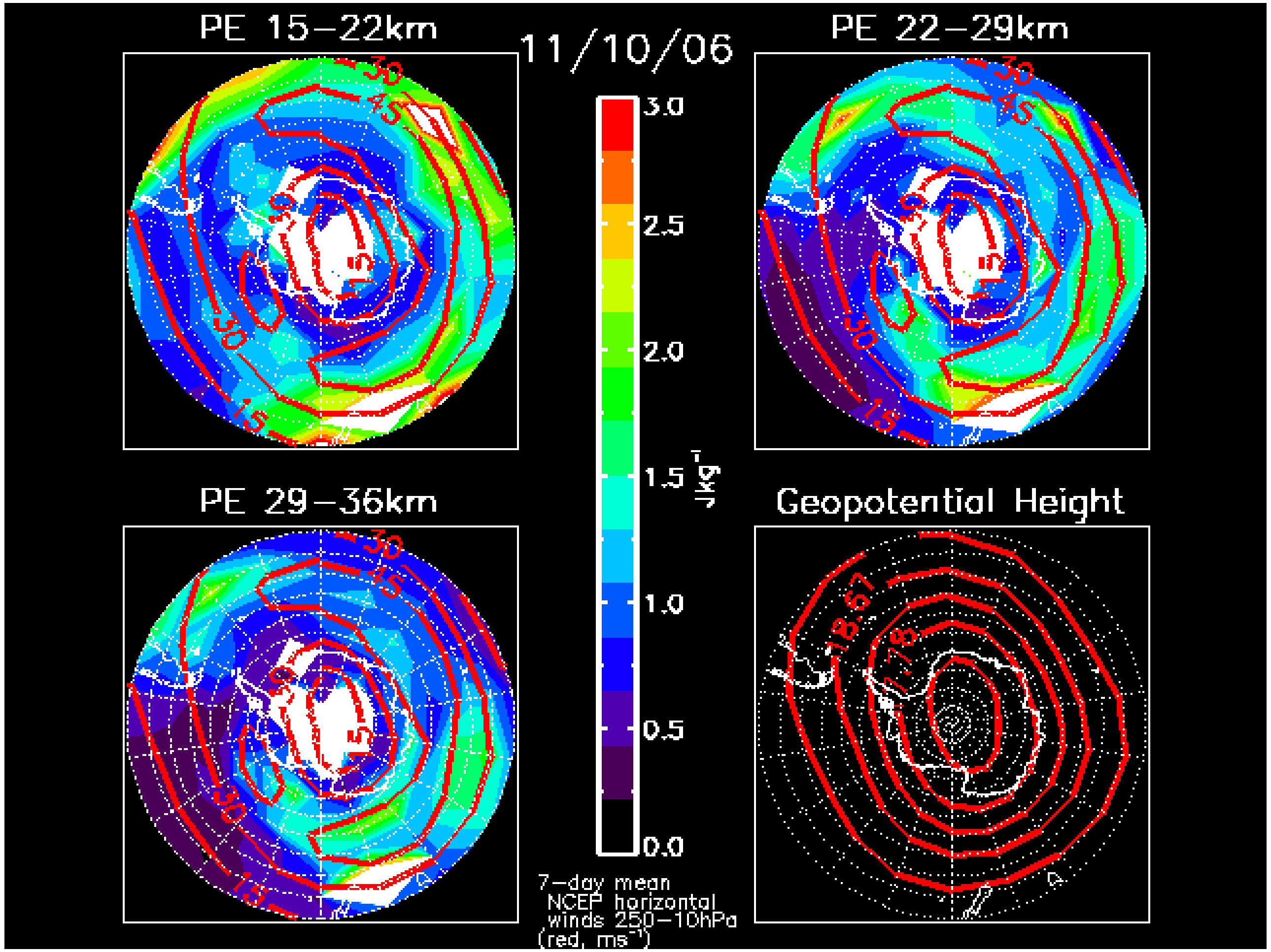

PE 15–22km
11/10/06
PE 22–29km
PE 29–36km
Geopotential Height
3.0
2.5
2.0
1.5
1.0
0.5
0.0
Jkg^{-1}
7–day mean NCEP horizontal winds 250–10hPa (red, ms^{-1})

COSMIC

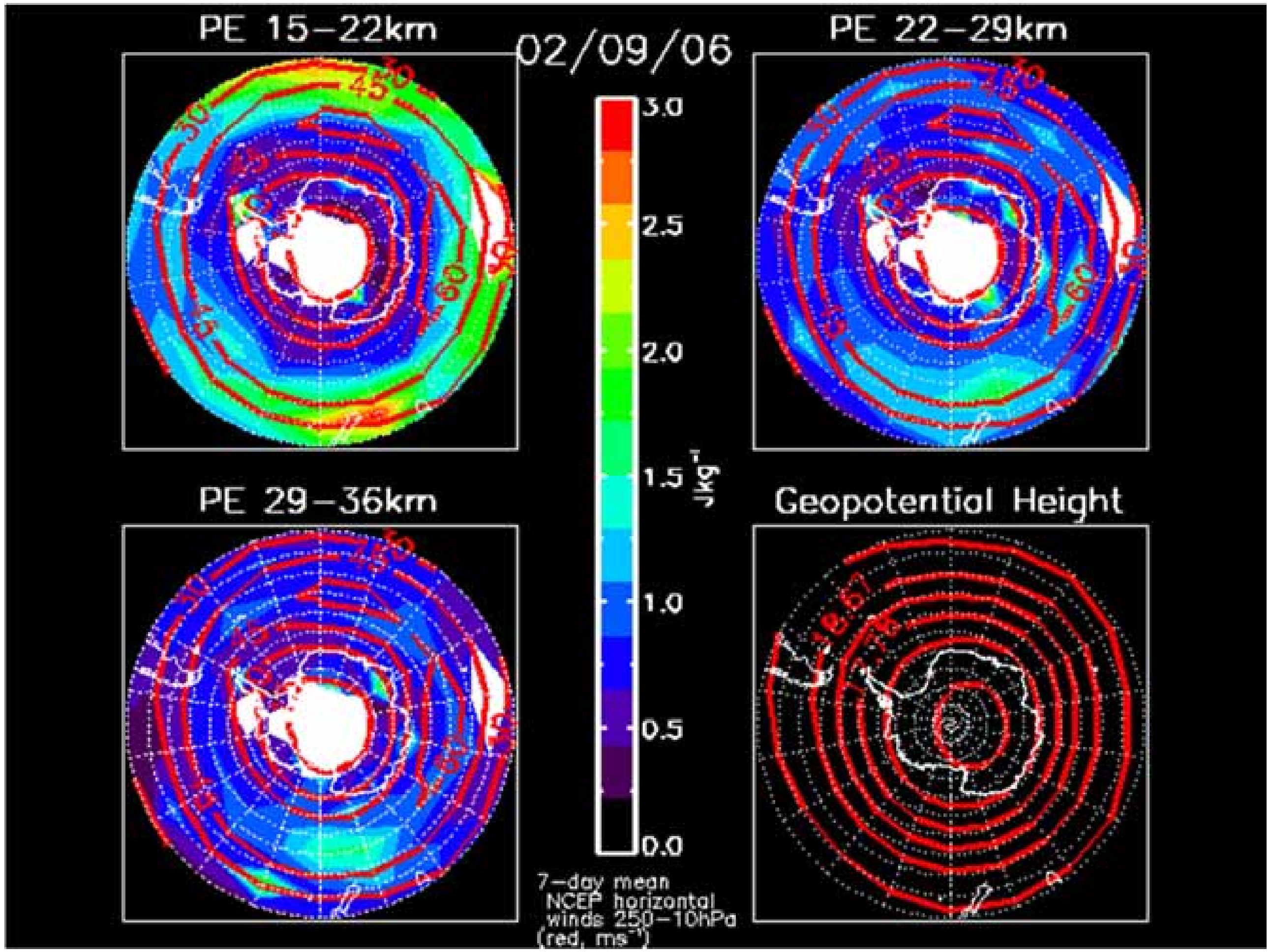

Movie

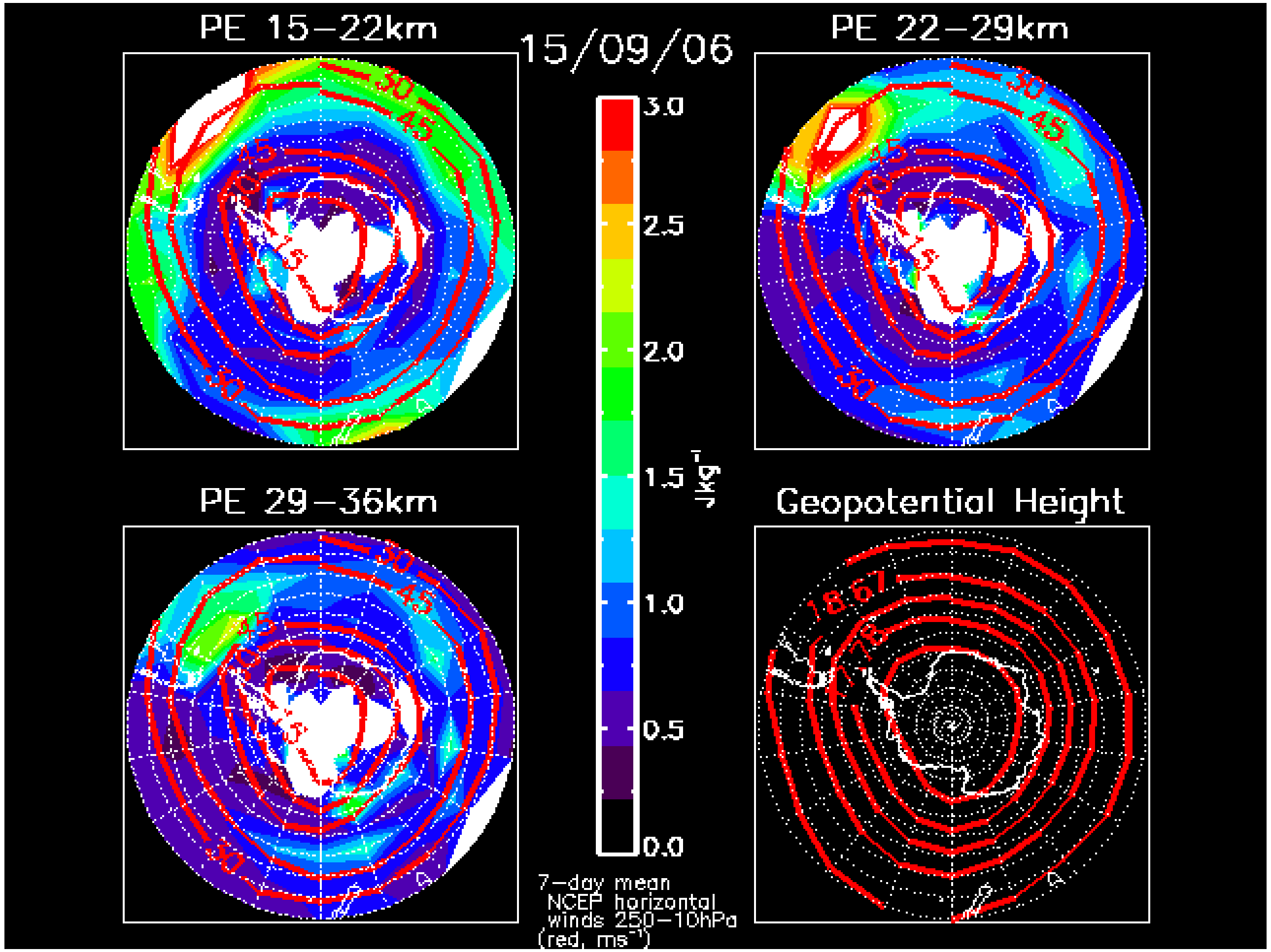

PE 15–22km
15/09/06
PE 22–29km
PE 29–36km
Geopotential Height
3.0
2.5
2.0
1.5
1.0
0.5
0.0
Jkg^{-1}
7–day mean
NCEP horizontal
winds 250–10hPa
(red, ms^{-1})
30
45
15
18.67

Structure of the polar vortex and wave variance (Ep) distribution

COSMIC

May-December 2007 in Antarctica at 500 K (about 19-20 km)

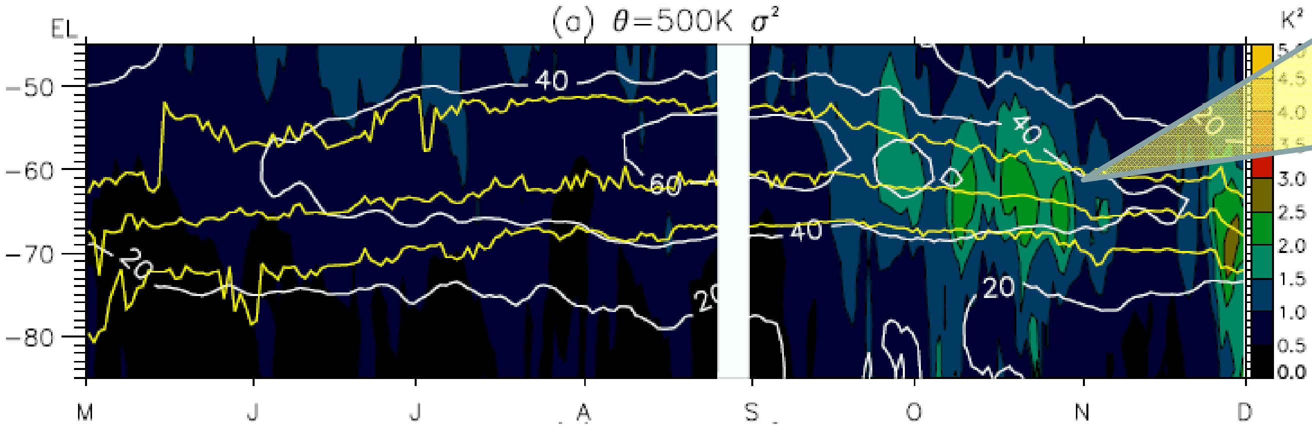

During winds decreased from 60m/s to 40 m/s in late-Sep to Oct (spring), large wave variance is observed inside the vortex boundary with symmetric distribution

October-May 2006/7 for the Arctic vortex at 500 K

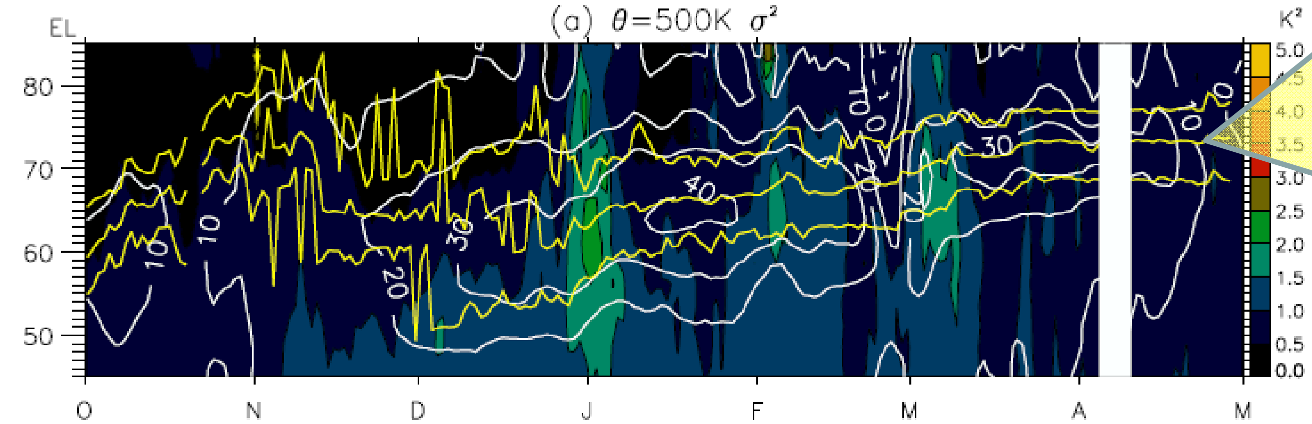

Enhancement of Ep does not occur during the vortex decay phase. But, large Ep in early Jan, Feb and March coincides with SSW (sudden stratospheric warming)

Contour: Ep, White line: 5-day smoothed UKMO zonal mean zonal winds (m/s, eastward solid),
Yellow line: vortex edge (thick) and vortex boundary region (between the thin yellow lines).

A gravity wave climatology for Antarctica compiled from CHAMP/GPS radio occultations, by A.J.G. Baumgaertner and A.J. McDonald, JGR, 2007(doi:10.1029/2006JD007504)

CHAMP

Longitude variation of Ep in 2003, averaged over 60-90S

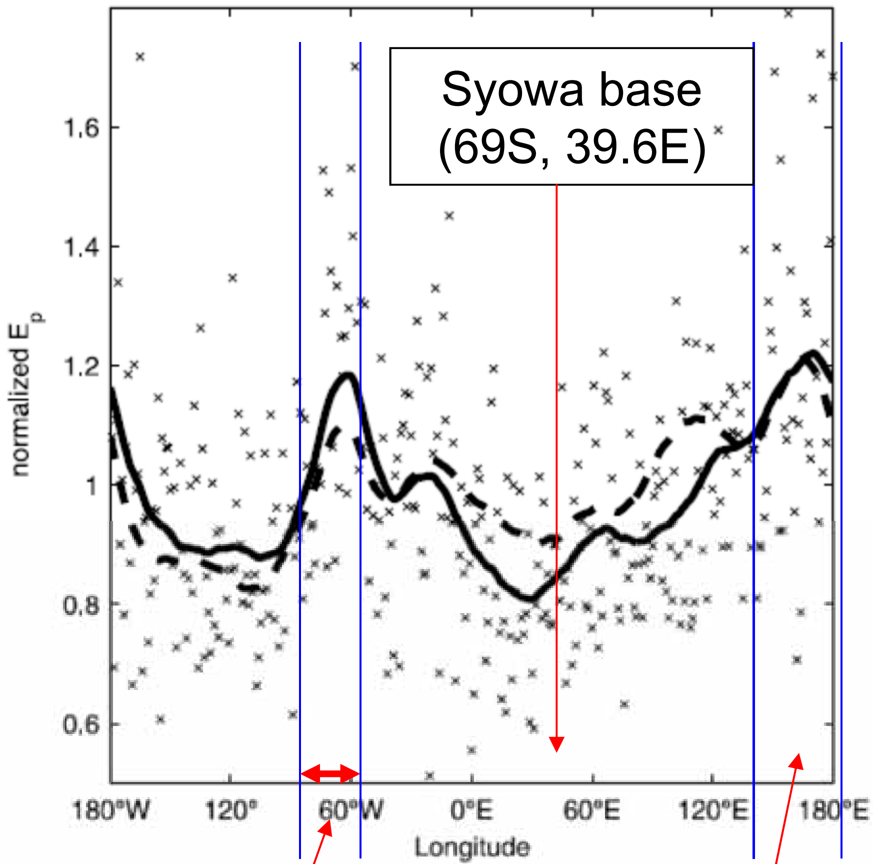

Figure 5. Longitudinal dependence of E_p at 18–22 km (solid line) and 23–27 km (dotted line) for 2003. Crosses show the unsmoothed values (1° longitudinal resolution) at 18–22 km.

Antarctic Peninsula (60-70W)

Trans-antarctic Mountains (about 160E)

Topography is an important source of gravity waves in the two regions. The relation is less pronounced at 23-27 km probably due to the filtering effects.

Yoshiki and Sato (2000) reported that the gravity wave activity at 15-20km over Syowa has a weak correlation with tropospheric winds, so, they suggested stratospheric sources for wave generation.

Outline of this lecture: Atmospheric Coupling Processes

- ✓ A linear theory of atmospheric gravity wave
  - Dispersion relation of atmospheric gravity waves
  - Convective instability and wave breaking/saturation
  - Critical level interaction between a gravity wave and wind shear
  - Importance of wave drag force (wave breaking) to maintain the general circulation of the middle atmosphere
- ✓ Radar observations of wave breaking process:
  - gravity wave saturation and turbulence generation (the MU radar).
- ✓ Global distribution of gravity wave activity with GPS radio occultation (RO) measurements:
  - Generation mechanisms; tropical convection, topography (mountain waves), Jet stream & polar night-jet, etc.
- ✓ Correlation between sporadic E and stratospheric gravity waves
  - Generation of orographic waves over Andes and Antarctica
  - A global distribution of sporadic E revealed with GPS-RO
- ✓ Coupling between the lower atmosphere and the MLT (mesosphere lower thermosphere) winds in the tropics
  - Tropical convection and gravity waves in the stratosphere
  - Correlation between short-period GW and Mesospheric SAO
  - Relation between S-QBO and M-QBO (M-QB Enhancement)

Dynamical Coupling of Atmosphere and Ionosphere in the Equatorial Region by Upward Propagating Atmospheric Waves

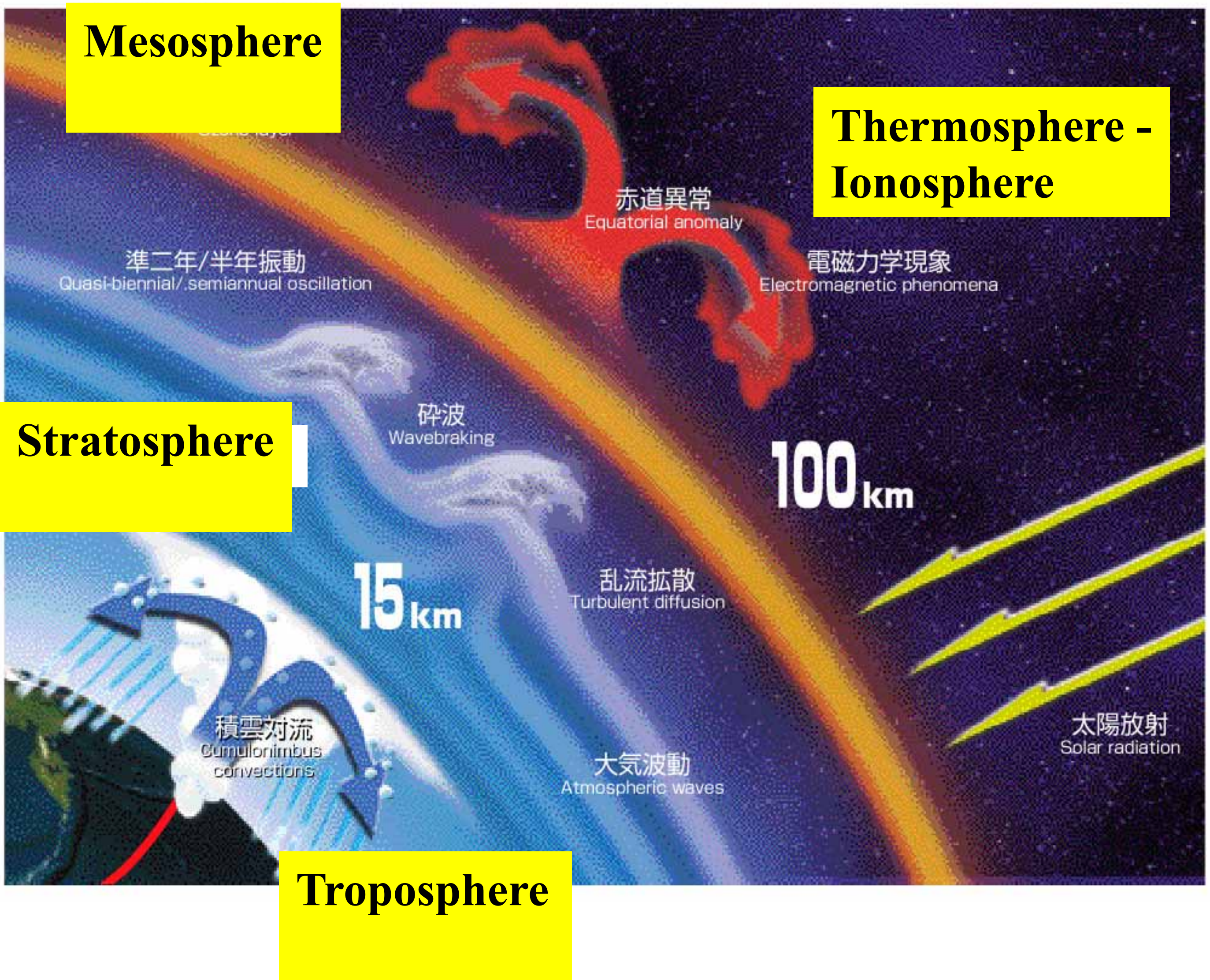

Estimation of Horizontal TEC (total electron content) from GPS occultation measurements

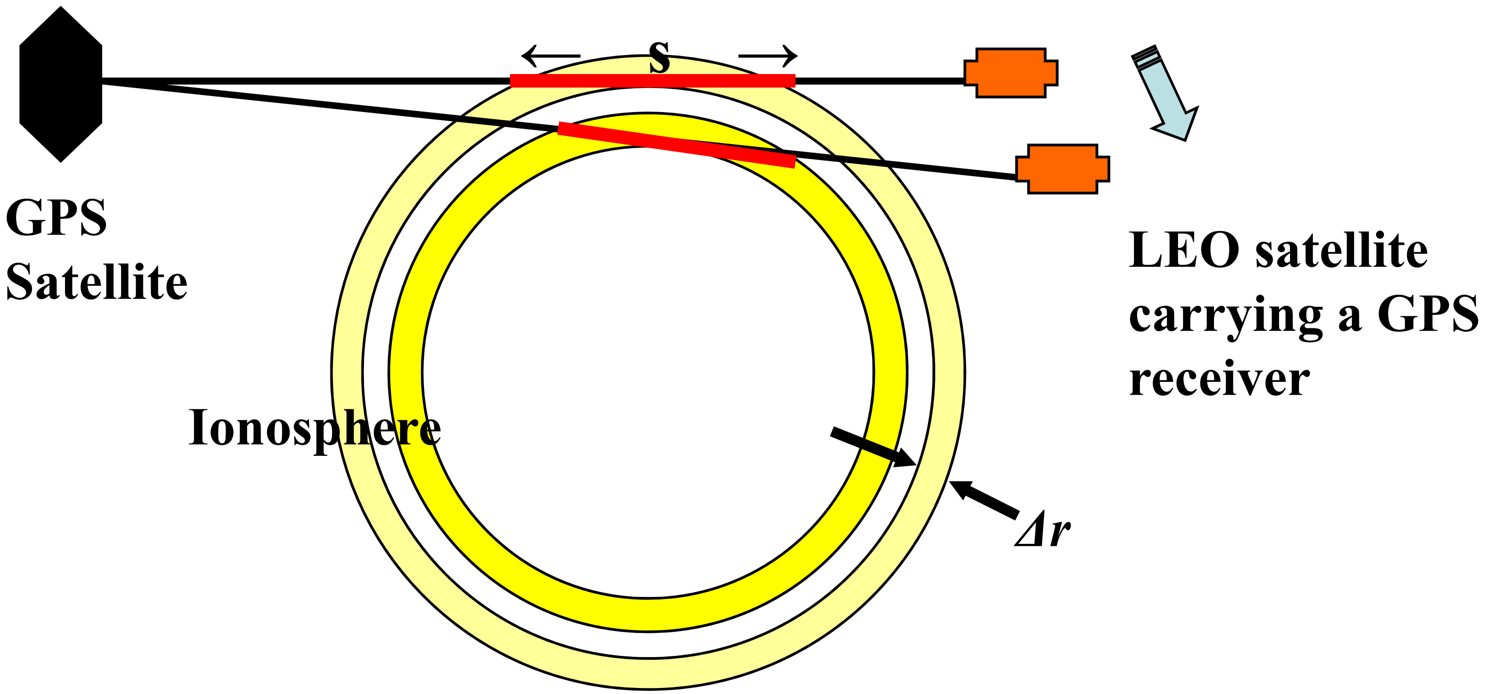

(1) Assuming that ***TEC*** is mostly attributed to the tangent point (***h***) of a straight GPS ray path, horizontal ***TEC*** (***hTEC***) is determined as function of ***h***.

(2) Fluctuating components of ***hTEC(h)*** is calculated by a sliding 7 km-window.

(3) Thin layers of ***Ne*** disturbances are assumed to have a constant vertical scale (***Δr*** ∼600 m in this study). Then, ***ΔhTEC*** is scaled to ***ΔNe*** by dividing with a constant factor, $s=2\,(2r\,\Delta r)^{1/2}$ ($r=6370 + 100$ km).

We do not investigate the absolute values of ***ΔNe***, but, we are mainly interested in the global distribution of ***ΔNe***.

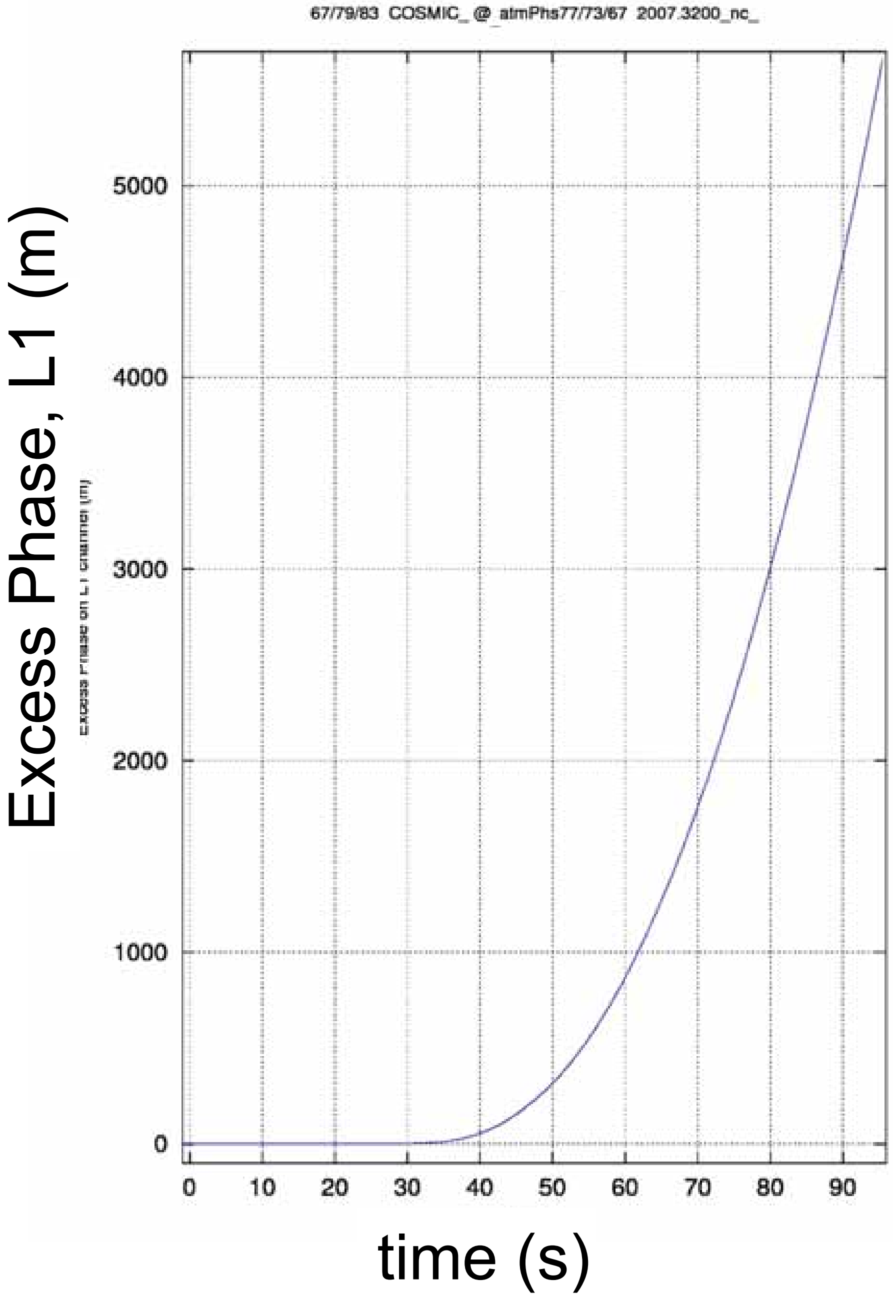
67/79/83 COSMIC_@_atmPhs77/73/67 2007.3200_nc_
Excess Phase, L1 (m)
0
1000
2000
3000
4000
5000
0 10 20 30 40 50 60 70 80 90
time (s)

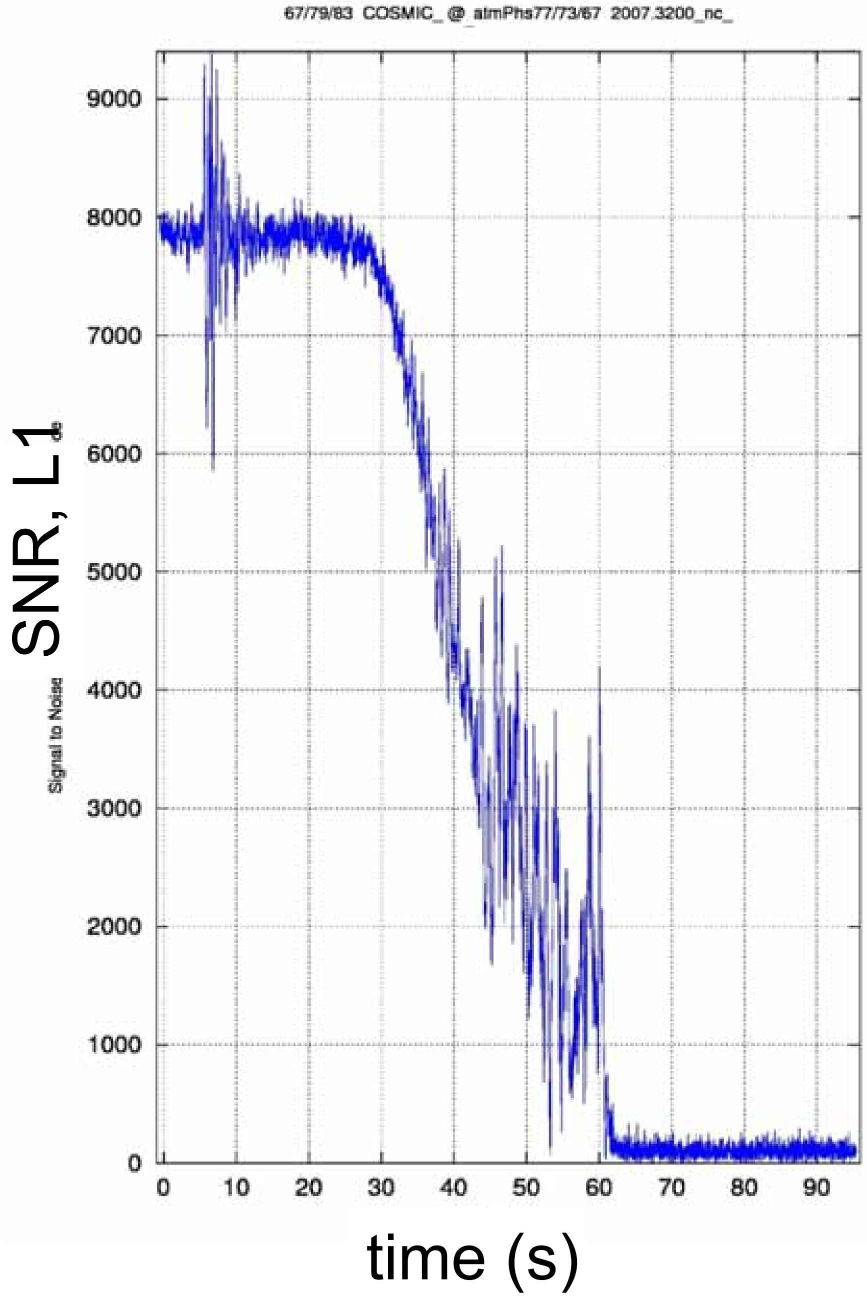
67/79/83 COSMIC_@_atmPhs77/73/67 2007.3200_nc_
SNR, L1
Signal to Noise
0
1000
2000
3000
4000
5000
6000
7000
8000
9000
0 10 20 30 40 50 60 70 80 90
time (s)

Electron density (Ne) profile observed with COSMIC GPS-RO

Fluctuating components of Ne after applying a high-pass filter with a cut-off at 7 km

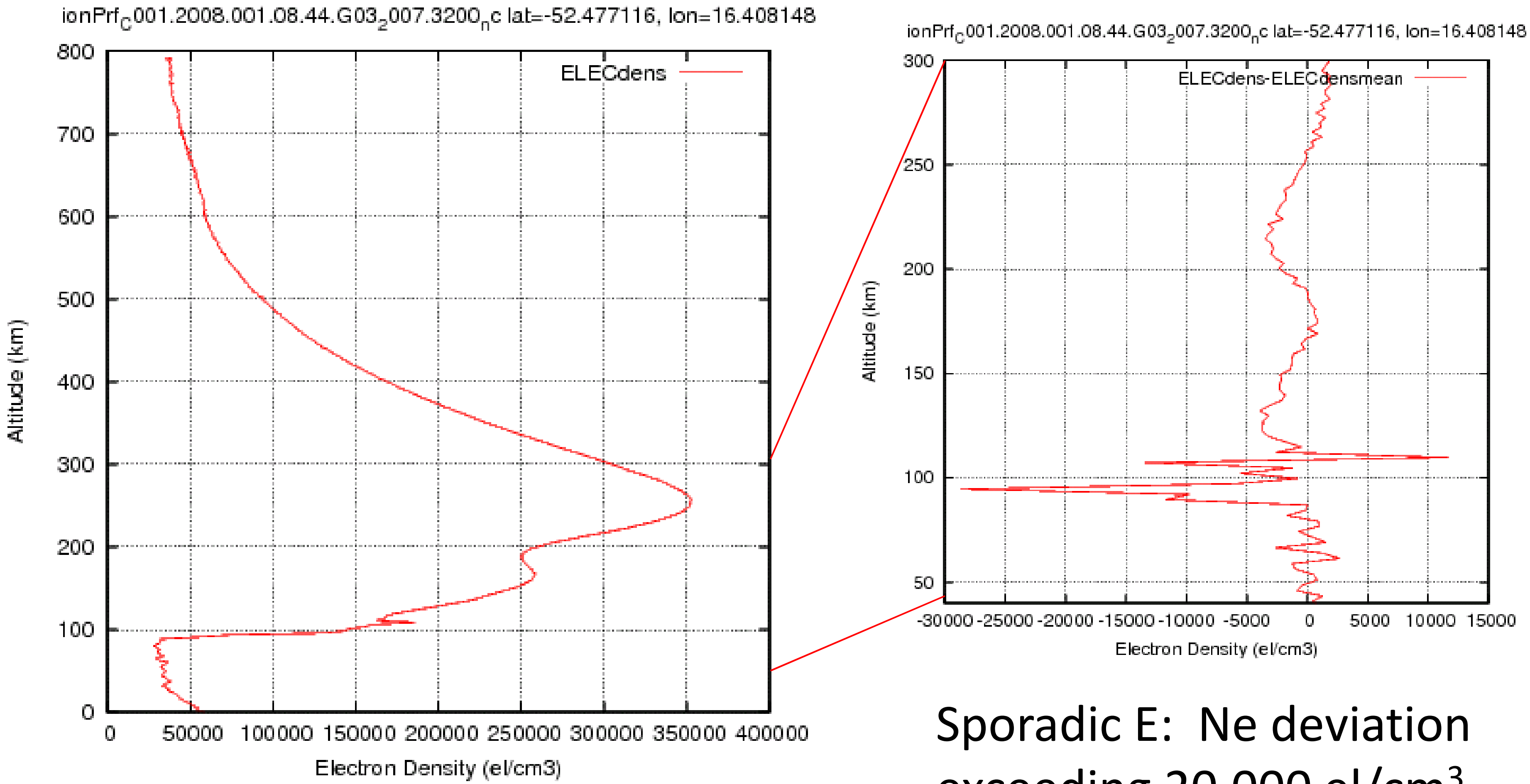

Sporadic E: Ne deviation exceeding 20,000 el/cm^3 at 50-200 km altitude

Example 2

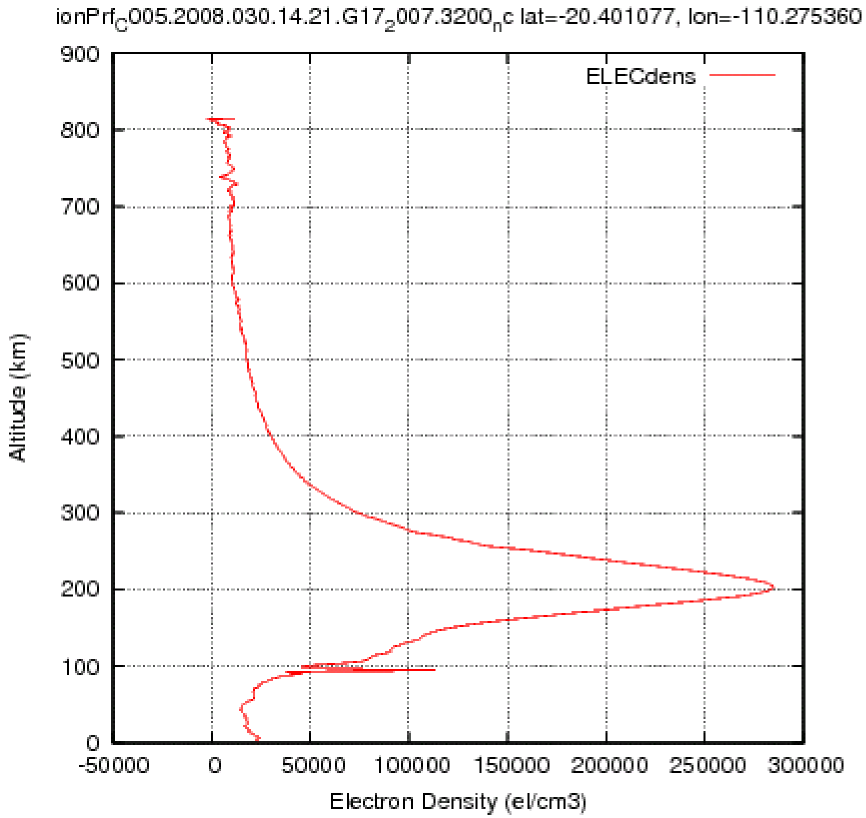

ionPrf_C005.2008.030.14.21.G17_2007.3200_nc lat=-20.401077, lon=-110.275360
ELECdens
Altitude (km)
Electron Density (el/cm3)
900
800
700
600
500
400
300
200
100
0
-50000
0
50000
100000
150000
200000
250000
300000

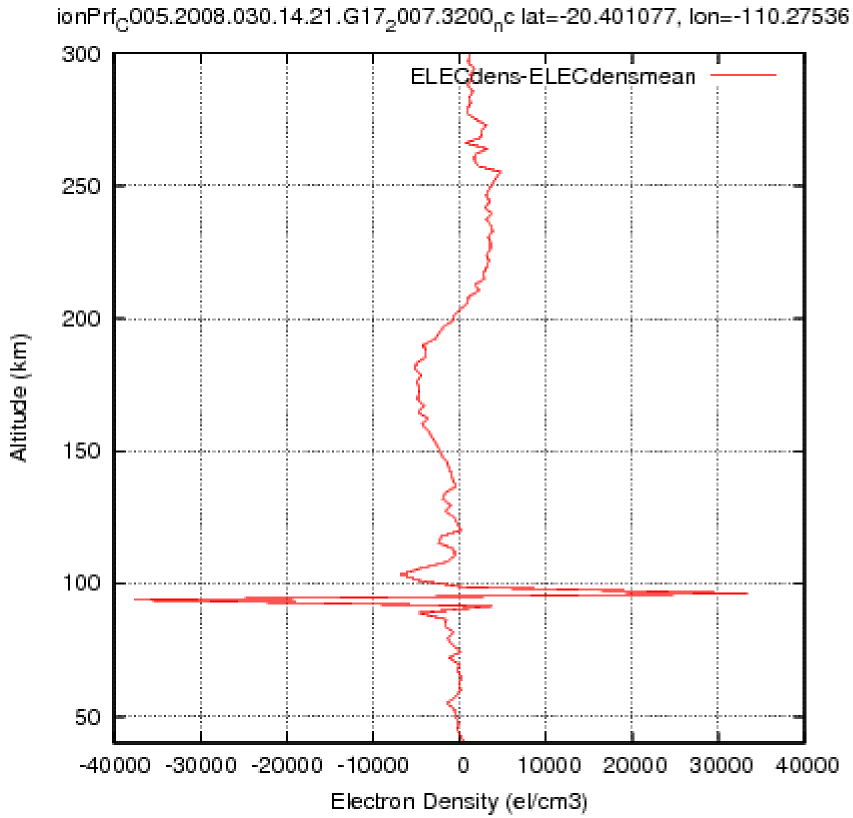

ionPrf_C005.2008.030.14.21.G17_2007.3200_nc lat=-20.401077, lon=-110.27536
ELECdens-ELECdensmean
Altitude (km)
Electron Density (el/cm3)
300
250
200
150
100
50
-40000
-30000
-20000
-10000
0
10000
20000
30000
40000

Orographic Generation of Mountain Waves

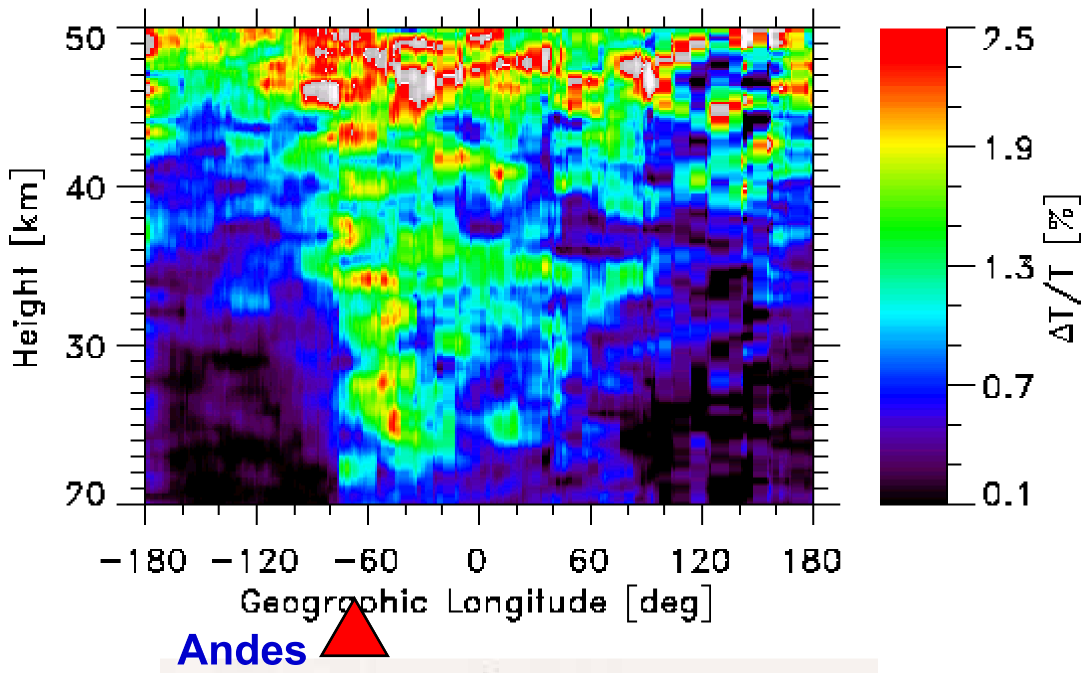

Longitude-Height Section of *T'/T* over Andes from GPS/MET data

(*T'/T*) with λ<7 km at 35-55 S in October, 1995.

Enhanced *T'* appears in the stratosphere at 50-70 W (over Andean mountains).

Vertical wind velocity

Stream line

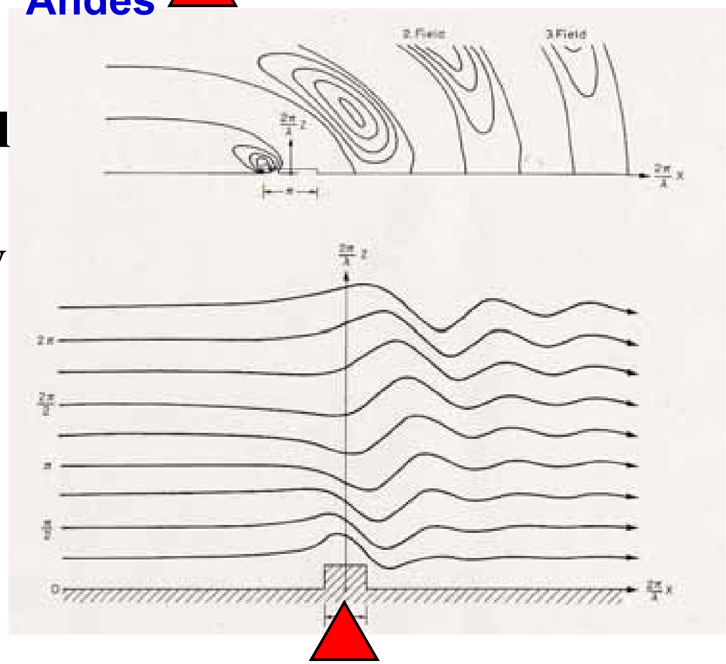

Mountain waves by interaction of surface winds with topography

(Gossard and Hooke, 1975)

Convergence of *Ne* (sporadic E) by the combined neutral wind shear and geomagnetic effects

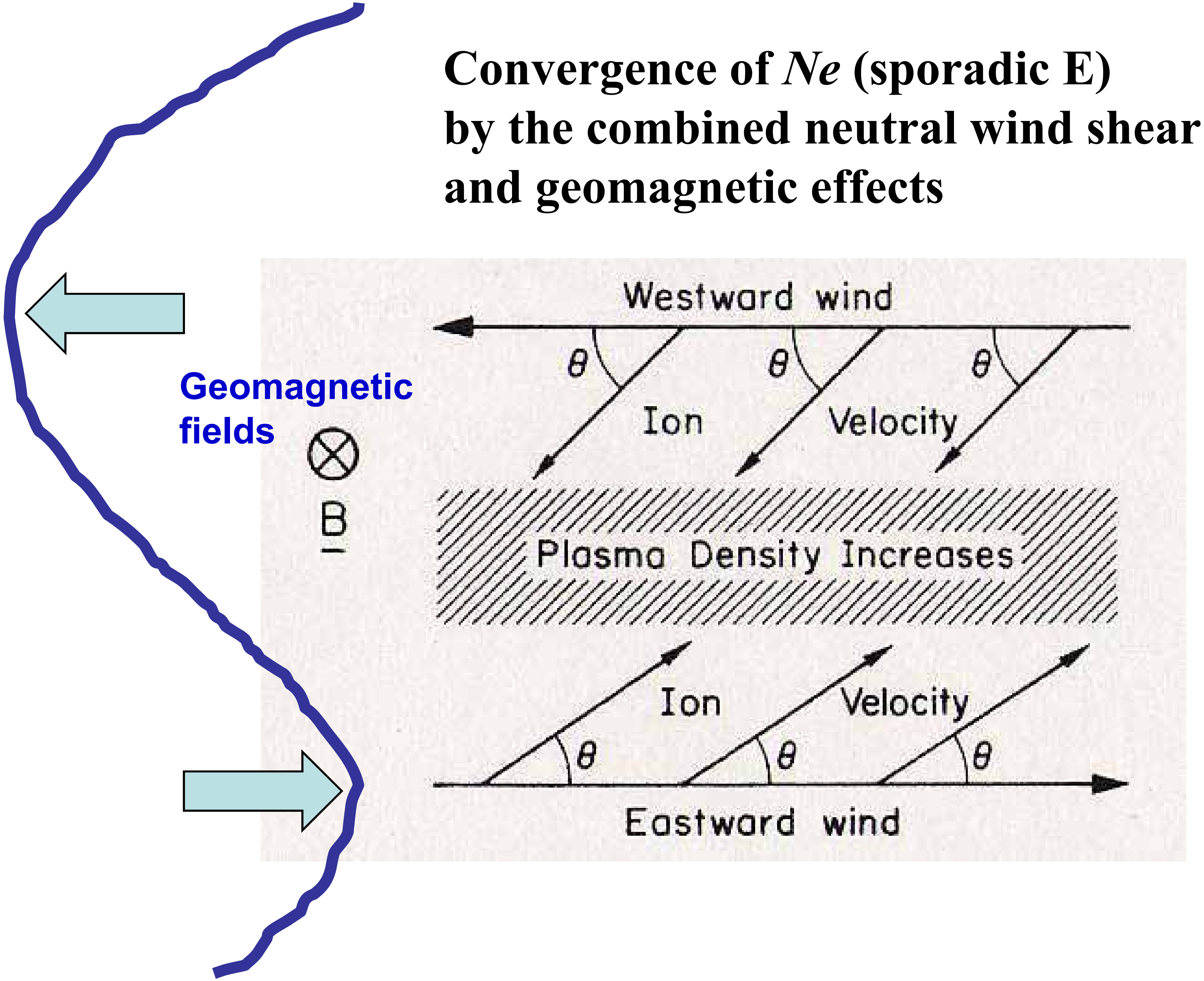

Horizontal winds associated with Atmospheric Waves

(Hines, 1974; Kelley, 1989)

Orographic Generation of Mountain Waves

GPS/ MET

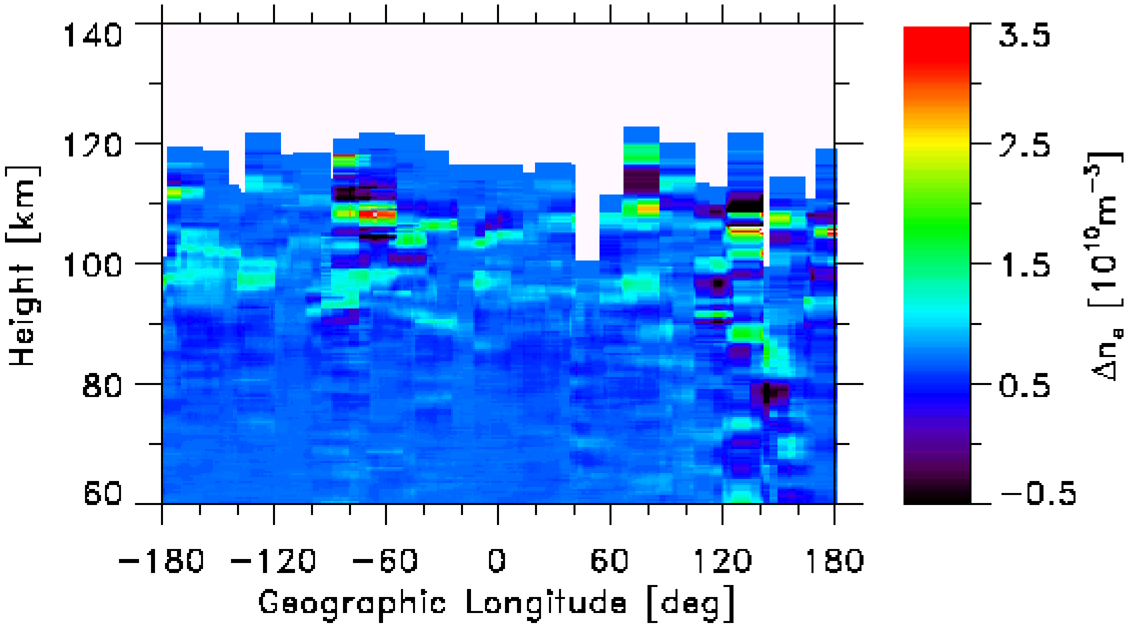

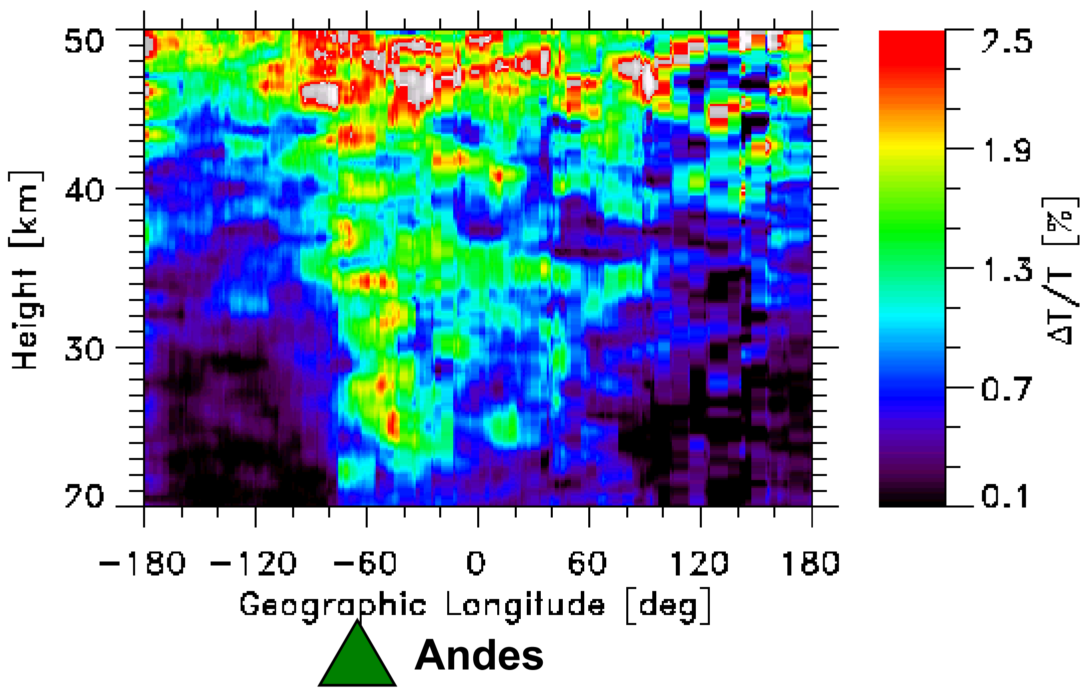

Longitude-Height Section of *Ne* and *T'/T* over Andes from GPS/MET

***Ne* perturbations with λ<7 km at 40-55 S in October, 1995**

Large *Ne* fluctuations (sporadic E) are seen around 110 km at 60-80 W.

(*T'/T*) with λ<7 km

At 50-70 W, enhanced *T'* appears in the stratosphere over Andes.

Distribution of *ΔNe* and $(T'/T)^2$ at 35-55S in October , 1995

GPS/ MET

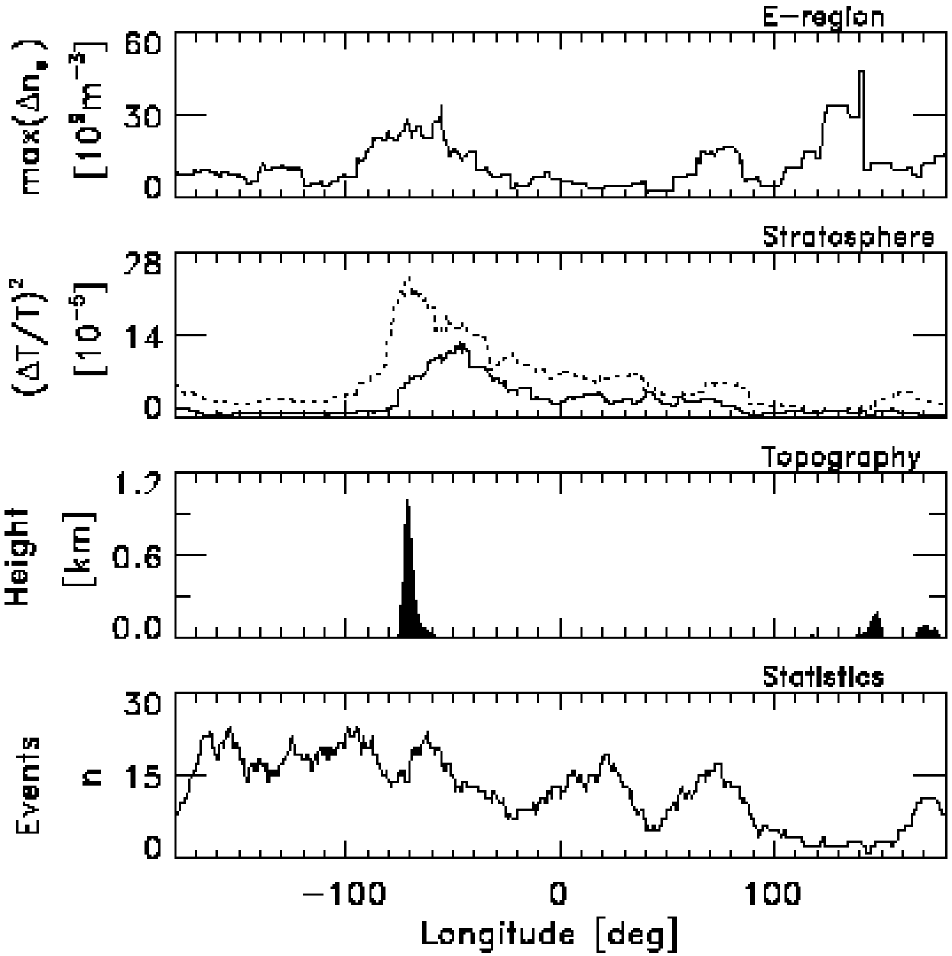

Maximum of electron density perturbations (*ΔNe*) at 80-120 km

$(T'/T)^2$ with λ< 7 km at 22-28 km (solid) and 32-38 km (dotted)

Topography at 35-55 S (A peak at 60-80 W corresponds to the Andean mountain)

Number of GPS/MET data

1. **$(T'/T)^2$ are clearly enhanced over the Andes, indicating orographic generation of mountain waves.**
2. **In the ionosphere, large *ΔNe* is frequently detected in the same longitude range.**

GPS/MET

Global Distribution of Electron Density Perturbations (ΔNe) with a Vertical Scale Smaller than 7 km at 105-110 km

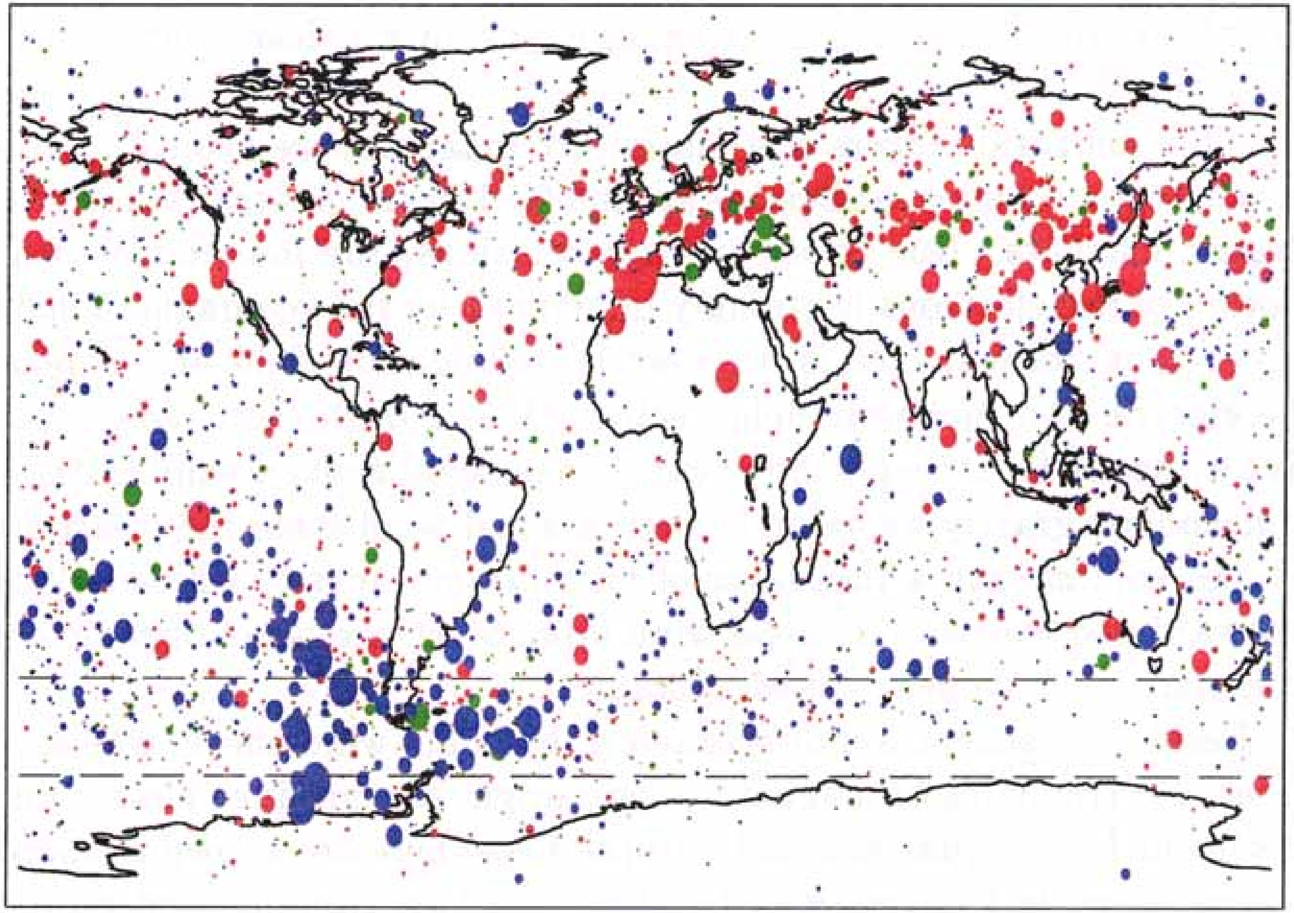

Red:
June/July 1995
Green:
October, 1995
Blue:
February, 1997

Radius of a dot is proportional to *ΔNe*

(1) Large *Ne* perturbations are frequently detected in summer over continents.
(2) In particular, near the Andes in the southern hemisphere, mountain waves seem to propagate up to the ionosphere, and generate a convergence of *Ne* (sporadic E) by the combined wind shear and geomagnetic effects.

Longitude Distribution of Topography, Humidity, Temperature Variance and Electron Density at 5-25°S on February 2-16, 1997

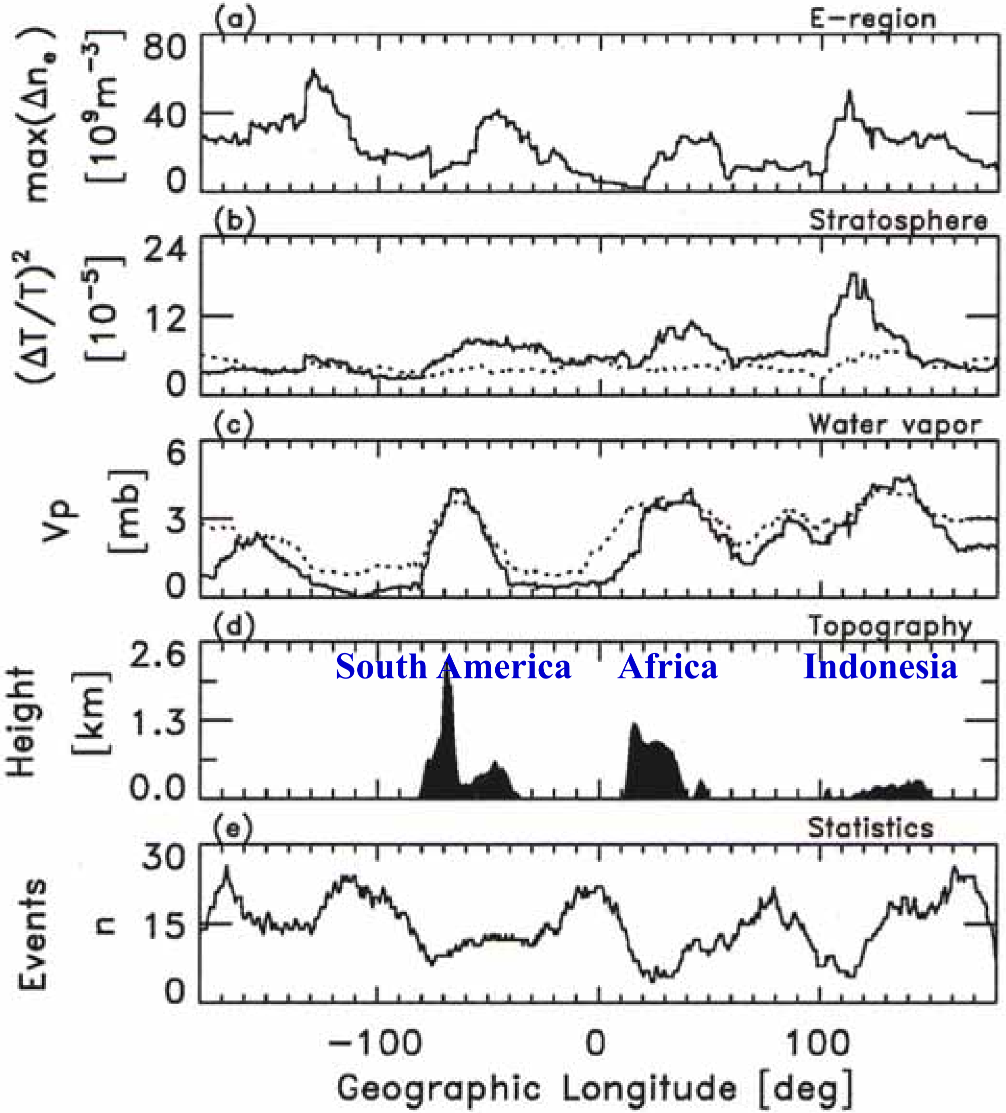

← Maximum of *Ne* perturbations in the MLT region (80-120 km)

← Temperature variance at 22-28 km (solid) and 32-38 km (dot)

← Water vapor pressure at 6 km from GPS/MET (solid) and ECMWF (dot)

← Mean height of surface topography at 5-25S

← Number of occultation events from GPS/MET

Good correlation between *ΔNe*, *Ep* and humidity is recognized.

Outline of this lecture: Atmospheric Coupling Processes

✓ **A linear theory of atmospheric gravity wave**
- **Dispersion relation of atmospheric gravity waves**
- **Convective instability and wave breaking/saturation**
- **Critical level interaction between a gravity wave and wind shear**
- **Importance of wave drag force (wave breaking) to maintain the general circulation of the middle atmosphere**

✓ **Radar observations of wave breaking process:**
- **gravity wave saturation and turbulence generation (the MU radar).**

✓ **Global distribution of gravity wave activity with GPS radio occultation (RO) measurements:**
- **Generation mechanisms; tropical convection, topography (mountain waves), Jet stream & polar night-jet, etc.**

✓ **Correlation between sporadic E and stratospheric gravity waves**
- **Generation of orographic waves over Andes and Antarctica**
- **A global distribution of sporadic E revealed with GPS-RO**

✓ **Coupling between the lower atmosphere and the MLT (mesosphere lower thermosphere) winds in the tropics**
- **Tropical convection and gravity waves in the stratosphere**
- **Correlation between short-period GW and Mesospheric SAO**
- **Relation between S-QBO and M-QBO (M-QB Enhancement)**

Earth Planets Space, **58**, 33–36, 2006

A global distribution of sporadic E events revealed by means of CHAMP-GPS occultations

M. Garcia-Fernandez and T. Tsuda

Research Institute for Sustainable Humanosphere, Kyoto University, Japan

(Received March 23, 2005; Revised June 22, 2005; Accepted August 10, 2005; Online published January 27, 2006)

With the advent of the GPS/MET mission, the atmospheric sciences were given a new tool to enhance studies related to global and seasonal variations of different atmospheric parameters. In particular, it has proof valuable for the study of the ionospheric irregularities in the E layer, which before were performed basically on a local basis by ground based instruments. Using similar techniques applied to GPS/MET data to process the 50 Hz sampling rate GPS data to study the E layer electron density distribution, this work shows the global and seasonal distributions of the ionospheric irregularities of electron density, during high solar activity, by using the CHAMP satellite GPS data from January 1st 2002 to May 31st 2004. As pointed out by several theories on the E layer and previous studies with ground based data, the results presented here show that these irregularities have strong geographical and seasonal dependence, with enhancements in the auroral regions, in mid-latitudes and during the summer season.

Key words: Ionospheric irregularities, E layer, occultation, CHAMP.

CHAMP

Jan 2002 – May 2004
175,500 profiles
(222/day)

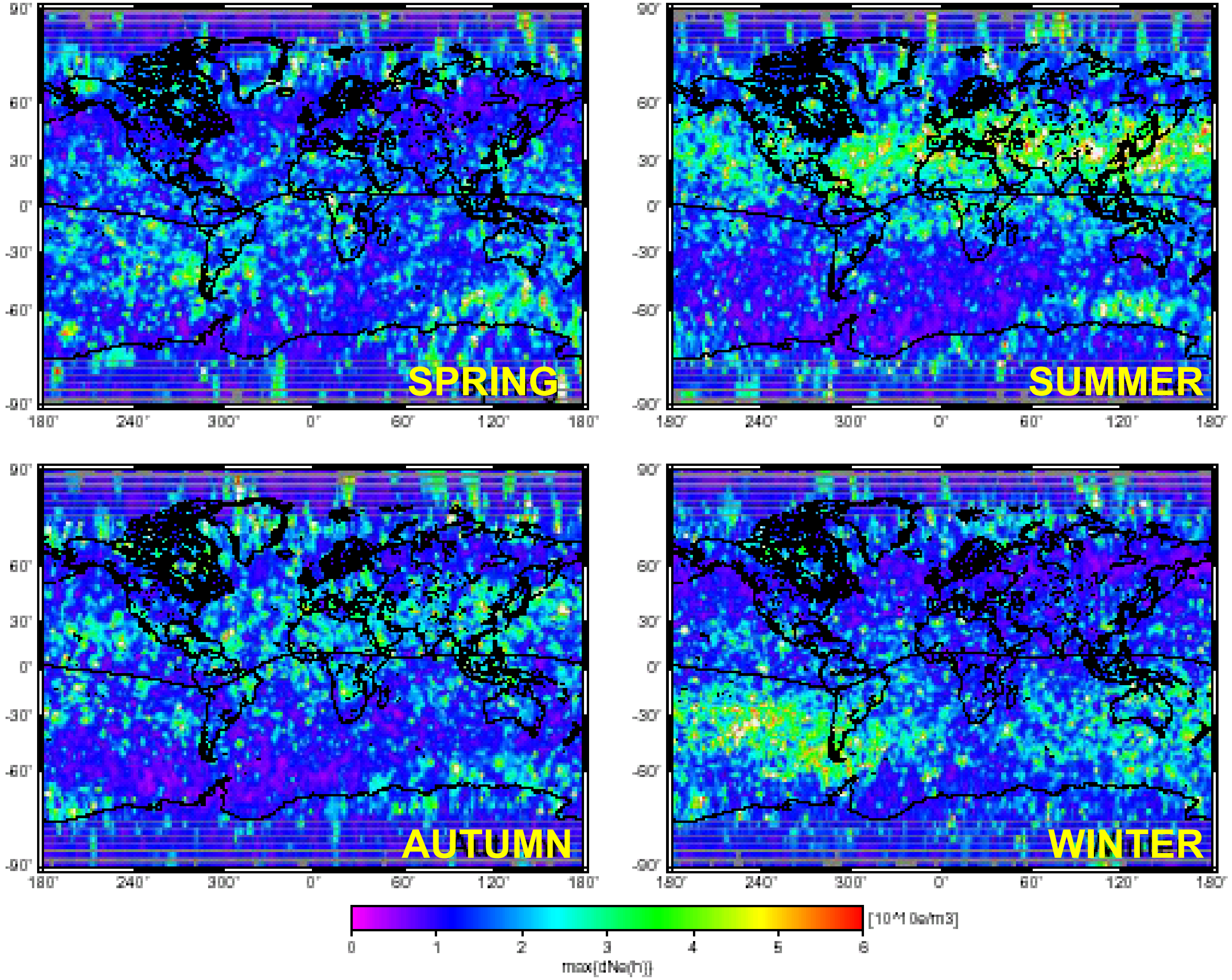

DAYTIME 5-22 LT

Fig. 2. World and seasonal distribution of ionospheric irregularities in the E region, corresponding to daytime period (5LT to 22LT). Periods shown are centered at the solstices or equinoxes, therefore Spring: day of year (doy) 046 to 126, Summer: from doy 127 to 218, Autumn: from doy 219 to 310 and Winter: from doy 311 to 045. GPS occultation data of CHAMP satellite from January 1st 2002 to May 31st 2004 have been processed.

A global climatology of ionospheric irregularities derived from GPS radio occultation

C. Arras,[1] J. Wickert,[1] G. Beyerle,[1] S. Heise,[1] T. Schmidt,[1] and C. Jacobi[2]

GEOPHYSICAL RESEARCH LETTERS, VOL. 35, L14809, doi:10.1029/2008GL034158, 2008

[1] GPS radio occultation measurements from CHAMP, GRACE-A and FORMOSAT-3/COSMIC are used to derive global information on small-scale ionospheric irregularities such as sporadic E layers between January 2002 and December 2007. The investigations are based on the analysis of amplitude variations of the GPS radio occultation signals. The global distribution of ionospheric irregularities shows strong seasonal variations with highest occurrence rates during summer in the middle latitudes. The long-term data set of CHAMP allows for first climatological studies, while the data coverage increases significantly with the combination of CHAMP, GRACE and FORMOSAT-3/COSMIC measurements. This allows for global maps of sporadic E occurrence rates of very high spatial resolution where the influence of the Earth's magnetic field becomes visible in global sporadic E maps for the first time.

Citation: Arras, C., J. Wickert, G. Beyerle, S. Heise, T. Schmidt, and C. Jacobi (2008), A global climatology of ionospheric irregularities derived from GPS radio occultation, *Geophys. Res. Lett.*, *35*, L14809, doi:10.1029/2008GL034158.

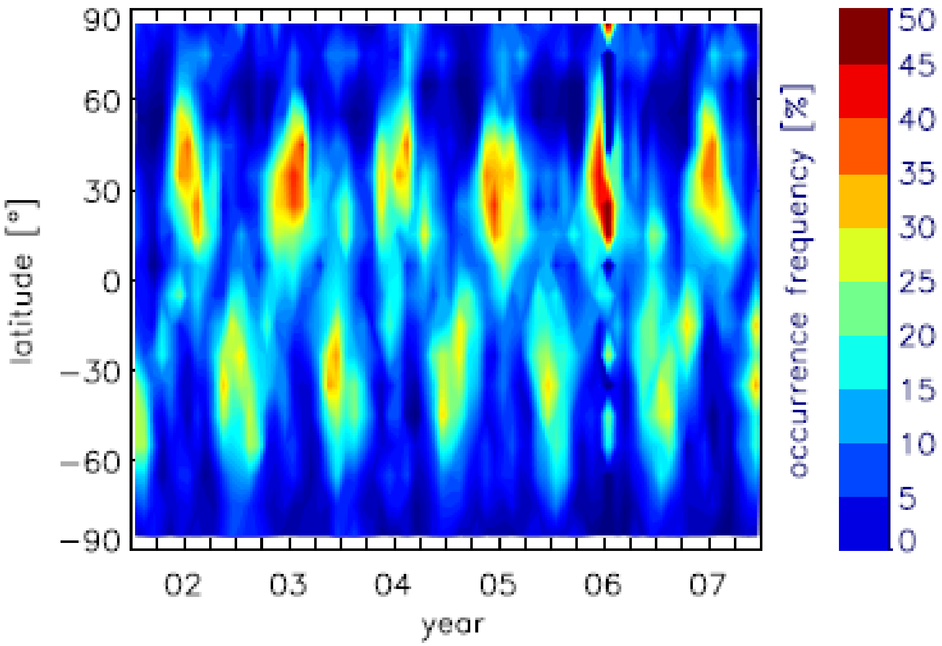

Figure 2. Time series of monthly relative E_s occurrence in dependency of geographical latitude (10° resolution) for the period January 2002 to December 2007 based on CHAMP data.

A global climatology of ionospheric irregularities derived from GPS radio occultation

C. Arras,[1] J. Wickert,[1] G. Beyerle,[1] S. Heise,[1] T. Schmidt,[1] and C. Jacobi[2]

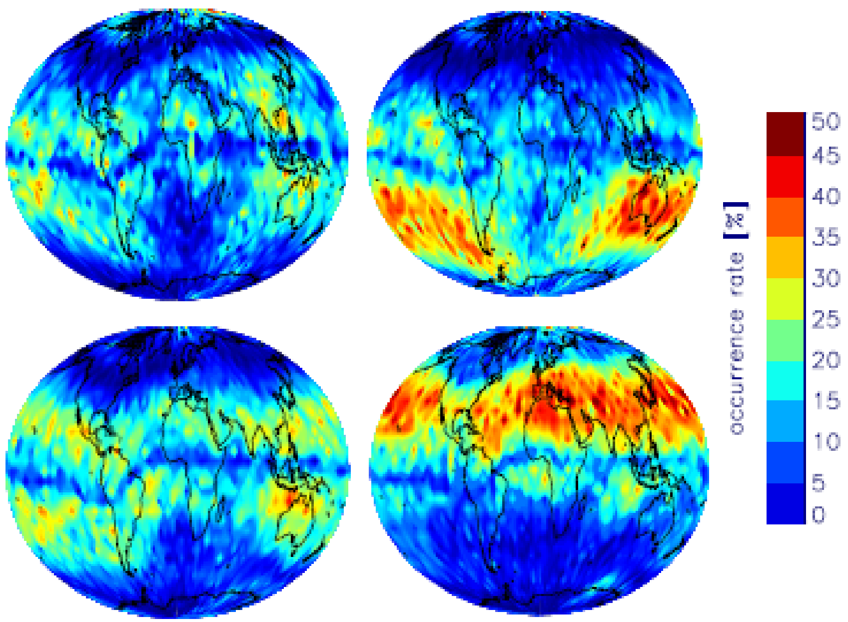

Figure 3. Seasonal occurrence of E_s detected with CHAMP, GRACE and FORMOSAT-3/COSMIC with a resolution of $5° \times 5°$. Plots for the (top left) autumn (September, October, November) 2006 and (top right) winter (December, January, February) 2006/2007. Data from (bottom left) spring (March, April, May) 2007 and (bottom right) summer (June, July, August) 2007.

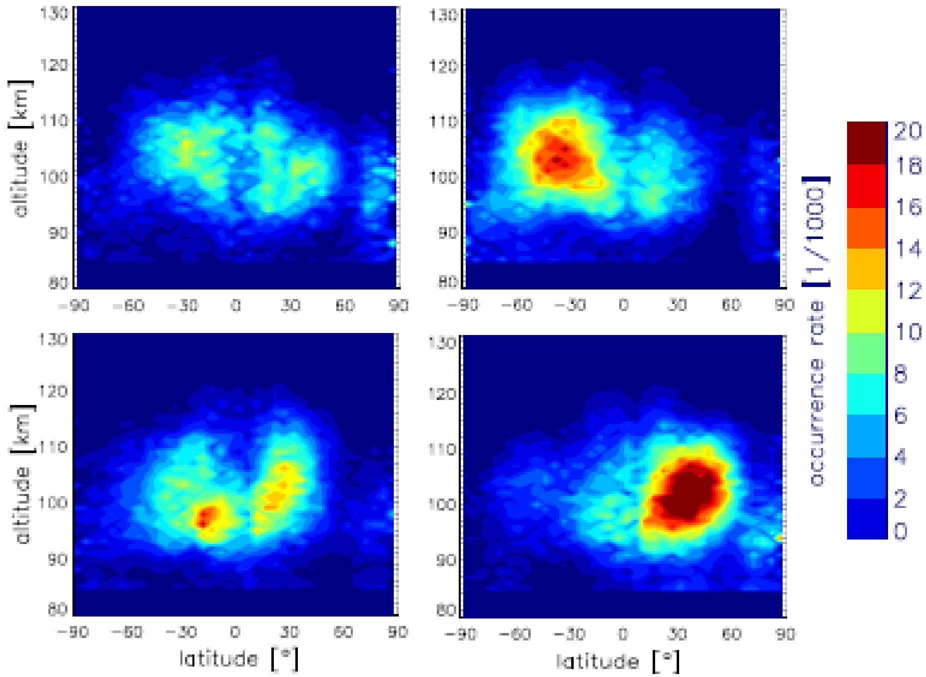

Figure 4. Relative E_s occurrence in latitude-altitude cross-sections in a $5° \times 1$ km resolution for the period autumn 2006 to summer 2007 in the same time intervals as in Figure 3.

Number of GPS RO data from January to June 2008 in a longitude-latitude cell of 10°x10°

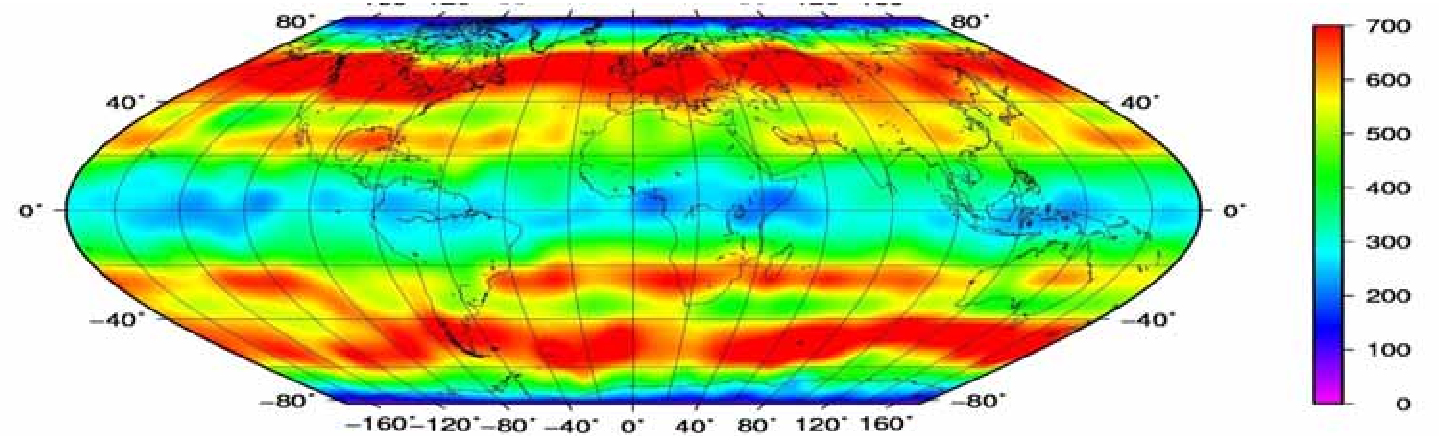

Number of sporadic E events

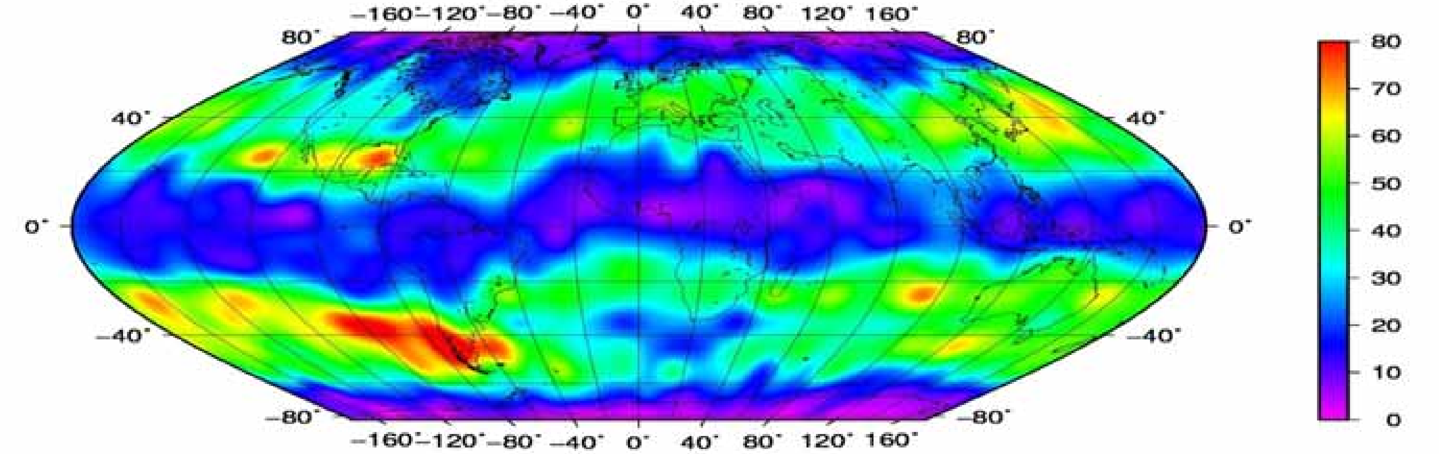

Occurrence rate of sporadic E events

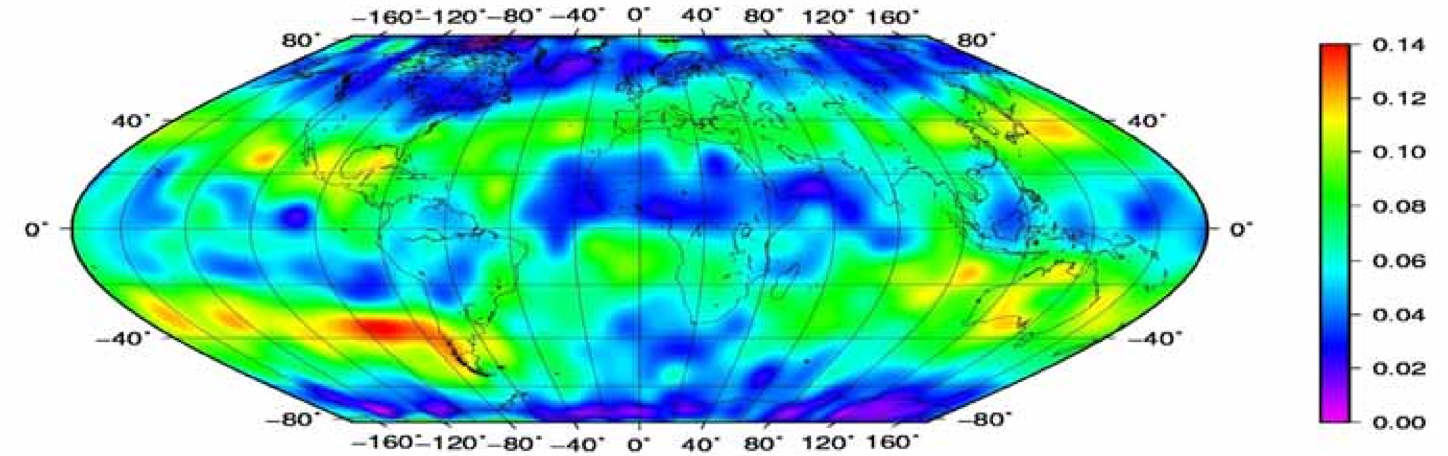

Number of GPS RO data from January to June 2008 in a longitude-latitude cell of $10^o x 10^o$

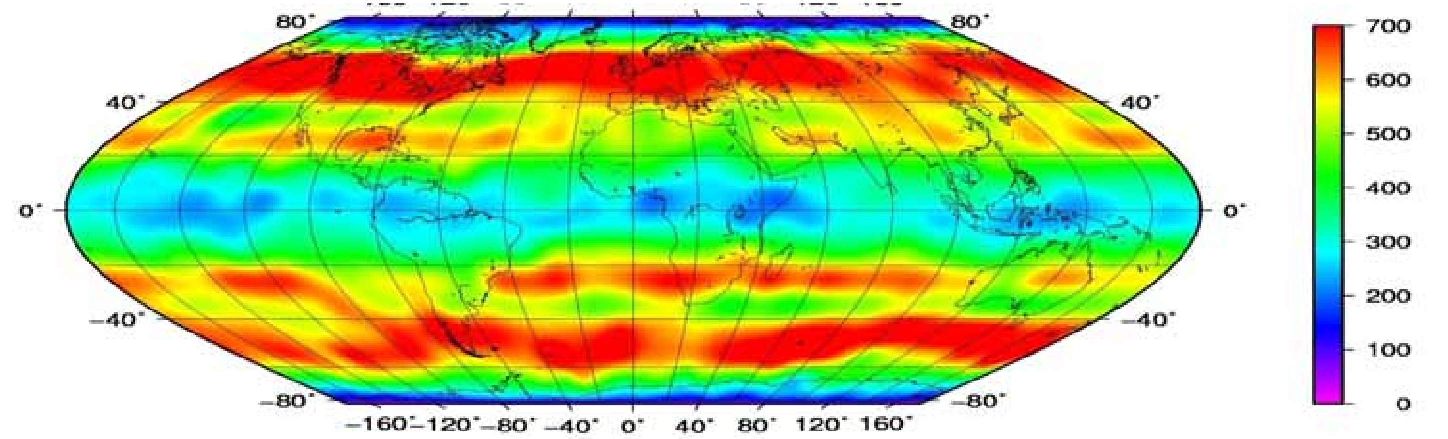

Number of sporadic E events

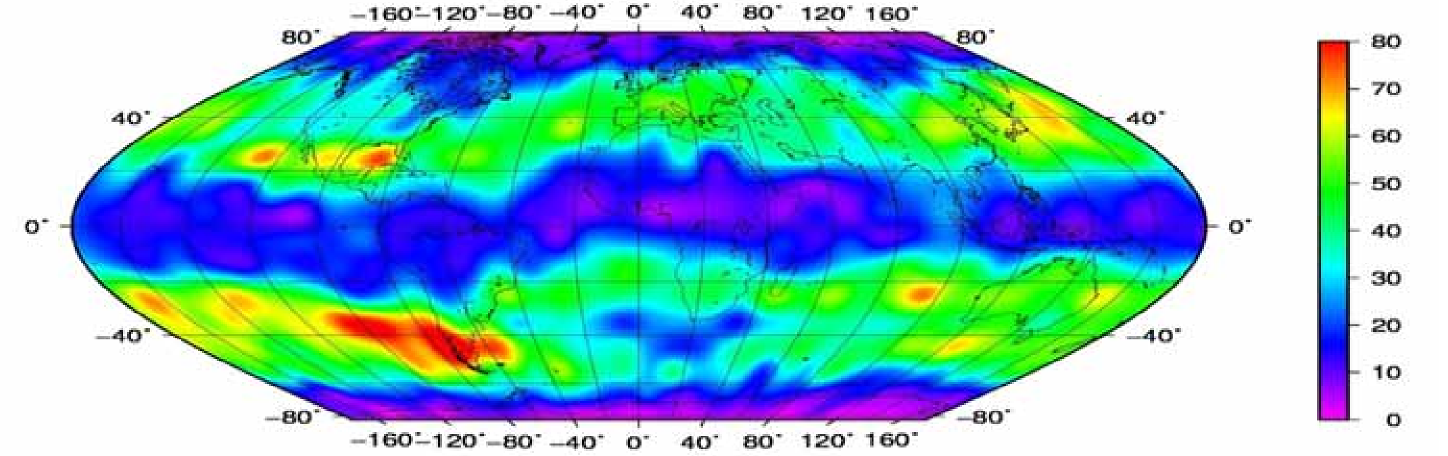

Occurrence rate of sporadic E events

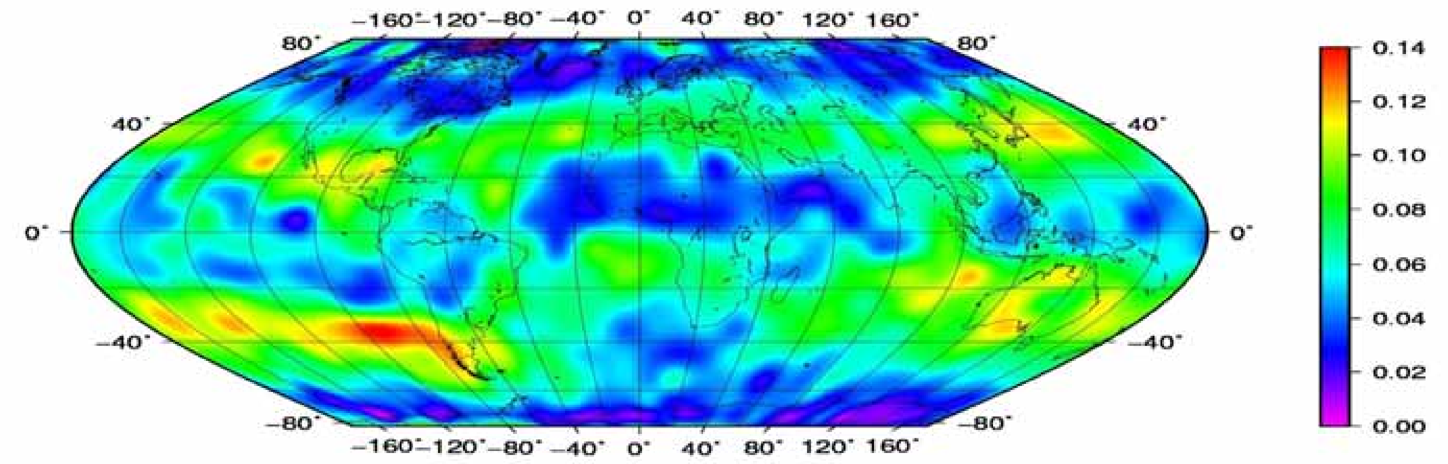

Outline of this lecture: Atmospheric Coupling Processes

✓ A linear theory of atmospheric gravity wave
- Dispersion relation of atmospheric gravity waves
- Convective instability and wave breaking/saturation
- Critical level interaction between a gravity wave and wind shear
- Importance of wave drag force (wave breaking) to maintain the general circulation of the middle atmosphere

✓ Radar observations of wave breaking process:
- gravity wave saturation and turbulence generation (the MU radar).

✓ Global distribution of gravity wave activity with GPS radio occultation (RO) measurements:
- Generation mechanisms; tropical convection, topography (mountain waves), Jet stream & polar night-jet, etc.

✓ Correlation between sporadic E and stratospheric gravity waves
- Generation of orographic waves over Andes and Antarctica
- A global distribution of sporadic E revealed with GPS-RO

✓ Coupling between the lower atmosphere and the MLT (mesosphere lower thermosphere) winds in the tropics
- Tropical convection and gravity waves in the stratosphere
- Correlation between short-period GW and Mesospheric SAO
- Relation between S-QBO and M-QBO (M-QB Enhancement)

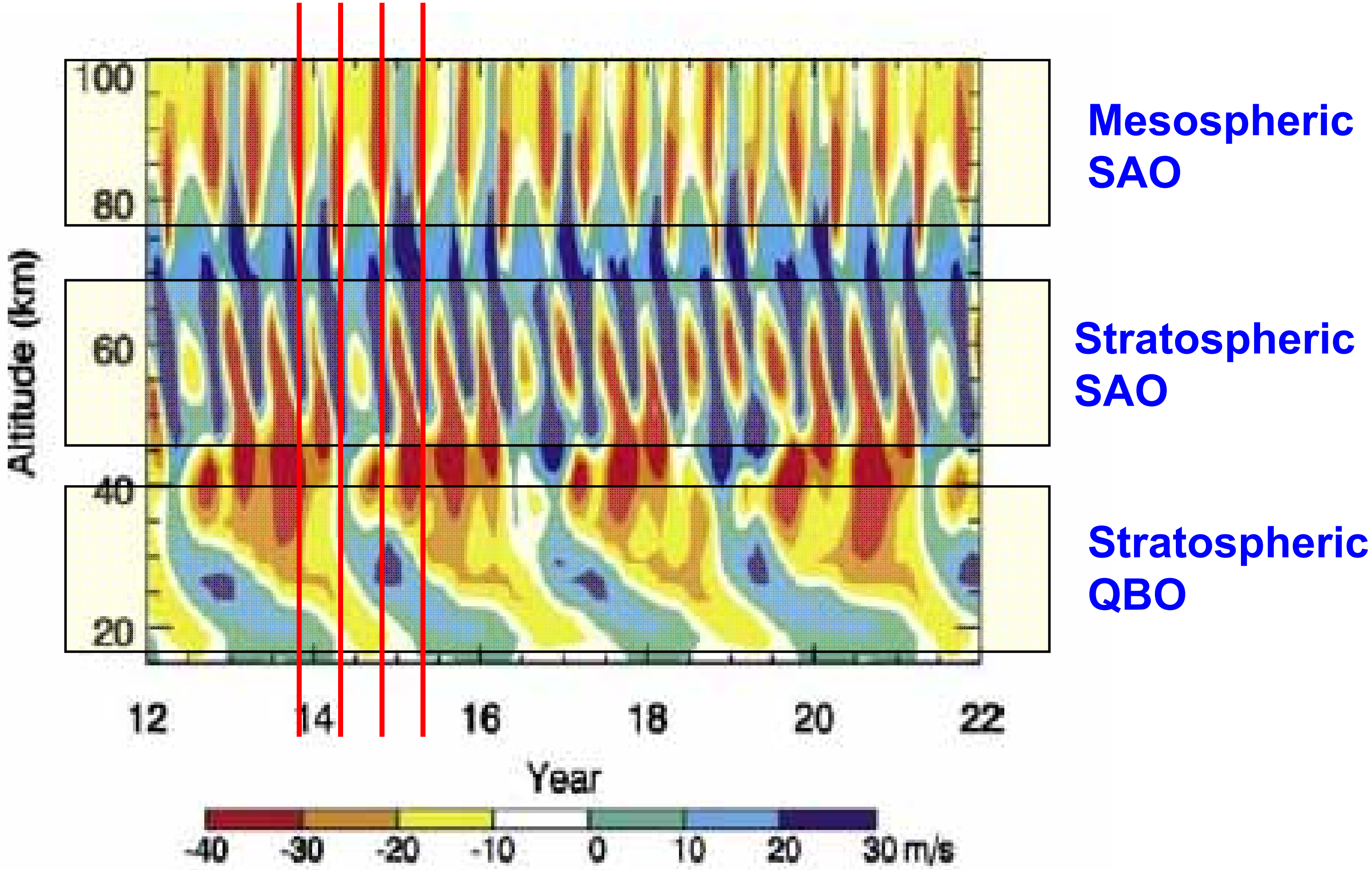

Figure 1. Altitude-time section of model equatorial zonal winds from a simulation with fixed solar UV (see text). Contour interval is 10 m s^{-1}. Westerly (eastward) flow is positive.

NRL Chemical/Dynamical Model of the Middle Atmosphere (CHEM2D) a two-dimensional, zonally-averaged model (McCormack, 2003)

Location of MF/Meteor Radars Used in This Study

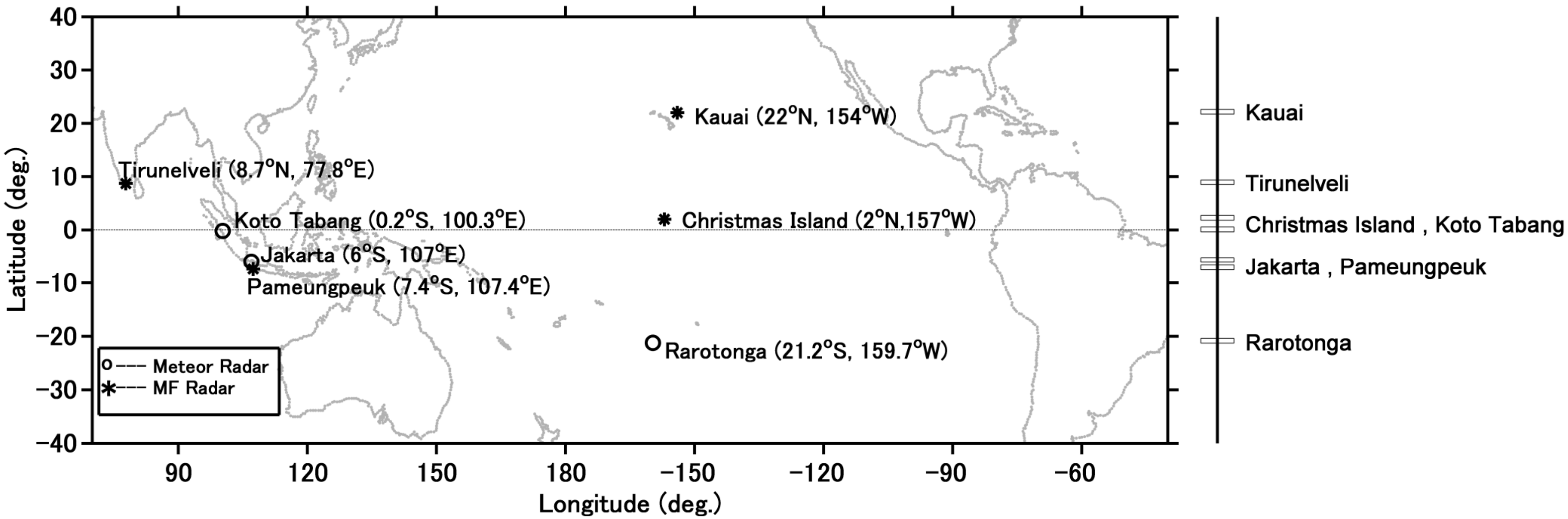

Data availability

22N Kauai : 1990-2006
9N Tirunelveli : 1993-2009
Equator Christmas Island : 1990-1997
and Koto Tabang : 2003-2010
7S Jakarta :1993-1999
and Pameungpeuk : 2004-2010
21S Rarotonga : 2003-2008

Radars located at similar latitudes (although differing in longitude on the Equator) are treated as one set.

Monthly mean zonal winds (after removing tidal contributions)

❖ Semi-annual oscillation at all locations

Within ±9° winds are westward biased

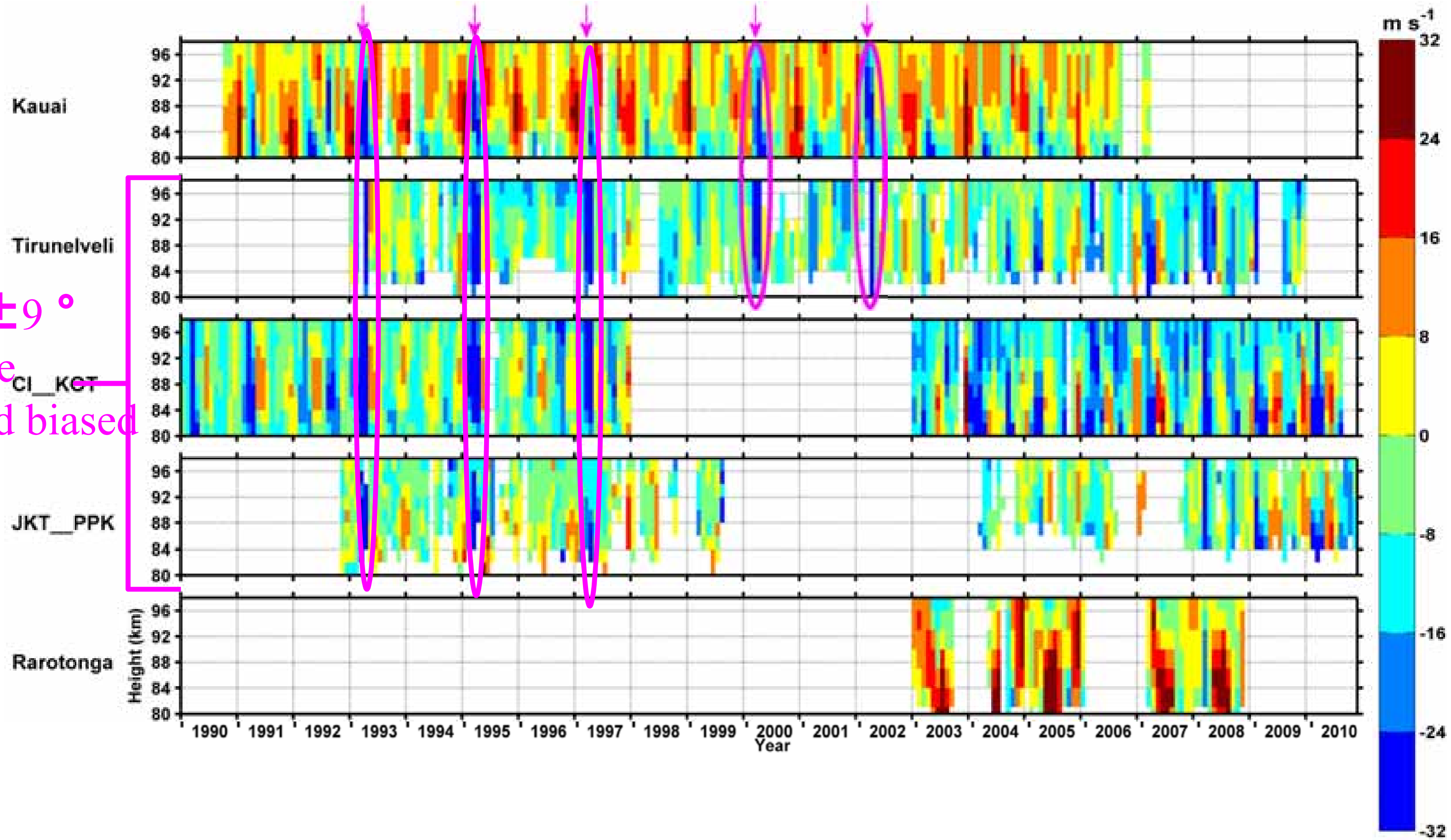

Comparison between the Radar Winds (left) and URAP (right) at 88 km

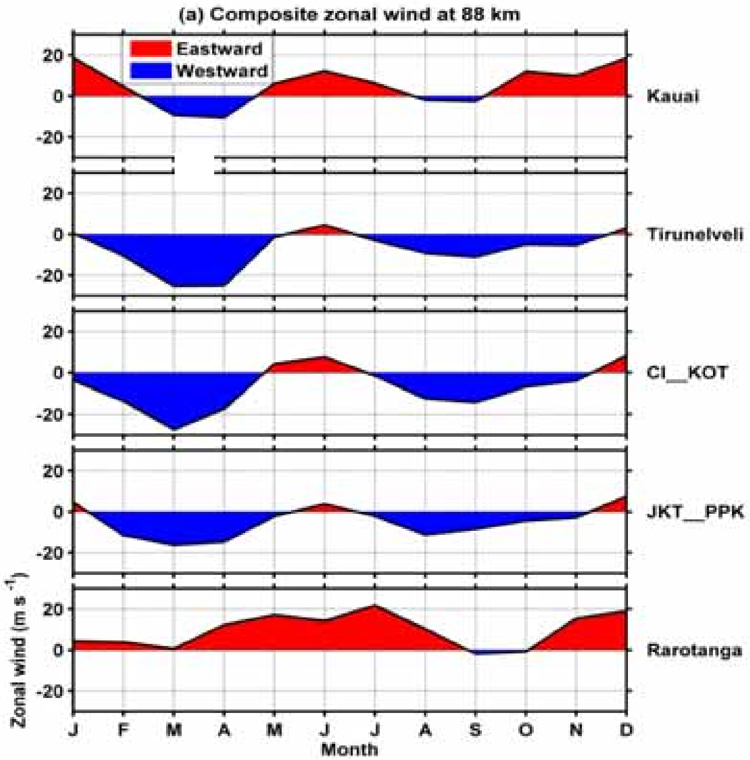

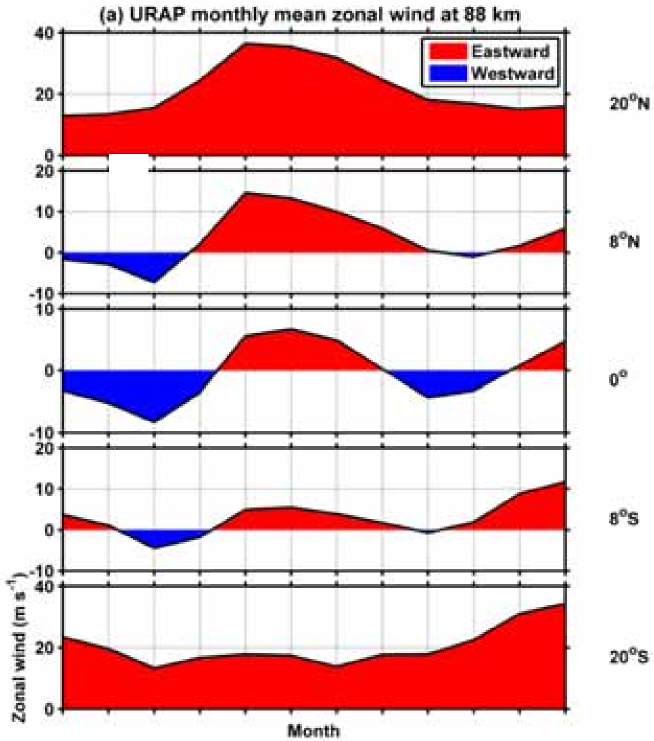

URAP: UARS (Upper Atmosphere Research Satellite) Reference Atmosphere [Swinbank and Ortland, 2003]

- ❖ Westward winds are stronger than the eastward winds and persist for longer time at Tirunelveli (9N) , Ch-Is & Koto Tabang (Eq), and JKT-PPK (7S).
- ❖ Westward winds during March equinox are stronger than in September equinox.
- ❖ Eastward winds are slightly larger than westward at Kauai (22N).
- ❖ At Rarotonga (21S) the winds are mostly eastward.

- ❖ URAP eastward winds are larger than the radar winds.
- ❖ At Tirunelveli (9N), and JKT_PPK (7S) the radar westward winds are larger than the URAP winds

Monthly mean eastward (top) and northward (bottom) winds in the MLT region (80-98 km) observed with the Tirunelveli MF radar

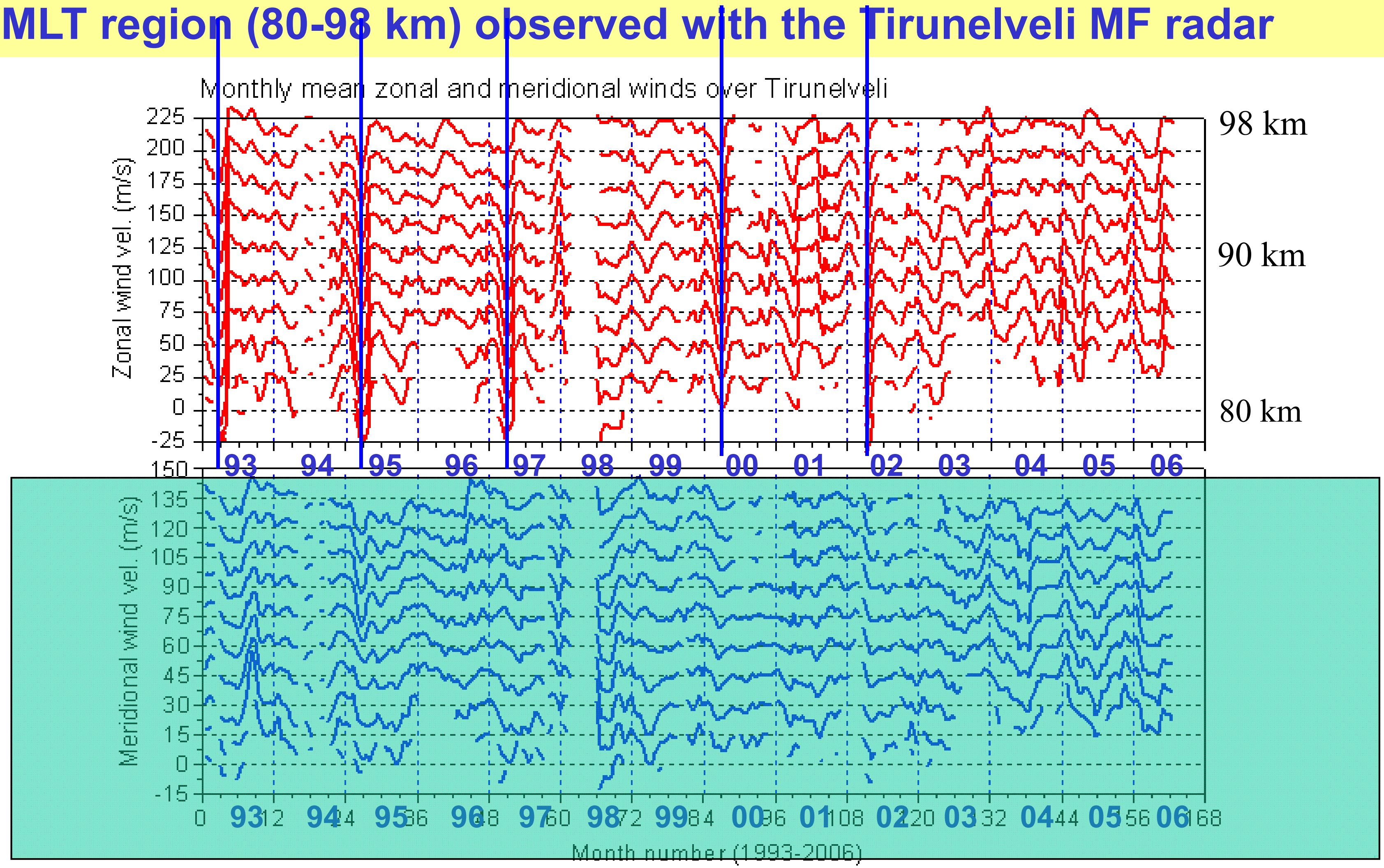

Monthly mean zonal wind showed SAO, the first westward phase of which showed interannual variability (interpreted as MQBO by Burrage et al. 1996)

Monthly mean meridional wind generally shows AO, which was clear in 1993-1997 and 2002-, but the amplitudes were considerably depressed in 1999-2002.3

Zonal winds in the MLT region observed with the Tirunelveli MF radar (top) and, in the stratosphere with radoiosonde at Singapore (bottom) in 1993-2006

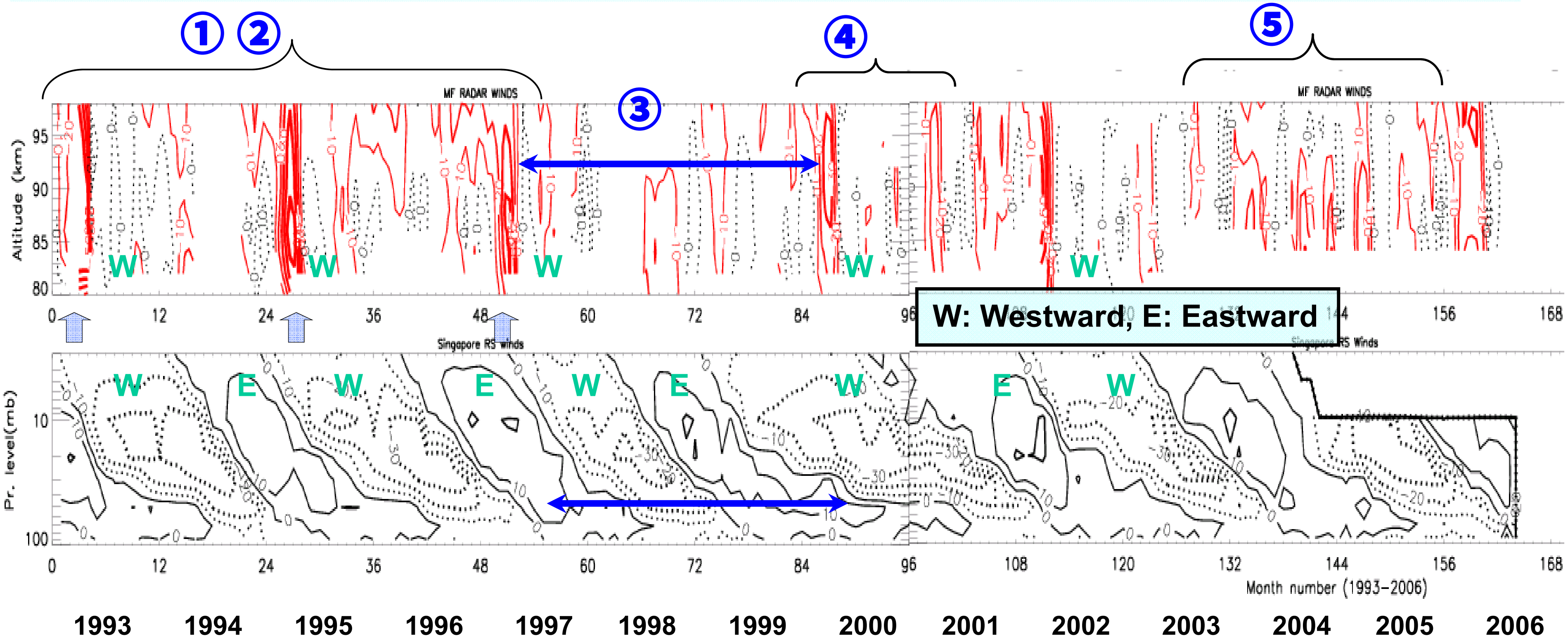

① In 1993-1997, **large westward winds of SAO** occurred in March-April, coinciding with **the eastward phase of S-QBO**.

② The maximum westward winds was about 80 m/s in 1993, 60 m/s in 1995 and 40 m/s in 1997, showing a decreasing trend.

③ But, in 1999 the M-QBO amplitudes became as small as about 10 m/s, and **the next M-SAO enhancement occurred in March-April, 2000 (3 year interval), which correlated well with S-QBO**.

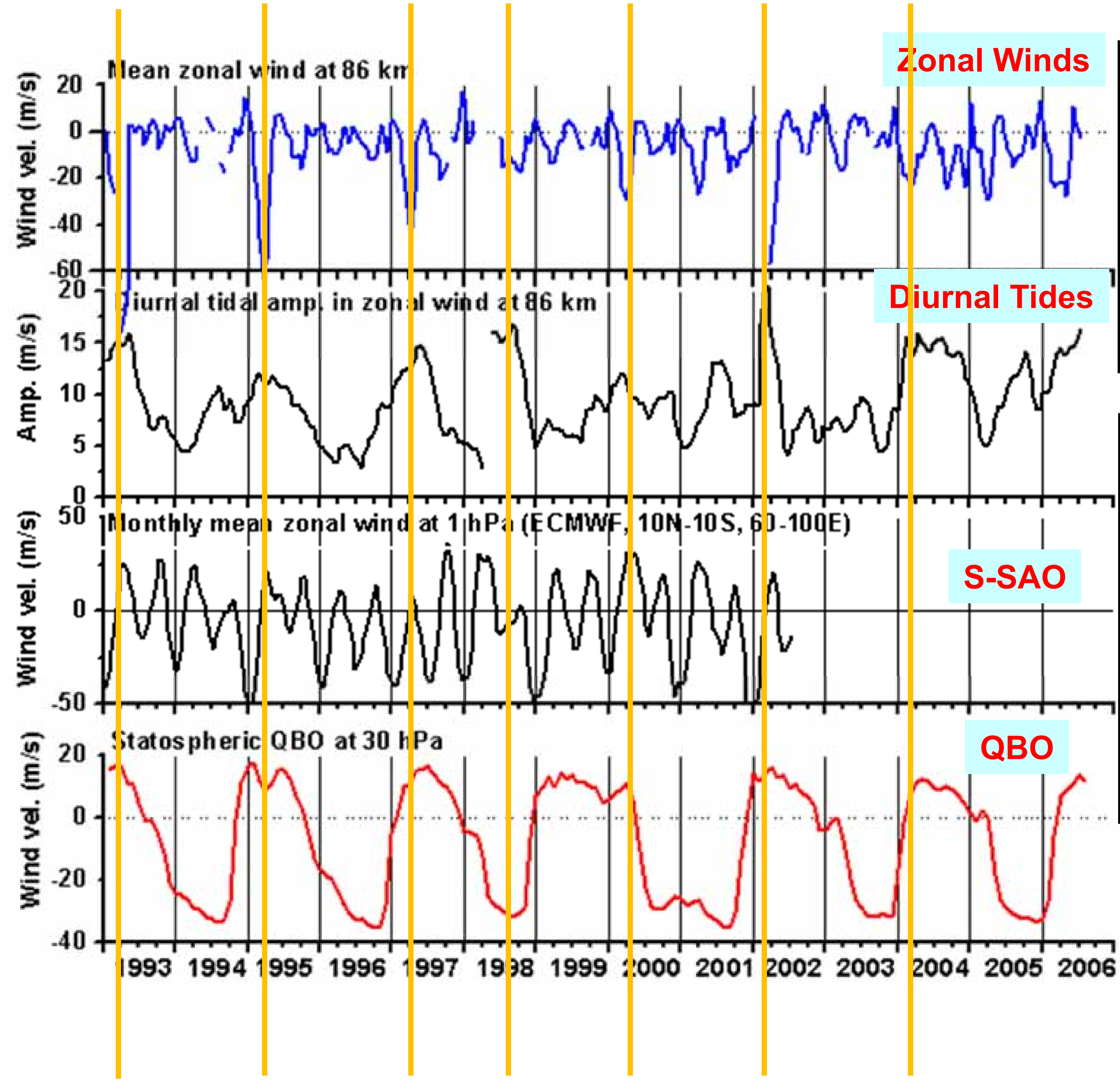

S-SAO (ECMWF): Zonal winds at 1 hPa (stratopause) exhibited SAO with eastward/westward winds during equinox/ solstice months.

When **the eastward phase of S-QBO and S-SAO** coincided, the westward winds of **M-SAO** was enhanced.
Note the **diurnal tide** also showed large amplitudes.

Daily mean zonal wind and GW variance ($u'^2+v'^2$)

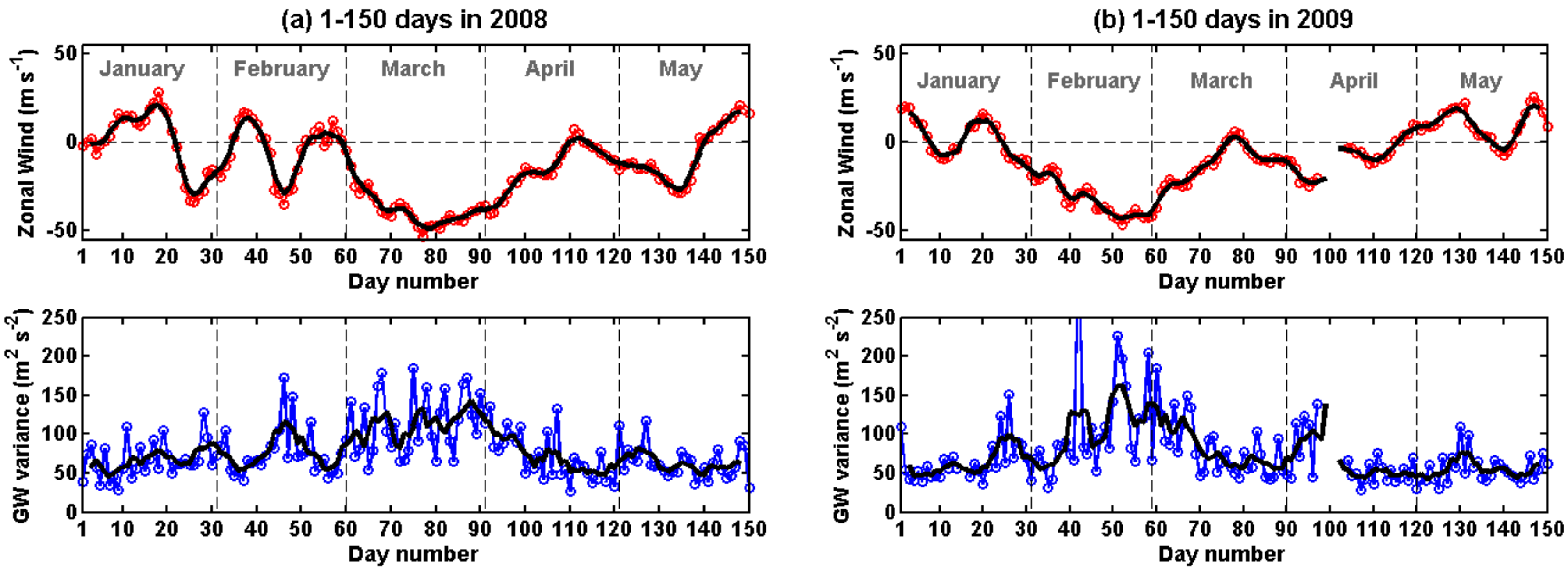

Enhanced GW activity (bottom panel) coincided with the westward maximum of the zonal winds (top panel), suggesting a relation of the wave drag force in driving SAO in the mesosphere.

N.Venkateswara Rao, T.Tsuda and Y. Kawatani, Ann. Geophys., 2012

Climate And Weather of the Sun-Earth System

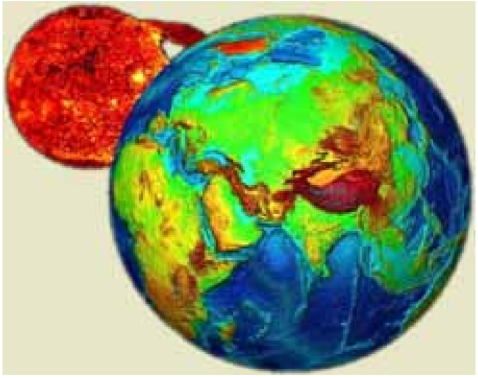

CAWSES-II Towards Solar Maximum

Summary

- Upward propagating atmospheric waves are essential in maintaining the general circulation of the middle atmosphere.
- Ground-based observations confirmed the dynamical stress by breaking of atmospheric gravity waves.
- A global distribution of generation sources for gravity waves is revealed by satellite observations, esp. GPS RO.
- Mountain waves over Andes and Antarctica seem to trigger generation of sporadic E layers.
- MF/meteor radar observations show a good correlation between the stratospheric QBO and the mesospheric SAO, suggesting a coupling of these regions by upward propagating waves.

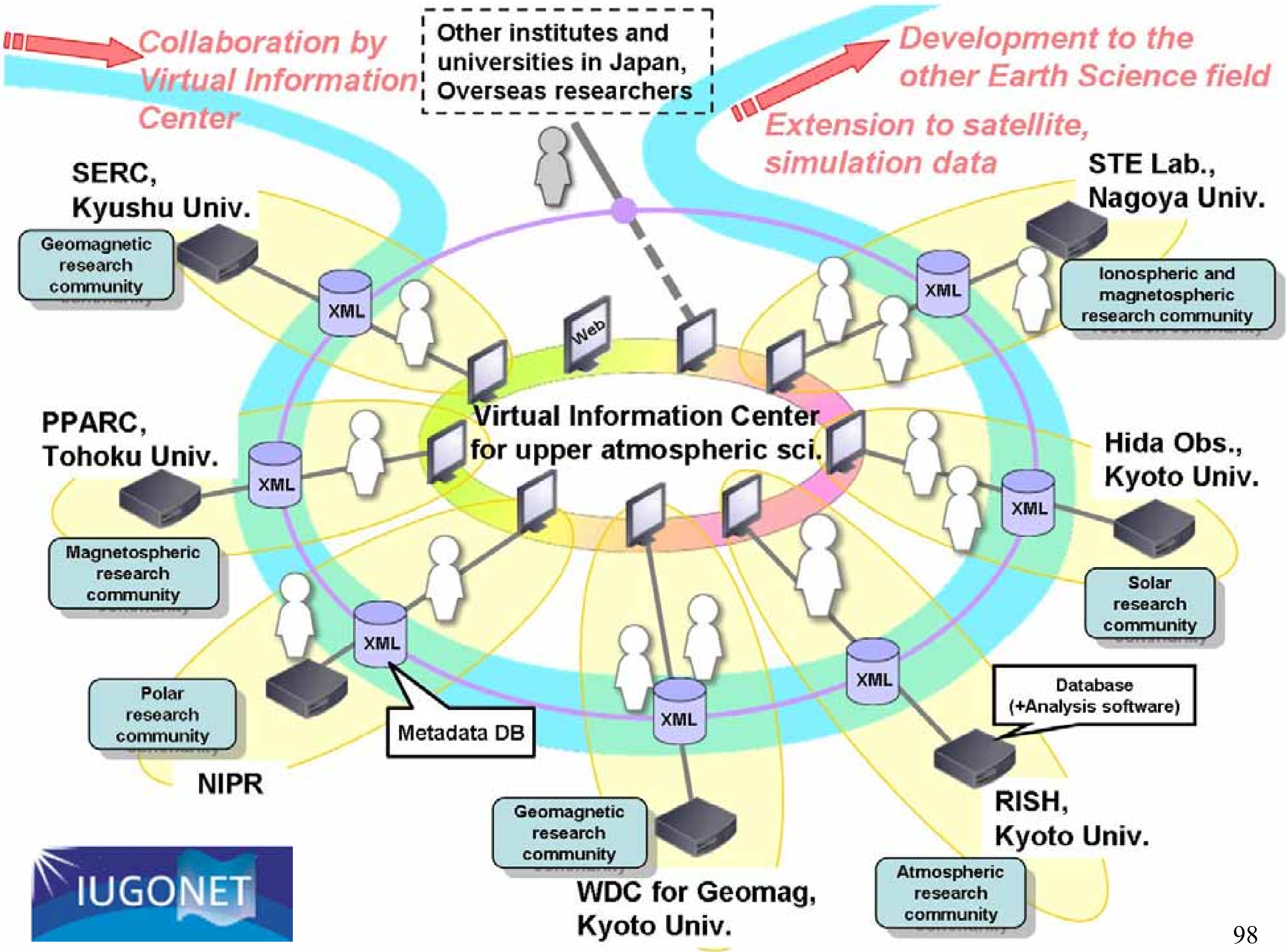
Collaboration by Virtual Information Center
Other institutes and universities in Japan, Overseas researchers
Development to the other Earth Science field
Extension to satellite, simulation data
SERC, Kyushu Univ.
Geomagnetic research community
STE Lab., Nagoya Univ.
Ionospheric and magnetospheric research community
Web
XML
Virtual Information Center for upper atmospheric sci.
PPARC, Tohoku Univ.
Magnetospheric research community
Hida Obs., Kyoto Univ.
Solar research community
Polar research community
NIPR
Metadata DB
Database (+Analysis software)
RISH, Kyoto Univ.
Atmospheric research community
Geomagnetic research community
WDC for Geomag, Kyoto Univ.
IUGONET

Data-Base and Virtual Observatory

- To investigate long-term variations in STP, we need to create integrated links between a variety of ground-based observations at various locations.
- Such databases, however, were available only to each group that conducted the observations, and were used only for specific phenomena,.
- The Inter-university Upper atmosphere Global Observation NETwork (IUGONET) project is continued in 2009-2014 by the five universities and institutes (NIPR, Tohoku-U, Nagoya-U, Kyoto-U, and Kyushu-U) in Japan.
- We collaborate to build a metadata-base system (MDB) archiving information; such as observation period, location, instrument, data format, etc, which is useful for researchers in efficiently finding and obtaining various observational data spread across the community.
- The MDB system will significantly facilitate the analyses of a variety of observational data, which will lead to more comprehensive studies of the mechanisms of long-term variations in STP.
- Moreover, since this project adopts an internationally widely used metadata format and uses a freely available repository software to build the MDB system, our developing tool will contribute to the promotion of international interdisciplinary studies in the CAWSES-II.

(For details of IUGONET, please refer to http://www.iugonet.org/en/)


Terima Kasih Banyak